Draft v. 2011 July 27
Preprint typeset using LaTeX style emulateapj v. 5/2/11

arXiv:1107.2570v2 [astro-ph.CO] 9 Sep 2011

THE STAR FORMATION REFERENCE SURVEY.
I. SURVEY DESCRIPTION AND BASIC DATA

M. L. N. Ashby[1], S. Mahajan[1,2], H. A. Smith[1], S. P. Willner[1], G. G. Fazio[1], S. Raychaudhury[2], A. Zezas[1,3], P. Barmby[4], P. Bonfini[3], C. Cao[5], E. González-Alfonso[6], D. Ishihara[7], H. Kaneda[7], V. Lyttle[4], S. Madden[8], C. Papovich[9], E. Sturm[10], J. Surace[11], H. Wu[12], and Y.-N. Zhu[12]

Draft v. 2011 July 27

ABSTRACT

Star formation is arguably the most important physical process in the cosmos. It is a fundamental driver of galaxy evolution and the ultimate source of most of the energy emitted by galaxies. A correct interpretation of star formation rate (SFR) measures is therefore essential to our understanding of galaxy formation and evolution. Unfortunately, however, no single SFR estimator is universally available or even applicable in all circumstances: the numerous galaxies found in deep surveys are often too faint (or too distant) to yield significant detections with most standard SFR measures, and until now there have been no global, multi-band observations of nearby galaxies that span all the conditions under which star-formation is taking place. To address this need in a systematic way, we have undertaken a multi-band survey of all types of star-forming galaxies in the local Universe. This project, the Star Formation Reference Survey (SFRS), is based on a statistically valid sample of 369 nearby galaxies that span all existing combinations of dust temperature, SFR, and specific SFR. Furthermore, because the SFRS is blind with respect to AGN fraction and environment it serves as a means to assess the influence of these factors on SFR. Our panchromatic global flux measurements (including *GALEX* FUV+NUV, SDSS *ugriz*, 2MASS JHK_s, *Spitzer* 3–8 μm, and others) furnish uniform SFR measures and the context in which their reliability can be assessed. This paper describes the SFRS survey strategy, defines the sample, and presents the multi-band photometry collected to date.

Subject headings: Infrared: galaxies; — catalogs — stars: formation

1. INTRODUCTION

Star formation has been the most important single physical process since recombination. Not only have stars created most of the luminous energy in the Universe, they have produced the heavy elements needed for planets and life. Star formation has naturally been the subject of vast numbers of studies, leading, for example, to our current understanding of the star formation history of the Universe (*e.g.*, Lilly et al. 1996, Hopkins & Beacom 2006; Madau et al. 1998) and the discovery of the Schmidt Law (Schmidt 1959; updated by Kennicutt et al. 1998) relating the SFR in galaxies to the gas surface density.

A general inadequacy of existing work is the lack of a self-consistent treatment of SFR across the full electromagnetic spectrum: ultraviolet (UV) continuum only samples the SFR in the absence of dust; Hα and [O II] measure *ionizing* photons coming from only the high-mass ($\gtrsim 5\,M_\odot$) population. Emission in the polycyclic aromatic hydrocarbon (PAH) bands is taken as a SFR measure (*e.g.*, Madden et al. 2006; Wu et al. 2005) but may be unreliable for low-luminosity (or low-metallicity) galaxies (Hogg et al. 2005) or in the presence of a hard radiation field. Far-infrared dust re-radiation samples a broad range of star formation ($\sim$1–10 $M_\odot$ for reasonable IMFs) but only becomes a precise SFR measure in the optically-thick limit (Kennicutt 1998). Nonthermal radio emission comes from Type II supernova remnants (*e.g.*, Rieke et al. 1980) and therefore only samples higher-mass SF.

Star formation activity is by no means evenly distributed throughout galaxies. Instead, stars form within the densest regions of giant molecular clouds; this phenomenon manifests in the *IRAS* bands as far-infrared radiation when the (hot) young stellar objects deeply embedded in their natal clouds illuminate the surrounding interstellar material (*e.g.*, Parker 1991), which then reradiates that energy at long wavelengths. In a detailed case study of Milky Way GMC complexes (*e.g.*, the California

---

[1] Harvard-Smithsonian Center for Astrophysics, 60 Garden St., Cambridge, MA 02138, USA [e-mail: `mashby@cfa.harvard.edu`]
[2] School of Physics and Astronomy, University of Birmingham, Edgbaston, Birmingham B15 2TT, UK
[3] University of Crete, Physics Department & Institute of Theoretical and Computational Physics, 71003 Heraklion, Crete, Greece
[4] Department of Physics & Astronomy, University of Western Ontario, London, ON N6A 3K7, Canada
[5] School of Space Science and Physics, Shandong University at Weihai, Weihai, Shandong 264209, China
[6] Universidad de Alcalá de Henares, Deptamento de Física, Campus Universitario, E-28871 Alcalá de Henares, Madrid, Spain
[7] Graduate School of Science, Nagoya University, Furo-cho, Chikusa-ku, Nagoya, Aichi 464-8602, Japan
[8] Service d'Astrophysique, CEA/Saclay, l'Orme des Merisiers, 91191 Gif-sur-Yvette, France
[9] Department of Physics, Texas A & M University, College Station, TX 77843-4242
[10] Max-Planck-Institute for Extraterrestrial Physics (MPE), Gieenbachstrae 1, D-85748 Garching, Germany
[11] Spitzer Science Center, MS 220-6, California Institute of Technology, Jet Propulsion Laboratory, Pasadena, CA 91125, USA
[12] Key Laboratory of Optical Astronomy, National Astronomical Observatories, Chinese Academy of Sciences, 20A Datun Road, 100012 Beijing, China

Nebula) Lada, Lombardi, & Alves (2010) demonstrated a remarkably tight correlation between SFR and the total mass of *dense* gas, lending further support to this view.

There is considerable evidence in the literature that our understanding of star formation depends on making consistent use of all available wavebands. For example, Kartaltepe et al. (2010) showed that without photometry at wavelengths longer than $100\,\mu$m, total far-IR luminosities (and thus SFRs) are typically underestimated by 0.2 dex; in some cases the discrepancy can be much larger. This can be interpreted as an inability to adquately measure emission from a cold dust component (if present) when such far-IR data are lacking. These issues are now becoming better understood as a result of *AKARI* and *Herschel* programs that reach deeper into the far-IR than could *IRAS*, *ISO*, or *Spitzer*. The situation remains complex, however. In *Herschel*-selected galaxies, dust attenuation appears to strongly impact the UV detection fraction and the relationship between UV and IR SFR indicators (Buat et al. 2010). There are strong hints of systematic discrepancies between *AKARI* and *IRAS* photometry at $\sim 100\,\mu$m (Jeong et al. 2007; Figs. 1 and 7 of Takeuchi et al 2010). These unresolved issues can in principle be addressed with thoughtful controls. But there are also systematic effects intrinsic to the galaxies themselves. For example, there is evidence that the specific SFR (sSFR, the SFR per unit stellar mass) depends on stellar mass (*e.g.*, Sobral et al. 2011, Elbaz et al. 2011). For many years there have been suggestions that dust temperature was dependent on luminosity (*e.g.*, Sanders et al. 2003). And there is as yet no systematic treatment of the contribution of the older, quiescent stellar components to the SFR tracers most commonly used.

To better understand the complexities of star formation, a comprehensive treatment examining the influence of all the major parameters — stellar mass, dust mass and temperature, and metallicity — on SFR indicators is needed. The importance and timeliness of this subject is attested by numerous recent efforts to grapple with the nuances of SFR estimation. Notable examples include the *Spitzer* Infrared Nearby Galaxies Sample (SINGS; Kennicutt et al. 2003; Calzetti et al. 2010), the Local Volume Legacy Survey (LVLS; Dale et al. 2009), the *Herschel* Reference Survey (HRS; Boselli et al. 2010), the Great Observatories All-sky LIRG Survey (GOALS; Armus et al. 2009), and the Multi-Wavelength Extreme Starburst Sample (MESS; Laag et al. 2010), among others. Each of these undertakings has been designed to attack specific aspects of the star-formation phenomenon, but each also has limitations that prevent it from providing a comprehensive picture of star formation in galaxies.

This paper presents the Star Formation Reference Survey (SFRS), a sample of nearby galaxies having a unique capacity to describe star formation under all conditions in which it occurs in the local Universe. Section 2 describes the selection criteria used to define the SFRS. Section 3 presents the SFRS datasets obtained to date. Section 4 shows how the SFRS complements the above-mentioned projects, presents an estimate of AGN prevalence and the ramifications for far-infrared SFR measures, and briefly describes SFRS-related observing campaigns now in progress.

2. SAMPLE SELECTION

The complexities of the real Universe mean that an understanding of global galaxy properties will inherently be statistical in nature. Progress, even in the local Universe, requires uniform measurements of the properties of a well-chosen, sufficiently large number of galaxies that they sample star formation across *the full range of galaxy properties*. In other words, having the proper study sample is critical to the success of this undertaking.

The SFRS selection criteria were defined objectively to guarantee that the sample spans the full range of properties exhibited by star-forming galaxies in the local Universe. We began with the *IRAS* $60\,\mu$m luminosity as an unbiased (but perhaps not always correct!) star formation tracer by virtue of the breadth and uniformity of *IRAS* coverage and because of the proximity of the $60\,\mu$m band to the SED peak associated with star formation. Although the selection was based squarely on the $60\,\mu$m flux, this should not be taken as an assertion that all issues of interpretation have been resolved. Some fraction of the $60\,\mu$m luminosity, at least in some galaxies, must arise from dust illuminated by the older stellar population. Addressing this matter is one of the aims of the SFRS project and a primary motivation for the assembly of the datasets described in Sec. 3.

The parent sample for the present study is the PSCz catalog (Saunders et al. 2000), a full-sky database of 15,000 nearby star-forming galaxies brighter than 0.6 Jy at $60\,\mu$m. Most PSCz objects are closer than $z = 0.2$. The PSCz is not biased toward relatively rare ultraluminous objects (unlike the 1 Jy sample of Kim, Veilleux, & Sanders 2002) and is more representative than more restricted samples (*e.g.*, the *IRAS* Bright Galaxy Sample; $F_{60} > 5.24$ Jy; Sanders et al. 2003). PSCz galaxy luminosities range from $L(60\,\mu\mathrm{m}) = 10^7$ to $10^{12}\,\mathrm{L}_\odot$.

Star-forming galaxies have a wide range of properties, but aside from absolute luminosity, the specific SFR and the color temperature of far infrared dust emission are arguably the most important. These parameters reflect the relative importance of present and past star formation and the densities of the regions where stars are forming. High color temperature is usually taken to indicate that dust grains are close to the newly-formed stars, *i.e.*, it is a measure of active star formation. A low color temperature (high F_{100}/F_{60} ratio), on the other hand, can be interpreted as reflective of a situation in which the ambient UV field from older stars in the galaxy disk is illuminating dust in the ISM. Figure 1 illustrates one way in which dust temperature and luminosity relate. Nearly all 'cool' galaxies (*i.e.*, those with a far-IR flux density ratio $F_{100}/F_{60} \geq 2$) reside in the low-luminosity regime. The situation is different for 'warmer' ($F_{100}/F_{60} < 2$) galaxies, however – this population is roughly evenly divided between high- and low-luminosity sources. To capture this behavior in a study sample, it is not adequate to make a simple luminosity cut: one must account for the dust temperature or be at risk of under-representing the mode (warm or cool) at which star formation occurs for some luminosities.

Figure 1 also reveals a dichotomy in the relationship of sSFR and luminosity. While essentially all the low-sSFR galaxies are low-luminosity objects, those with high sSFRs are a mix, with both low- and high-luminosity galax-

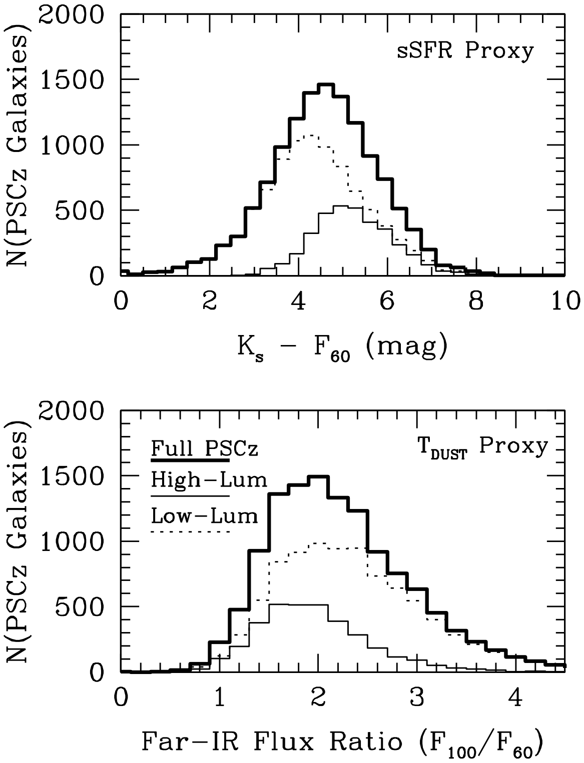

Fig. 1.— Histograms of sSFR and dust temperature proxies within the parent PSCz galaxy sample. Thick lines show galaxy numbers for the full sample. The PSCz has been divided into two subsamples at $\nu L_\nu(60\,\mu\text{m}) = 10^{9.5}$ L$_\odot$. Thin solid lines indicate the distributions for the high-luminosity subsample, and dashed lines indicate the distributions for the low-luminosity subsample. *Top panel:* Abscissa is the ratio of K_s to $60\,\mu$m flux densities expressed as the difference in AB magnitudes. *Bottom panel:* Abscissa is the ratio of 100 to $60\,\mu$m flux densities (F_ν).

TABLE 1
Bin Boundaries Applied to Parent PSCz Sample

Parameter	Q1/Q2	Q2/Q3	Q3/Q4
sSFR Proxy ($K_s - F_{60}$)	3.78	4.56	5.34
T_{DUST} Proxy (F_{100}/F_{60})	1.71	2.14	2.69

Note. — The quartile boundaries applied to the sSFR and T_{DUST} proxies used to define the SFRS sample. The third selection dimension, $60\,\mu$m luminosity, was binned in decades starting at log(L$_{60}$) = $10^{6.5}$ L$_\odot$ with an additional half-decade bin boundary at 10^{10} L$_\odot$, near the peak of the distribution (Fig. 2).

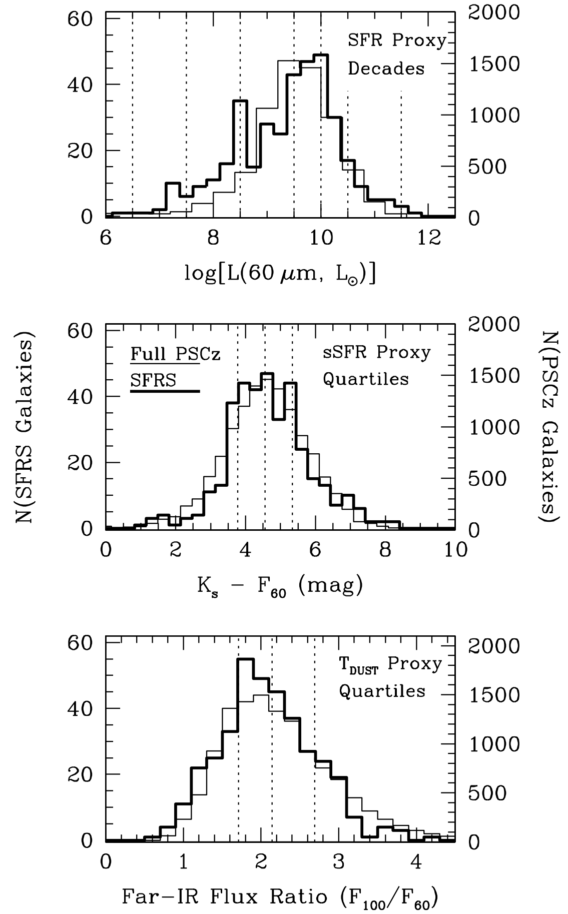

Fig. 2.— The distributions of the SFRS galaxies in each of the three parameter spaces used to select the sample. Thick histograms indicate the SFRS galaxies and are referenced to the left-hand axes, while thin histograms represent the larger PSCz sample from which the SFRS sample is drawn, and are referenced to the right-hand axes. The distributions are very similar in all three panels. The vertical dotted lines in each panel indicate the boundaries defining the bins (Tab. 1).

ies present. A selection on luminosity alone is therefore extremely unlikely to include sources with the full range of sSFRs that exist, and a high-luminosity selection will miss the low-sSFR sources entirely.

A full sampling of star-forming galaxy properties requires that the SFRS be defined in a three-dimensional space spanning the *full ranges* occupied by PSCz galaxies in $60\,\mu$m luminosity, flux ratio F_{60}/K_s, and far-IR flux density ratio F_{100}/F_{60}. In this scheme 2MASS K_s serves as a proxy for stellar mass, the far- to near-infrared flux ratio measures specific SFR, while the far-IR flux density ratio acts as a measure of dust temperature. This three-dimensional parameter space was binned by decade in $60\,\mu$m luminosity and by quartiles in both the $K_s - 60\,\mu$m color and the F_{100}/F_{60} flux density ratio (Fig. 2). The bins are defined in Table 1. This ensured that the sample contains all existing combinations of high- and low-sSFR with far-IR color *and* luminosity. The changeover from cool dust/low sSFR to warm dust/high sSFR occurs around $L(60) = 10^{9.5}$ to $10^{10.5}$ L$_\odot$, which is the most heavily populated decade in luminosity. We therefore split this range into two half-decades in $L(60)$ to sample this important regime more finely. The result is 4×4 bins in each of two colors and eight bins in luminosity: 128 bins altogether.

After the bin boundaries were determined from the complete PSCz, a representative subsample was selected as follows. First, only galaxies with measured positive redshifts were included. Second, galaxies outside the Sloan Digital Sky Survey (SDSS) and NRAO VLA Sky Survey (NVSS; Condon et al. 1998) of the northern Galactic cap were excluded. This constraint ensures that visible and radio detections, and hence radio-derived SFRs, would be available for all galaxies and simultaneously minimizes foreground confusion because the Galactic plane is >20° distant from all sources. Out

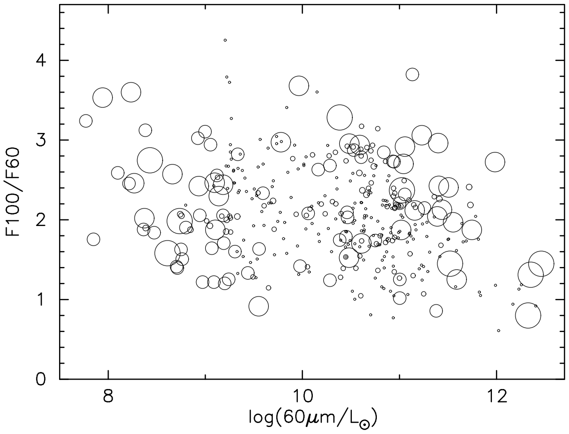

FIG. 3.— The three-dimensional SFRS galaxy distribution projected into the two-dimensional space defined by 60 μm luminosity and far-IR flux density ratio. The symbol size is inversely proportional to weight: large symbols indicate relatively rare objects that occupy sparsely-populated bins; they significantly enlarge the parameter space explored by our sample and may be under-represented by programs not implementing selections similar to the SFRS.

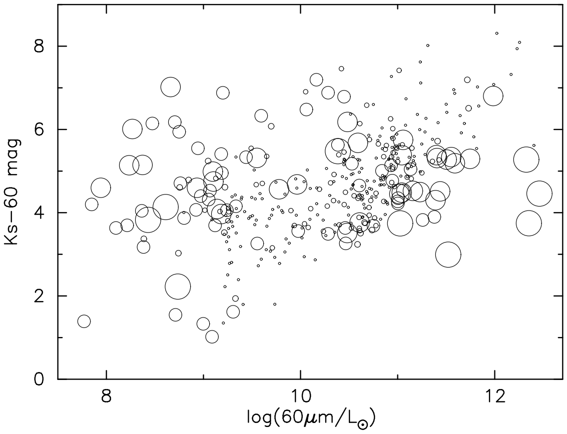

FIG. 4.— The three-dimensional SFRS galaxy distribution projected into the two-dimensional space defined by 60 μm luminosity and near- to far-IR color (specific SFR proxy). Symbols as in Fig. 3.

of the 15,000 PSCz galaxies, 2564 meet these restrictions. Third, the few nearest galaxies were eliminated in order to avoid time-consuming *Spitzer* mapping of objects with large angular diameters and the attendant uncertainties in calculating global measurements. The exact distance limit was made luminosity-dependent: at $L(60) < 10^{7.5}$ L$_\odot$ and $L(60) > 10^{10}$ L$_\odot$, all galaxies were eligible because they were either sufficiently small or distant that they could be imaged efficiently with *Spitzer*. At intermediate luminosities, galaxies with recession velocities $cz < 0.05 * L(60)^{1/2}$ km s^{-1} were excluded, where $L(60)$ is expressed in units of L$_\odot$. This criterion excluded 194 galaxies. Because all these restrictions are based strictly on galaxy positions in three-dimensional space, they in no way bias the sample, and they ensure that low-luminosity sources are retained.

The final SFRS consists of a representative number of galaxies from each bin. The number chosen from each bin containing N galaxies was $\sqrt{N}$, rounded up to a maximum of 10 galaxies. The specific galaxies chosen were the brightest within each bin. This selection sets the sample size at 369 galaxies and guarantees that the sample will be representative of the much larger PSCz, and by inference, representative of star forming galaxies generally. The distributions of the sample galaxies in the two-dimensional projections of the three-dimensional selection space are illustrated in Figs. 3 and 4. The SFRS distributions are very similar in all three selection parameters (Fig. 2) to those for the full PSCz. The resulting sample is thus statistically well-defined, *and covers the entire range of star formation properties seen locally: five decades in luminosity (and thus SFR); a factor of nearly 200 in specific SFR, and all masses, morphologies, and sizes.*

The relative prevalence of a galaxy of any type within the sample is reflected in its weight: each SFRS galaxy in a given selection bin is assigned a weight determined by the ratio of the total number of PSCz galaxies in that bin to the number of sample galaxies drawn from that bin into the SFRS sample. Relatively rare galaxy types have low weights, while those from heavily populated bins have large weights. The names, positions, individual weights, and *IRAS* 60 and 100 μm fluxes used to define the sample are given in Table 2. These weights project the SFRS sample back to the parent PSCz population. Additional weighting based on the volume in which a galaxy would enter the PSCz would be needed to define a true volume-limited sample.

Because of the rigid selection criteria, the well-known quasar 3C 273 and the the blazar OJ 287 are members of the SFRS. Each is the only galaxy in its bin (weight≡1). While we retain these objects to preserve the demographics of our selection, they can be ignored for studies relating purely to star formation.

3. BASIC DATA

In addition to the 2MASS and *IRAS* data used to define the selection criteria, many other resources are available. These are summarized in Table 3 and described in detail beginning with Sec. 3.2.

3.1. *Distances*

A significant fraction of the SFRS galaxies are very nearby, and can have peculiar velocities comparable to their Hubble flow velocities. Tully et al. (2008) have recently accumulated redshift-independent distance measurements for nearby galaxies by using alternate methods including the Tully-Fisher relation (Tully & Fisher 1977), Cepheids (Freedman et al. 2001), the luminosity of stars at the tip of the red giant branch (Karachentsev et al. 2004, 2006), and surface brightness fluctuations (Tonry et al. 2001). These measurements yield *quality* distances for nearby ($v < 3000$ km s^{-1}) galaxies with distance modulus uncertainties < 0.1 mag. Tully et al. (2008) estimated the distances of additional galaxies based on their association with groups/clusters. In total, their catalog[13] includes 3,529 distance measurements (Tully, 2010, private communication.) for galaxies with $v < 10,000$ km s^{-1}, of which 127 are in the SFRS.

For the 242 galaxies lacking quality distances, the heliocentric velocities in the PSCz catalog were converted to a corrected recession velocity taking into account the

---

[13] The Extra-galactic Distance Database, http://edd.ifa.hawaii.edu/

TABLE 3
SUMMARY OF AVAILABLE DATA FOR SFRS GALAXIES

Bandpass	Observatory	Sample Coverage
1.4 GHz	VLA/NVSS	100%
12,25,60,100 μm	*IRAS*	100%
65,90,140,160 μm	*AKARI* FIR All-Sky Survey	95%
24 μm	*Spitzer*/MIPS	70%
3.6, 4.5, 5.8, 8.0 μm	*Spitzer*/IRAC	100%
JHK_s	2MASS	100%
ugriz	SDSS	100%
Optical Spectra	SDSS (fiber)	57%
Hα	NAOC	30% (campaign ongoing)
0.13–0.28 μm	*GALEX*	90% to date

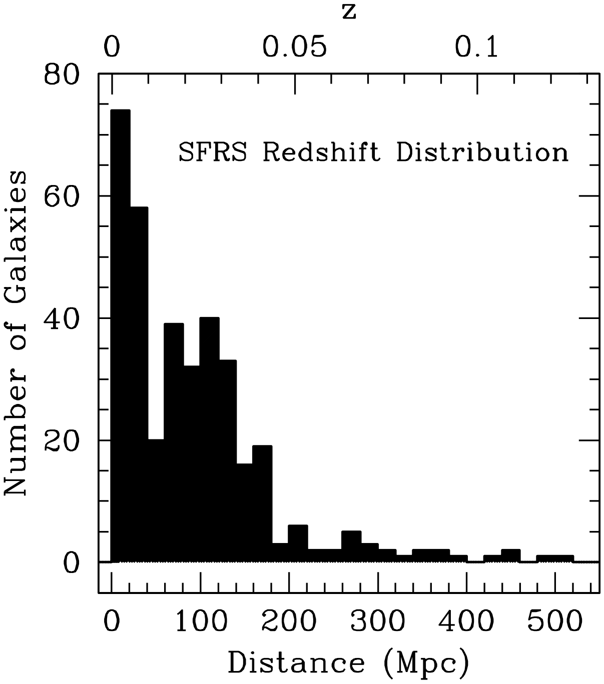

FIG. 5.— The distance/redshift distribution of the SFRS, in 20 Mpc bins. Because of the 60 μm *IRAS* selection, most of the sample galaxies are nearby ($z < 0.05$), but the distribution has a tail of higher-luminosity galaxies towards higher redshifts. The plot has been scaled to emphasize the nearby galaxies; the four most distant objects are not shown (3C 273, IRAS 11267+1558, IRAS 13218+0552, and OJ 287, at 660, 740, 850, and 1260 Mpc, respectively; Table 2).

velocity field of Virgo, the Great attractor and the Shapley supercluster, following Mould et al. (2000). All cataloged PSCz heliocentric velocities agree with those provided by the NASA Extra-galactic Database (NED)[14], within the uncertainties.

The resulting corrected velocities were used to estimate distances for all SFRS galaxies, assuming $H_0 = 73$ km s^{-1} Mpc^{-1}. The distances are given in Table 2, and the overall distance distribution is plotted in Figure 5. The SFRS galaxies tend to be bright by virtue of their proximity (60% are nearer than 100 Mpc, and 90% are closer than 180 Mpc) and are therefore easily accessible from a wide range of telescopes.

3.2. *IRAC Photometry*

The IRAC (Fazio et al. 2004) observations of most SFRS sources (*i.e.*, all those lacking suitable archival data) were carried out during Cycle 5 (PID 50128) using standard observing parameters. Each of the 273 galaxies targeted by PID 50128 was observed with at least 6×12 s full-array exposures using a cycling dither with a medium dither scale. All sources were observed in both IRAC fields of view, yielding a total exposure time of at least 72 s in each of the four IRAC bands at 3.6, 4.5, 5.8, and 8.0 μm. This relatively low exposure time consistently yielded $S/N > 1000$ for these very bright galaxies. All sources not included in PID 50128 had already been observed by other programs, and the corresponding data were downloaded from the archive.

The archival and PID 50128 data were reduced together in as homogeneous a manner as possible. The basic IRAC data reduction was carried out by team members at the University of Western Ontario and at the Center for Astrophysics. In both instances it was based on the corrected Basic Calibrated Data (cBCD). The cBCD frames were object-masked and median-stacked on a per-AOR (Astronomical Observing Request) basis. The resulting stacked images were visually inspected and subtracted from individual cBCDs within each AOR. This was done to eliminate long-term residual images arising from prior observations of bright sources by the 3.6, 5.8, and 8.0 μm arrays. The 4.5 μm detector array did not suffer from residual images during *Spitzer*'s cryogenic mission. Subtracting the median stacks also minimized gradients in the celestial backgrounds around each source. After these preliminaries, the data for each galaxy were mosaiced into four spatially-registered mosaics using IRACproc (Schuster et al. 2006). IRACproc augments the capabilities of the standard IRAC reduction software (MOPEX). The software was configured to automatically flag and reject cosmic ray hits based on pipeline-generated masks together with a sigma-clipping algorithm for spatially coincident pixels. IRACproc calculates the spatial derivative of each image and adjusts the clipping algorithm accordingly. Thus, pixels where the derivative is low (in the field) are clipped more aggressively than are pixels where the spatial derivative is high (point sources). This avoids downward biasing of point source fluxes in the output mosaics. The mosaics were resampled to $0''.84$ per pixel, so each pixel in the final mosaic subtends half the solid angle of the native IRAC pixels.

---

[14] http://ned.ipac.caltech.edu/

Photometry was carried out with SExtractor (ver. 2.5.0; Bertin & Arnouts 1996). Because our interest lies in global photometry and in particular in ensuring accurate global SEDs, we first registered all IRAC and *GALEX* mosaics (for which *GALEX* data were available; Sec. 3.7) to a common spatial scale using SWarp (version 2.17.1) and then applied SExtractor in two-image mode to photometer the galaxies. In two-image mode, SExtractor performs detection and characterization of the surface brightness distribution in one image and applies that surface brightness distribution to a second image. This was necessary because the infrared and ultraviolet mosaics in many instances have significant morphological differences; two-image mode prevents this fact from biasing the global color measurements. We used the IRAC $3.6\,\mu$m mosaic — the best tracer of the stellar light distribution — as the detection image and photometered the *GALEX* and IRAC mosaics using the surface brightness distribution at $3.6\,\mu$m to define the apertures. In a few cases where UV-bright features dominate, it was necessary to use the *GALEX* NUV image as the detection image in order to ensure that the SExtractor captures all the light in all six *GALEX* and IRAC bands. The IRAC photometry appears in Table 4.

3.3. *Radio Continuum Flux Densities*

Most of the radio observations come from the NVSS, a snapshot survey of 82% of the celestial sphere at 1.4 GHz (Condon et al. 1998). The survey's key features are that it used VLA D-array, and the images were cleaned and restored with a $45''$ beam (Condon et al. 1998). Typical rms brightness fluctuations in the survey are $0.45\,\mathrm{mJy\,beam^{-1}}$, and the survey catalog reaches the 50% completeness level at $S = 2.5\,\mathrm{mJy}$. In practice, the SFRS sources were retrieved from the online catalog[15] with a $30''$ search radius. Such queries returned results for 342 of the SFRS galaxies, all with unique matches. Figure 6 of Condon et al. (1998) shows a 1% chance of finding a spurious match within this distance of an arbitrary position. Ten additional matches, two of them double, were found in a search radius of $60''$, and two additional matches were found with a $90''$ search. The probability of spurious matches at these distances is 5–10%, but such large position errors are highly unlikely for correct matches unless the source itself is very extended.

Condon et al. (2002) gave flux densities based on NVSS data for 192 of the SFRS galaxies. In all but 14 cases, the flux densities are essentially identical to the ones from the automated lookup. For the 14 discrepant cases and also for all cases where the NVSS position differed from the adopted galaxy position by more than $10''$, we examined the NVSS images[16] together with the *IRAS* and IRAC infrared images. Most of the discrepancies were caused by blends of two radio sources, one of them being the SFRS galaxy and the second a nearby galaxy or QSO. This cause (blended sources) was found to explain discrepancies both in total measured flux and for discrepancies in the reported coordinates. In about half of the cases, the blended source was identifiable on the IRAC image or in NED. Most of the time, the *IRAS* (*i.e.*, SFRS) source was attributable to a single galaxy, but in some cases two galaxies are likely to contribute. The radio blends were deconvolved using IMFIT in the Common Astronomy Software Applications (CASA) package[17], in each case with the minimal set of free parameters that led to a satisfactory fit[18]. Another cause of discrepancy was extended radio sources. The NVSS catalog fit Gaussians to all sources, but in some cases this is not an accurate description of the galaxy. In these cases, the radio flux was measured in a circular, rectangular, or polygonal beam as appropriate for the particular galaxy. In general, our results agree with those of Condon et al. (2002) but differ slightly because we took into account information from the *IRAS* images in determining how to fit the radio sources.

A final 16 SFRS sources either were not detected in the NVSS or had very low signal to noise. These were observed with the VLA in D configuration in 2008 July (program AA 319).[19] The observations used the same observing frequencies and bandwidth as those of the NVSS but were $\geq$7 minutes long as opposed to 30 s for the NVSS in the relevant declination bands. Data reduction was with CASA and followed the NVSS procedure in using superuniform weighting with `npix`= 5. The reductions differed in using $7\overset{''}{.}5$ pixels and a restoring beam set by the actual baselines and weightings of each observation; typical beams were $30''\times40''$. The two frequencies observed were imaged and cleaned separately and the resulting images averaged; the separate images were also inspected and source flux densities measured on each of them as well as on the combined image. This was especially important for three galaxies with bright radio sources (M87, 3C 273) in the outer part of the VLA primary beam. Flux densities were measured via Gaussian fitting (CASA IMFIT), by adding up pixels in rectangular areas, or where needed by deconvolution as discussed above. In many cases, the limiting noise source is sidelobes from strong, imperfectly cleaned sources in the field. The tabulated uncertainties are our best estimate taking these into account, especially by comparison of the images at the two frequencies and of different methods of measuring flux density.

All the radio flux densities are given in Table 5. Uncertainties are higher for sources marked as "extended" because the peak surface brightness is the best-measured parameter, and uncertainty in the source size contributes to the uncertainty in flux density. Unrecognized blends may give spuriously high flux densities, but this is likely to be the case for only a very few objects.

3.4. *MIPS 24 μm Photometry*

Many SFRS galaxies are not well-detected by *IRAS* at 12 and $25\,\mu$m, leaving an obvious gap in the suite of useful SFR estimators (*e.g.*, Calzetti et al. 2010). To fill this gap we photometered all available archival *Spitzer*/MIPS observations (Rieke et al. 2004) and were awarded time to observe the remainder of the sample via our own observing program (PID 50132, PI Fazio).

---

[15] http://www.cv.nrao.edu/nvss/NVSSlist.shtml, lookup done in 2010 in catalog dated 2004

[16] http://www.cv.nrao.edu/nvss/postage.shtml

[17] http://casa.nrao.edu/index.shtml

[18] When small-diameter objects could be identified, their positions were held fixed, and objects were forced to be point sources whenever possible. Extended objects had position angles held fixed when those could be determined from visible or IR data.

[19] The AA 319 observations also included two galaxies that were in an early version of the SFRS sample but were later deleted.

Our MIPS 24 μm campaign was active from the start of 2008 November until the exhaustion of *Spitzer*'s cryogen in 2009 May. A total of 178 SFRS galaxies were observed, all of them in Phot mode. Most used a small field size, 10 s exposures per position, and 2 cycles. For six relatively large galaxies, a large field size was used to ensure a sufficiently large source-free background was present in the final mosaics to permit an accurate background subtraction. In one instance (NGC 3338), a raster map had to be used to cover the full spatial extent of the source plus the nearby field.

All PID 50132 data were reduced using standard techniques. We used object-masked median stacks of all exposures of each target to eliminate array artifacts from the enhanced basic calibrated data (eBCD) before mosaicing. All mosaics were pixellated to $2\farcs5$.

The archival observations were a heterogenous dataset employing a variety of exposure times and observing strategies. Our analysis of these 101 observations therefore began with the post-BCD data products, which retain some array-based artifacts but were nonetheless suitable for deriving global photometry. Two galaxies (NGC 4314 and 4418) exhibited saturation at their cores in the archival data, but apart from this we retrieved mosaics covering the full extent of a total of 101 of our sample galaxies. Together with the 178 objects from PID 50132, a total of roughly 3/4 of the SFRS galaxies yielded useful mosaics.

We photometered all sources identically using SExtractor, accounting for differences in pixellation by an appropriate choice of convolution kernel. Typically the sources were detected with S/N ratios of hundreds or even thousands in mosaics that were very far from being confused with unrelated background or foreground sources. Using the effective radii measured by SExtractor (`KRON_RADIUS`), we applied appropriate aperture corrections to the total fluxes following Table 4.13 of the MIPS Instrument Handbook. No special effort was made to identify and exclude foreground stars, but because of the typically very high galactic latitude of the sources this should not significantly bias the photometry.

The MIPS photometry was verified in two ways. First, all the SExtractor-generated background and object checkimages were inspected to make sure that the backgrounds were smooth on scales larger than the galaxies themselves and that SExtractor had identified all the pixels associated with a particular galaxy. Second, the results were compared to those reported for the 15 SFRS galaxies in common with the SINGS and LVLS samples (Table 6; Dale et al. 2007; Dale et al. 2009). All agree within 1σ except for NGC 5474 and NGC 4395. The measurement for NGC 5474 (0.14 Jy) is 1.7σ lower than the SINGS measurement (0.18 Jy). Among 15 independent measurements, a single discrepancy at the 1-2σ level is acceptable agreement. NGC 4395 is arguably a different case because the photometry is discrepant at the 3σ level. This galaxy is unusually extended with a particularly uneven surface brightness profile. The failure of the curve-of-growth to converge on a single level strongly suggested the MIPS photometry for NGC 4395 was biased low. For this single object the Dale et al. (2009) measurement was therefore adopted in preference to our own measurement.

The final aperture-corrected global MIPS 24 μm photometry is given in Table 7. The corresponding aperture corrections are given in Table 8. Because the detections have such high S/N ratios, the random (measurement) uncertainty is dominated by the systematic uncertainty in the absolute calibration of MIPS. According to the MIPS Instrument Handbook this uncertainty is between 4 and 8 percent; we therefore adopt 8% uncertainty as the most conservative estimate of the true error in all the MIPS photometry. For reasons having to do purely with scheduling, the galaxies lacking MIPS 24 μm photometry tend to be those at lower Right Ascensions; eventually this lack will be corrected using photometry from the WISE mission.

3.5. *Far-Infrared Photometry from Planck*

Planck (Planck Collaboration 2011a) is a space-based mission now carrying out an all-sky survey in six bands from 25–1000 GHz with a spatial resolution that progresses from $\sim 30'$ to $5'$ depending on the band. Although its main mission is to measure spatial anisotropies in the Cosmic Microwave Background, in the course of its repeated surveys of the sky it has detected thousands of foreground sources. The 1700+ detections resulting from the first pass through the sky are tabulated in the *Planck* Early Release Compact Source Catalog (Planck Collaboration 2011b). Because the SFRS galaxies are bright, a significant number are detected by *Planck*: 176, 78, and 28 are detected by *Planck's* High-Frequency Instrument (Lamarre et al. 2010) at 350, 550, and 850 μm, respectively. This far-infrared photometry provides new and valuable constraints on the cold dust content of the detected SFRS galaxies, *e.g.*, Planck Collaboration (2011c) found evidence for cold ($T < 20\,K$) dust in their analysis of combined *IRAS*+*Planck* SEDs. The relevant photometry is presented in Table 7. No doubt the SFRS detection fraction will increase as *Planck* accumulates more complete passes over the sky and reaches correspondingly fainter flux limits.

3.6. *Visible and Near-Infrared Observations*

The visible photometry was taken from the data release 7 of the Sloan digital sky survey (SDSS; Abazajian et al. 2009). The SDSS consists of an imaging survey of π steradians, mainly in the northern sky, in five passbands u, g, r, i, and z. The imaging was done in drift-scan mode, and the data were processed using the photometric pipeline PHOTO (Lupton et al. 2001) specially written for SDSS. All SFRS galaxies have photometry available in the five SDSS bands, although in six cases the cataloged values greatly understate the true values because they pertain only to the galaxy nuclei instead of the entire galaxy. We used the Petrosian magnitudes as the best measure of the total flux in the five SDSS bands (Blanton et al. 2001). The Petrosian magnitudes were calculated using the aperture set by the 'Petrosian radius' in the r-band, thus providing consistent measurements. SDSS Petrosian magnitudes should recover all the flux for an exponential galaxy profile independent of the axis ratio (Blanton et al. 2001) and about 80% of the flux for a de Vaucouleurs profile.

SDSS also acquired nuclear spectra for 210 SFRS galaxies. The spectra were obtained using two fiberfed double spectrographs covering a wavelength range of 3800–9200 Å. The resolution $\lambda/\Delta\lambda$ varies between 1850 and 2200. The SDSS fibers have a diameter of $3''$.

Near-infrared photometry was taken from the 2MASS extended source catalog. Although isophotal magnitudes had been used for the initial SFRS sample selection, total magnitudes were extracted from the 2MASS database for greater consistency with the global photometry measured in the other bands. 2MASS extrapolated total magnitudes are typically ~ 0.3 mag brighter than isophotal magnitudes. Typical measurement uncertainties are given as 0.03, 0.04, and 0.05 mag at J, H, and K_s, respectively. Sec. 4.3.2 discusses the *systematic* biases in the 2MASS photometry.

The SDSS and 2MASS photometry is presented in Table 9.

3.7. *GALEX Photometry in the Near- and Far-Ultraviolet Bands*

GALEX (Martin et al. 2005) is an astronomical satellite with sensitive wide-field ultraviolet imaging capability in two bands, the FUV (1350–1750Å) and NUV (1750–2800Å). The *GALEX* archive (release GR6) contains scientifically usable imaging (covering the full extent of our sources and therefore capable of yielding global flux measurements) in at least one of the *GALEX* bands for 332/369 SFRS galaxies, or 90% of the sample. The fraction observed by *GALEX* in the NUV will increase as the survey portion of the mission continues, although FUV imaging is no longer possible.

Almost three-quarters of these imaging data in both wavebands were taken as part of *GALEX*'s primary surveys[20] – the all sky survey (AIS) with an effective exposure time of ~ 0.1 ks and the relatively deep nearby galaxy survey (NGS) with an effective exposure time of ~ 1.5 ks. With a resolution of $4'' - 6''$, *GALEX* images have lower spatial resolution than *Spitzer*/IRAC. However, since almost a third of the SFRS galaxies lie $<$ 40 Mpc away, together with a 1.25 degree *GALEX* field of view, the moderate *GALEX* spatial resolution nonetheless allows for robust measures of spatially-integrated fluxes and color which are comparable to data at other wavelengths. The *GALEX* observations and an analysis of the UV properties of the SFRS galaxies are described by S. Mahajan et al. (2012, in preparation; hereafter Paper 2).

3.8. *Hα Imaging from the National Astronomical Observatory of China*

In the spring of both 2008 and 2009, Hα imaging was acquired for SFRS sample galaxies from the NAOC 2.16 m telescope in Xinlong, Hebei Province, China. The Beijing Faint Object Spectrograph and Camera (BFOSC) was used to obtain on-source integrations lasting between 1800 and 3600 s for each galaxy observed. The choice of exposure time was made based on prevailing conditions; longer exposures were used during bright-sky time or for relatively faint targets. The $10'\times10'.5$ BFOSC field of view illuminates a single CCD with 2048×2080 pixels. Each pixel subtends roughly $0''.3$, well below the typical seeing during our campaign ($2''.0 - 2''.5$). This spatial resolution is reasonably well-matched to the FWHM intrinsic to IRAC ($1''.66$ – $1''.98$). The BFOSC is equipped with a suite of 11 narrow Hα filters centered at wavelengths ranging from 6563 Å to 7060 Å at 50 Å intervals. The filter bandpasses are 70 Å wide. In the two observing campaigns carried out to date, a total of 105 SFRS galaxies were observed through one of these narrow-band Hα filters, the specific filter being chosen to cover the Hα+[NII] complex at the target's redshift. Observations were also made of each galaxy through the standard Johnson R band filter but with shorter exposure times (400 – 600 s) in order to measure the continuum flux.

The BFOSC data were reduced in the usual way. The lowest 32 rows of pixels were used for overscan correction. Standard IRAF tasks were used to subtract bias frames, construct and apply flatfields, coadd frames while simultaneously correcting for cosmic rays and known bad pixels using outlier rejection, and finally to photometer each of the 105 observed sources in both Hα and R. This work was carried out at the Chinese Academy of Sciences in Beijing. The quality of the final Hα mosaics is indicated by Fig. 6, which shows the outcome for UGC 8058, a typical case.

Figure 7 shows the relationship between the SFRs derived independently in Hα and the far-infrared for the 40 SFRS galaxies fully processed so far. The SFR estimates were made following the methods applied by Kewley et al. (2002) to 81 'pure' starburst galaxies in the Nearby Field Galaxy Survey (hereafter NFGS). Specifically, we estimated the Hα-based SFR as $\mathrm{SFR(H\alpha)} = 7.9 \times 10^{-42} L(\mathrm{H}\alpha)$ and the far-infrared SFR as $\mathrm{SFR(FIR)} = 4.5 \times 10^{-44} L(TIR)$ (Kennicutt 1998), where we have estimated the total far-infrared luminosity $L(TIR)$ as described in Sec. 4.2.

Kewley et al. (2002) demonstrated that for 81 NFGS galaxies selected at visible wavelengths to cover a range of luminosities, SFR(Hα) is discrepant with SFR(IR) in the sense that SFR(Hα) tends to be significantly lower than SFR(IR). The discrepancy was measured to be a factor of nearly three (2.7±0.3) and was shown to increase with increasing SFR. Both of those findings apply also to the SFRS galaxies shown in Fig. 7, but more so: as shown subsequently, the infrared-selected SFRS galaxies require a significantly larger mean reddening correction than did the NFGS galaxies to bring the Hα and far-infrared SFR indicators into agreement.

Most of the galaxies shown in Fig. 7 have *GALEX* photometry available. For all such objects an extinction correction $A_{H\alpha}$ appropriate for Hα was estimated based on the NUV photometry in Paper 2, which implemented the empirical IRX-based prescription following Eq. 1 of Buat et al. (2005). That estimate for A_{NUV} was then converted into an Hα extinction estimate $A_{H\alpha}$ assuming a Calzetti (2001) dust law: $A_{H\alpha} = 0.79(A_V + A_{MW}) = 0.79(0.77 \times A_{NUV} + A_{MW})$ where A_{MW} is the foreground extinction due to the Milky Way. Following this prescription the mean $\mathrm{A}_{H\alpha}$ was found to be 1.7 mag, corresponding to attenuation by a factor of 4.7. This likely reflects the fact that our sample is (primarily) infrared-selected, unlike the NFGS. A similar effect is seen for ultraviolet selection (Buat et al. 2005). Intriguingly, four galax-

---

[20] `http://galexgi.gsfc.nasa.gov/docs/galex/Documents/ERO_data_description_2.htm`

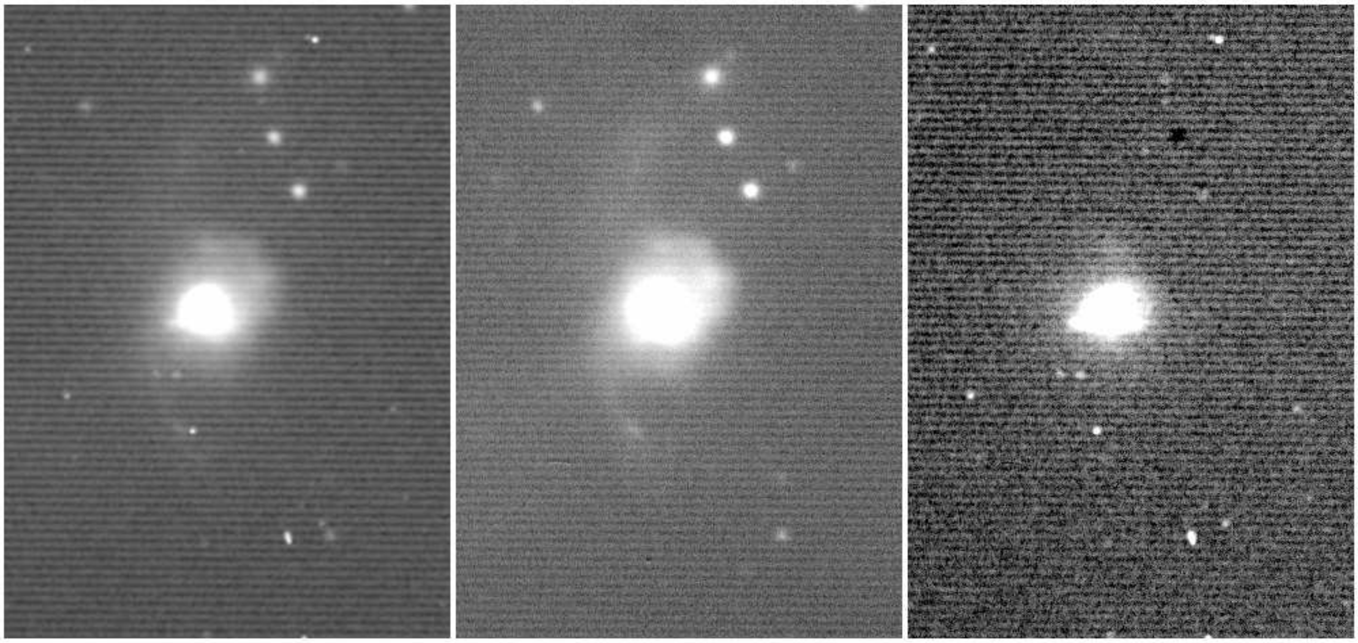

FIG. 6.— A typical example of the narrowband Hα imaging being collected for the SFRS sample; the images shown here are for UGC 8058. *Left panel:* the narrowband Hα emission-line image obtained at the NOAC. *Center panel:* the same field, seen in the continuum at *R*. *Right panel:* a difference image formed by subtracting the continuum image from the narrowband image, revealing the regions in which significant star formation is traced by the Hα emission.

ies (out of 34 with extinction estimates) lie more than an order of magnitude from the line of equality even when extinction-corrected. This suggests that for a minority of infrared-selected galaxies, either the intrinsic Hα emission does not accurately reflect the 'true' SFR. Alternately, the standard extinction corrections may not work well for such objects, as has been found for galaxies with large SFR(IR)/SFR(UV) ratios (Wuyts et al. 2011). The reason will remain unclear pending acquisition and analysis of Hα emission line intensities for the full SFRS. This will be possible as soon as the NAOC Hα imaging campaign is completed. In the summer of 2010 the BFOSC was upgraded with a new CCD having lower read noise. A subset of our team (led by H. Wu) has been awarded time in the 2011 observing season to complete the imaging campaign for the roughly two-thirds of the SFRS for which Hα imaging has not yet been obtained.

We have also begun a longslit spectroscopic campaign (Sec. 4.3.1) to obtain dust reddening estimates for all SFRS galaxies via the Balmer decrement and thereby address the possibility that A_{NUV} may not be the most reliable extinction indicator at visible wavelengths (Bell 2003). A detailed analysis of the global Hα emission line flux measurements for the full sample will be presented in a forthcoming paper (Y.-N. Zhu et al. 2012, in preparation).

4. DISCUSSION

4.1. *SFRS Compared to Other Nearby Galaxy Samples*

A number of recent survey programs have documented important aspects of star formation phenomenology. In addition to the studies mentioned above (SINGS, LVLS, and MESS), there are the NFGS (Kewley et al. 2002) and the Herschel Reference Survey (Boselli et al. 2010). The SFRS differs from these other efforts in significant ways.

SINGS is fundamentally different than SFRS because SINGS is comprised of a relatively small number (75) of very nearby, extended objects. SINGS therefore allows spatially-resolved measurements in numerous wavebands (Dale et al. 2007), but the SINGS galaxies sample primarily the low-luminosity end of the far-infrared luminosity function. This means SINGS isn't representative of star formation generally. Only five SINGS galaxies are present in the SFRS (Table 6).

The distinction between the LVLS and SFRS is less obvious because of the two-tiered optical+volume-limited

TABLE 6
GALAXIES IN COMMON WITH OTHER SURVEYS

Spitzer Infrared Nearby Galaxy Survey (SINGS)		
NGC 3049	NGC 3265	NGC 5474
NGC 3190	NGC 3773	
Local Volume Legacy Survey (LVLS)		
NGC 2500	NGC 4020	NGC 5474
NGC 2537	NGC 4244	NGC 5585
NGC 2552	NGC 4395	
NGC 3274	NGC 5204	
Herschel Reference Survey (HR)		
NGC 3245	NGC 4237	NGC 4548
NGC 3338	NGC 4294	NGC 4592
NGC 3370	NGC 4396	NGC 4607
NGC 3430	NGC 4412	NGC 4630
NGC 3659	NGC 4420	NGC 4689
NGC 3666	NGC 4424	NGC 4688
NGC 3686	NGC 4435	NGC 4701
NGC 3729	NGC 4438	NGC 4747
NGC 4116	NGC 4470	UGC 8041
NGC 4178	NGC 4491	NGC 5014
NGC 4207	NGC 4519	NGC 5303

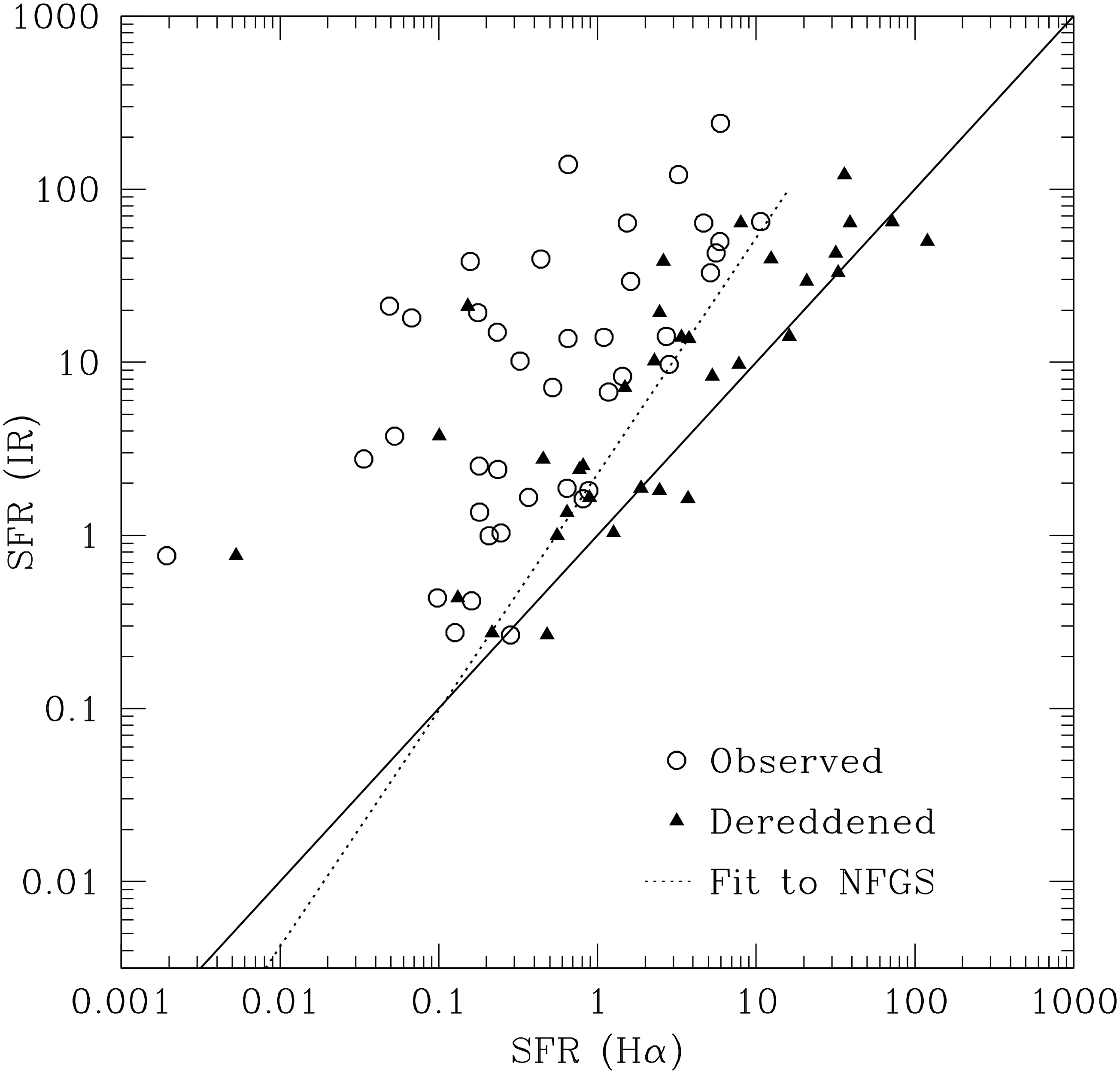

Fig. 7.— A comparison of far-infrared and Hα SFRs for an unrepresentative subset of the SFRS, following Fig. 1 of Kewley et al. (2002). Circles denote galaxies when SFR(Hα) is not correct for extinction due to dust. Solid triangles show the revised (larger) SFR(Hα) estimates that result when the extinction estimates from Paper 2 are applied. The solid line indicates where the points would fall if the Kennicutt (1998) relations were in agreement. The dashed line indicates the Kewley et al. (2002) fit to the corresponding data for the NFGS, not extinction-corrected.

nature of the selection used for the LVLS. The fundamental difference is that the LVLS is mostly comprised of low-luminosity dwarf galaxies, well below the break in the far-infrared luminosity function at $L_{FIR} = 10^{10.25}\,L_\odot$. Even so, the overlap between the LVLS and the SFRS samples is surprisingly small — only 10 objects (Table 6).

The MESS sample relies on a SDSS Hα emission-line strength selection criterion to define a sample of 138 IR-luminous galaxies that are very rapidly forming stars. MESS galaxy SFRs range from 11 to $61\,M_\odot\,yr^{-1}$. Because it uses a single selection criterion, MESS does not control for ISM temperature or stellar mass and so cannot be representative of even high-intensity star formation generally. Furthermore, Hα fluxes systematically understate total SFRs compared to the far-infrared unless relatively large and uncertain extinction corrections are made, and MESS selects against star-forming galaxiess with large extinction. By design, MESS samples only galaxies with large SFRs.

GOALS (Armus et al. 2009) is more akin to the SFRS because it relies on a restricted $60\,\mu$m brightness selection to construct the sample. All of the more than 200 GOALS galaxies are likewise bright, nearby objects for which an impressive range of multiband data have been made available, particularly HST and CXO imaging. But by design, GOALS selects for Luminous InfraRed Galaxies (LIRGs, galaxies with $L > 10^{11}\,\mathrm{L}_\odot$). The AGN fraction is significantly higher for high-luminosity galaxies. Indeed, it is a feature of the GOALS sample that it contains the full range of optical spectral types including many dominant AGNs as well as major-merger systems. While SFRS galaxies are by no means entirely free of AGN contributions (Sec. 4.2), they are a relatively minor contributor, and the fact that the SFRS spans the full range of both far-infrared color and luminosity simultaneously makes the SFRS less biased in characterizing star formation than GOALS.

The Herschel Reference Survey (Boselli et al. 2010) contains nearly as many galaxies as the SFRS (323 vs. 369) but does not capture the full range of star forming behavior because it is explicitly oriented toward high-density environments. Consequently, it contains a much larger fraction of elliptical galaxies (65/323) residing in Virgo and other major clusters. The *IRAS* 60 μm detection fraction is about 3/4, primarily because of a low detection fraction for HRS ellipticals. HRS contains 33 galaxies in common with the SFRS (Table 6), an overlap of about 10%. Most important, HRS approximates two morphology-based volume-limited surveys, together spanning 'only' three decades in 60 micron luminosity. HRS has or soon will have a comprehensive suite of *Herschel* far-IR photometry available, but its selection makes it optimized for the study of how environment affects dust content rather than as an unbiased study of star formation.

4.2. *AGN Content*

The SFRS does not discriminate for AGN activity. For this reason it should be an excellent means of estimating AGN prevalence generally as well as the relative importance of AGNs for the overall energy budget of any far-IR-selected sample, at least in the local Universe. Our ongoing campaign (Sec. 4.3.1) to acquire longslit spectra for all SFRS galaxies with the FAst Spectrograph for the Tillinghast Telescope (FAST; Fabricant et al. 1998) will eventually permit AGN detection to very faint levels via resolved emission line intensity ratios (*e.g.*, Kewley et al. 2006). But even though the faint AGNs will be out of reach or a time, it is nonetheless possible to identify the relatively luminous AGNs immediately via their global infrared colors, and to exploit the spectroscopy that does exist to arrive at a preliminary estimate of AGN prevalence.

The most sensitive method for identifying AGNs is probably the BPT diagram (Baldwin, Phillips, & Terlevich 1981; Kewley et al. 2001), an emission-line intensity ratio diagnostic that identifies AGNs via species that trace high-excitation conditions. Because it relies on visible lines, the BPT method will not find highly-obscured AGNs, but it can identify so-called 'transition' sources in which the contributions of star-forming activity and a central AGN are comparable. Figure 8 shows this method applied to a subsample of SFRS galaxies, *i.e.*, all 165 objects for which the set of four necessary emission line intensities have been measured by SDSS. Of these 165 sources, 30 are identified as AGNs according to the Kewley et al. line-ratio criterion. Another 45 objects were observed spectroscopically by SDSS but do not exhibit the emission lines linked with AGNs. These 45 galaxies are unlikely to host strong AGNs. Thus the AGN fraction identified by the BPT diagram is roughly 1/7.

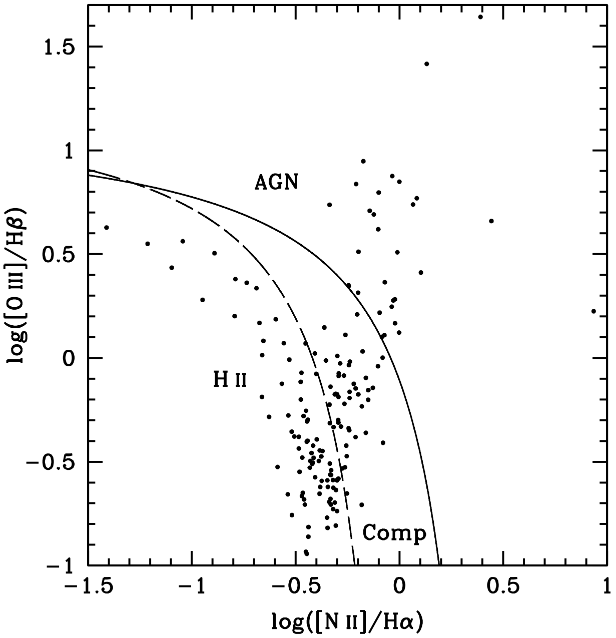

FIG. 8.— Line ratios from SDSS fiber spectra for 165 SFRS galaxies. Galaxies above the solid line are considered AGNs (Kewley et al. 2001), and those below the dashed line are considered purely star forming (Kauffmann et al. 2003), with emission-line intensity ratios closely matching those seen in HII regions. Those between the two lines are composite or transitional.

Figure 9 shows the IRAC color-color plot first used by Stern et al. (2005) to empirically discriminate galaxies with infrared SEDs dominated by active nuclei from those dominated by star formation. It identifies 19 of the 369 SFRS galaxies (∼5%) as AGNs according to the empirical Stern et al. criteria. For these sources, emission from an active nucleus is a significant or even dominant contributor to the mid-IR SED. Moreover, some of the 18 galaxies outside the Stern et al. "wedge" but having redder $[3.6] - [4.5]$ colors than the main group probably also contain AGNs. The most extreme such outliers are UGC 9560 (=II Zw 70) and UGC 5613, which have very different luminosities but are both strongly star-forming (Oconnell, Thuan, & Goldstein 1978; Poggianti & Wu 2000). An outlier with much smaller $[5.8] - [8.0]$ color is IC 486 (=UGC 4155), which is a Sey 1 (Bonatto & Pastoriza 1997). The outliers are thus a mixed group.

A third method to identify AGNs is based on the 25 μm (or 24 μm) flux density (Sanders et al. 1988), specifically $F_{25}/F_{60} > 0.2$. Despite their large 60 μm fluxes, many SFRS galaxies are not reliably detected by *IRAS* in the 25 μm band. We therefore used MIPS 24 μm flux measurements, where available, to form the flux density ratio F_{24}/F_{60}, because MIPS 24 μm fluxes track *IRAS* 25 μm fluxes very closely on average (Dale et al. 2009). The distribution of the 313 SFRS galaxies with such data is shown in Figure 10. The distribution is qualitatively similar to that of the Revised Bright Galaxy Survey (Sanders et al. 2003). Only a small minority of the sources (22/313, or about 7%) lie at $F_{24}/F_{60} > 0.2$,

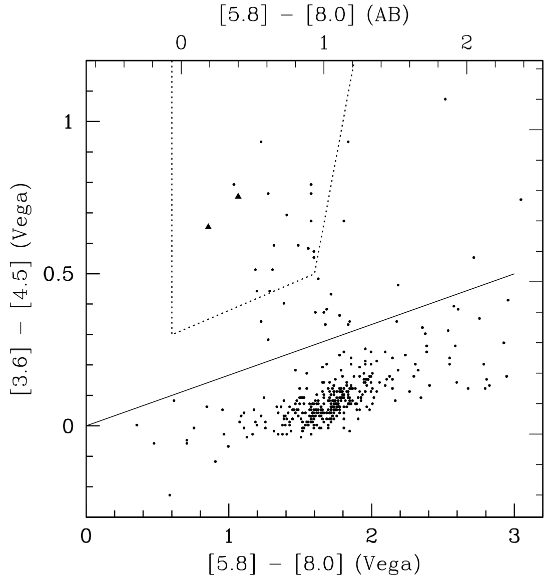

FIG. 9.— IRAC colors of SFRS galaxies. Colors are shown in both Vega and AB magnitudes on opposite axes. The solid triangles denote 3C 273 and OJ 287. The dotted line encompasses the empirically-determined region within which galaxy colors indicate the presence of an AGN (Stern et al. 2005). The solid line indicates the division between normal galaxies and outliers, which probably represent a mix of AGNs and strongly star-forming systems.

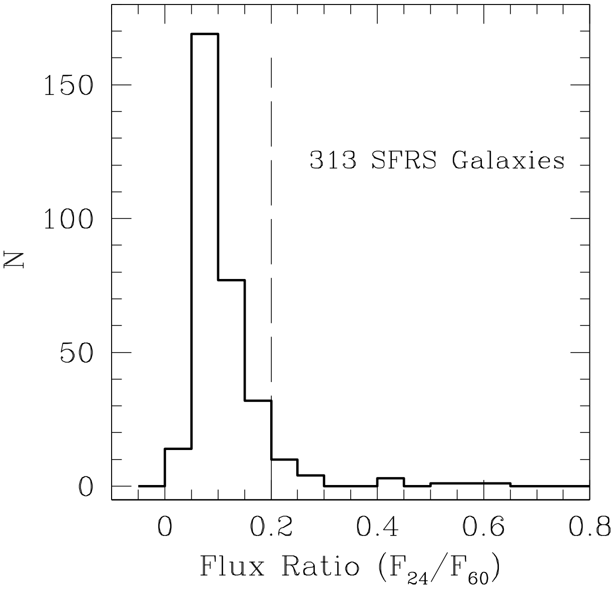

FIG. 10.— The distribution of the ratio F_{24}/F_{60} for 313 SFRS galaxies for which MIPS 24 μm fluxes (or their *IRAS* 25 μm equivalents) are available. The vertical line marks the value above which Sanders et al. (1988) suggest that a relatively large mid-infrared flux indicates that an AGN contributes to the SED. Out of 313 SFRS galaxies 22 meet this criterion. They are listed in Table 10.

which Sanders et al. (1988) identify as potentially arising from a significant contribution coming from an active nucleus. Most of the galaxies identified as AGNs in this way are also identified by one of the other two methods (Table 10).

No matter how they are identified, the AGNs in the SFRS do not have a noticeably different F_{60}/F_{100} ratio than the non-AGNs. Figure 11 is a far-infrared color-color diagram showing the 313 SFRS galaxies with either *IRAS* 25 μm or MIPS 24 μm flux measurements, including the 22 objects identified as AGNs by the Sanders et al. (1988) criterion. This suggests that for most galaxies in the sample, AGNs contribute relatively little of the far-infrared light. Conversely, the far-infrared emission is an uncontaminated tracer of star formation. This result is consistent with Mullaney et al. (2011), who found that the SEDs of AGNs drop rapidly at wavelengths longer than 40 μm. It is also consistent with the outcome of Netzer et al. (2007), who found that the far-infrared properties of QSOs is almost entirely due to star formation. This view is confirmed by an examination of the FIR-radio correlation (*e.g.*, Condon et al. 1992, Helou et al. 1985), the fact that the non-thermal radio emission and the thermal far-infrared emission correlate tightly over at least four orders of magnitude in far-infrared luminosity. Fig. 12 shows the FIR-radio correlation constructed using *total* infrared flux estimates $F(TIR) = 2.403\nu f_\nu(25\,\mu\mathrm{m}) - 0.2454\nu f_\nu(60\,\mu\mathrm{m}) + 1.347\nu f_\nu(100\,\mu\mathrm{m})$ in the usual way (Dale & Helou 2002) except that we employ MIPS 24 μm fluxes where available instead of the less precise *IRAS* 25 μm fluxes. The solid line in the lower panel of Fig. 12 is an unweighted least-squares fit to all SFRS galaxies (except 3C 273 and OJ 287, which have extremely high radio continuum luminosities arising from dominant central AGNs). If all galaxies flagged as hosting AGNs by at least one of the three criteria above are excluded from the fit, the slope changes very little (to 1.09 from 1.086) and the scatter about the fit does likewise (decreasing to 0.29 dex from 0.31 dex). Thus, if the two dominant AGNs are excluded from the fit, the FIR-radio correlation is not significantly affected by the presence of AGNs in 52/367 (roughly one of every seven galaxies). This underlines the utility of the thermal far-IR as an optimal probe of SFR.

The FIR-radio correlation obtained for the SFRS sample is higher than unity but nonetheless shallower than reported by Devereux & Eales (1989), roughly 1.1 instead of 1.28. This could be due to selection effects: Devereux & Eales (1989) employed an optical selection that sampled luminosities only up to $\sim 10^{11}\,\mathrm{L}_\odot$. Yun, Reddy, & Condon (2001) find a slope much closer to unity for their sample of bright infrared-selected galaxies, a result later confirmed by Bell (2003).

In summary, the three different AGN detection criteria identify three different AGN subsamples comprising from 5 to 10% of the SFRS study sample. There is only modest overlap among the three criteria (Table 10), which in hindsight validates the use of multiple tracers of AGN activity. AGNs are more prevalent at higher luminosities, despite the fact that they contribute little to the total far-infrared luminosities of star-forming galaxies. AGNs were detected in ~15% of the sample (52/369 galaxies) when all three detection methods were combined. Taken

TABLE 10
AGN Detections

Number	Name	Detection Method		
		Emission Lines	F_{24}/F_{60}	3.6–8.0 μm Colors
1	IC 486	Y	Y	...
7	IRAS 08072+1847	...	Y	...
30	OJ 287	Y	Y	Y
32	IRAS 08550+3908	Y	...	-
36	IRAS 08572+3915SW	...	...	Y
55	NGC 2893	...	Y	-
57	CGCG 238-066	Y	Y	-
64	CGCG 182-010	...	Y	-
76	IC 2551	...	Y	-
79	IRAS 10120+1653	Y	...	...
91	UGC 5713	...	Y	Y
100	UGC 5881	Y	...	...
107	CGCG 95-055	Y	...	...
109	UGC 6074	...	Y	...
118	IC 2637	Y	...	...
121	IRAS 11167+5351	...	...	Y
122	NGC 3633	...	Y	...
139	NGC 3758	...	...	Y
169	UGC 7016	Y	...	...
189	NGC 4253	...	Y	Y
194	NGC 4385	...	Y	...
198	NGC 4418	...	Y	Y
204	3C 273	...	Y	Y
233	MCG 8-23-097	Y	...	...
239	UGC 8058	...	Y	Y
244	NGC 4922	...	...	Y
248	UGC 8269	Y	...	...
253	IRAS 13144+4508	Y	Y	...
259	NGC 5104	Y	...	...
263	IRAS 13218+0552	...	...	Y
270	IRAS 13349+2438	...	Y	...
276	MK 268	Y	...	Y
277	NGC 5278	Y	...	...
278	NGC 5273	Y	...	...
281	UGC 8696	Y	...	Y
283	MK 796	...	...	Y
284	IRAS 13446+1121	Y	...	Y
286	NGC 5313	Y	...	...
288	NGC 5347	Y	Y	-
292	UGC 8850	...	Y	Y
296	NGC 5403	Y	...	...
303	CGCG 074-129	Y	Y	Y
309	IC 4395	Y	...	-
322	UGC 9412	...	Y	Y
329	IRAS 14538+1730	Y	...	...
332	UGC 9639	Y	...	...
339	IC 4553	Y	...	-
341	IC 4567	Y	...	...
343	NGC 5975	Y	...	...
350	UGC 10120	...	Y	Y
352	NGC 6040	Y	...	...
358	IRAS 16150+2233	Y	...	...
	Total	30	22	19
	Total AGNs (all methods)		52	

as a whole, these results suggest that the far-infrared selection described above (Sec 2) has successfully yielded a sample with bolometric luminosities dominated by star formation, and there is no compelling evidence that the AGNs significantly contaminate the far-infrared SEDS.

4.3. *Pending Observing Campaigns*

There are several ongoing observing campaigns for which significant data have been acquired but which are not yet complete. They are described below.

4.3.1. *Longslit Optical Spectroscopy with FAST*

Visible spectra from SDSS are available only for a fraction of the SFRS galaxies (Abazajian et al. 2009). Moreover, the SDSS spectra were obtained through fibers centered on the nuclei and so do not uniformly measure or constrain the excitation conditions within the galaxy disks. We are therefore reobserving SDSS galaxies with a long-slit spectrograph in order to: 1.) build a consistent set of disk+nuclear spectra with better sky subtraction, 2.) take advantage of the spatial dimension to implement accurate starlight subtraction, and 3.) measure rotation curves.

The observations are currently being carried out at the Fred Lawrence Whipple Observatory 1.5 m telescope at Mt. Hopkins with FAST. FAST is being used with a 2″ wide slit positioned along the major axis of the

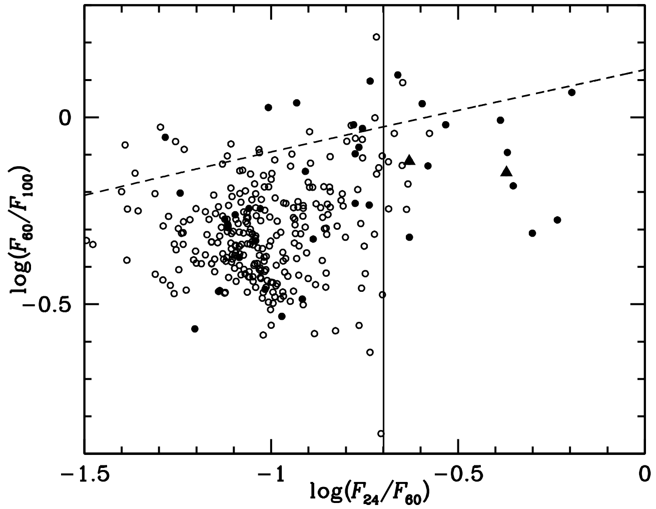

FIG. 11.— Far-infrared color-color diagram for 313 SFRS galaxies. The 24 μm flux densities come from MIPS if available or *IRAS* (25 μm) otherwise, and the 60 and 100 μm flux densities come from *IRAS*. Galaxies to the right of the vertical line meet the Sanders et al. (1988) criterion for an active nucleus that affects the far-infrared colors. The dashed line indicates the colors of isothermal dust with emissivity $\epsilon \propto \nu^{-1}$. Filled symbols indicate galaxies identified as AGN on the basis of nuclear SDSS spectra (Fig. 8) or the Stern diagram (Fig. 9). The solid triangles correspond to 3C 273 and OJ 287. The 56 SFRS galaxies having only upper limits at 25 μm are not plotted, but only 27 of them have 25 μm upper limits large enough to potentially allow them into the AGN territory.

galaxies. For galaxies which extend beyond the slit ends we obtain either a second spectrum along the minor axis of the galaxy, or a second spectrum at a sky position away from the galaxy. The spectra are obtained with a 600 l/mm grating in two tilt positions in order to cover the blue (3700 − 5700 Å) and the red (5500 − 7500 Å) part of the spectrum with resolutions of 2.2 Å and 2.7 Å respectively. Throughout the modest redshift range occupied by our sample, this setup covers the standard diagnostic emission lines in the optical band: [O II]λ3727 Å; Hβ; [O III]$\lambda\lambda$4959, 5007 Å; [O I]λ6300 Å; [N II]$\lambda\lambda$6548, 6583 Å; Hα; and [S II]$\lambda\lambda$6716, 6731 Å. The exposure time for each nucleus has been chosen in order to achieve a signal-to-noise ratio (S/N) of at least 40 at the Hα line, based on the available photometry from SDSS.

4.3.2. *PAIRITEL Near-IR Imaging*

As described in Sec. 2, 2MASS K_{20} magnitudes were used as a stellar mass proxy to define the SFRS sample because of the well-characterized and uniform data quality and the full-sky coverage. However, a campaign has been initiated to replace the 2MASS photometry with significantly deeper near-IR observations in the same three bands, because the 2MASS observations are somewhat shallow. They are not optimal for detecting the faint outskirts of even nearby galaxies, where relatively high sky backgrounds obscure the outermost, low surface-brightness features. This leads to a systematic downward bias in the 2MASS photometry that is at present not fully characterized. Kirby et al. (2008) found the discrepancy to be highly variable, ranging up to 2.5 mag in extreme cases. Karachentsev et al. (2002)

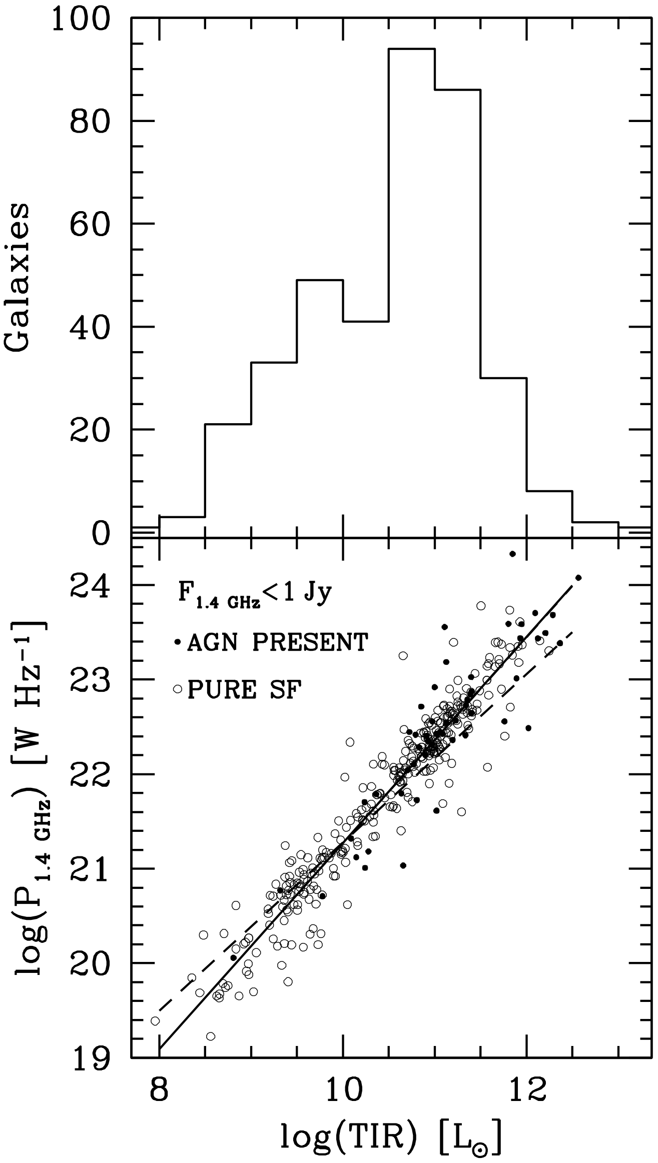

FIG. 12.— *Upper panel:* Histogram of total infrared luminosities calculated as described in the text. *Lower panel:* The FIR-radio correlation for 367 galaxies with radio continuum fluxes below 1 Jy, *i.e.*, all but the two SFRS galaxies (3C 273 and OJ 287) dominated by emission from an AGN at radio wavelengths. Open circles indicate the 52 sources (Table 10) for which at least one of the three AGN criteria described in Sec. 4.2 is met. Solid circles indicate sources not known to have any AGN contribution. The line is an unweighted least-squares fit to the entire distribution. The same fitting procedure, when performed only for the 315 'pure' star-forming galaxies, yields a correlation indistinguishable from that for all 367 galaxies on the scale of this plot. The dashed line illustrates a slope of unity.

found that the global 2MASS XSC photometry implied unphysical colors in some cases.

Deeper near-infrared observations will offer several advantages. They will greatly reduce both the measurement uncertainties and the bias in the existing photometry. They will better characterize the true extents and morphologies of the SFRS galaxies. They will also be a much better match to the existing *Spitzer*/IRAC data, which benefit from the very low backgrounds available from space. This will facilitate accurate K-corrections and stellar mass estimates planned for subsequent papers as well as reliable bulge/disk decompositions (because a greater extent and dynamic range in disk surface brightness is sampled).

Motivated by these considerations, the SFRS team sought and was awarded time for near-infrared imaging in 2009, 2010, and 2011 with the Peterson Automated Infrared Imaging Telescope (PAIRITEL; Bloom et al. 2006), the same telescope originally used for 2MASS. Useful JHK_s imaging (*i.e.*, flattened, background-subtracted, and astrometrically correct mosaics encompassing all the emission from the targets) has been acquired for 259 SFRS galaxies to date. Exposure times were typically 20 min on-source, but in some cases the exposures were shorter because of circumstances related to weather or instrumentation. The PAIRITEL observations typically reach two magnitudes deeper than 2MASS. Based on a preliminary analysis of the K_s imaging data reduced to date, it appears that the total magnitudes listed in Table 9 understate the galaxies' true output by about 0.3 mag (P. Bonfini, 2011facility, private communication). The goal is to complete the deep JHK_s coverage in the 2012a observing semester, after which the imaging and photometry will be presented together with a structural decomposition of the SFR galaxies (P. Bonfini et al., 2012, in preparation).

4.3.3. *Far-Infrared Detections by AKARI*

AKARI is a cryogenic space-based infrared telescope facility launched in 2006. Because it uses infrared detectors with pixels smaller ($0\farcm5$–$0\farcm9$; Jeong et al. 2007) than those used by *IRAS*, *AKARI* offers spatial resolution superior to that of *IRAS* despite having a primary mirror only slightly larger. For example, the Far-Infrared Surveyor (FIS) point spread functions have FWHMs ranging from $40''$ to $60''$ depending on the band (Kawada et al. 2007). *AKARI* therefore offers a way to improve upon *IRAS* photometry and likewise improve the fidelity of the far-IR SFRs inferred for our sample in cases of high foreground gradients arising from Galactic cirrus and/or confused *IRAS* sources, because *AKARI* has the potential to resolve out such contributions to the *IRAS* flux measurements.

Two all-sky surveys were carried out by the *AKARI* mission, covering >94% of the sky more than twice (Murakami et al. 2007). The central wavelengths of the six survey bands are 9 and 18 μm with the Infrared Camera (IRC; Ishihara et al. 2010) and 65, 90, 140, and 160 μm with the FIS (Kawada et al. 2007). All SFRS galaxies were detected in both the FIS and IRC all-sky surveys, which reached detection limits of 0.21 Jy at the 80% completeness level at 18 μm and a 5σ detection limit of 0.55 Jy at 90 μm. The 90 μm band is the most sensitive of the four FIS bands and covers a bandpass very similar to the *IRAS* 100 μm band. A subsequent paper (H. Kaneda et al., in preparation) is planned to refine the far-IR SFR estimates with the full suite of *AKARI* photometry.

5. CONCLUSION

The Star Formation Reference Survey, by virtue of its reliance on a restricted but representative far-IR selection, ensures the capability to study *obscured* star formation in all of its varied manifestations in the local Universe. Its panchromatic resources, spanning UV to radio wavelengths and featuring 100% complete photometry in the visible to mid-infrared regimes ($ugrizJHK_s$ and four IRAC bands) provides an opportunity to quantitatively assess the degree to which far-IR emission reflects total (not just obscured) SFR. This comprehensive collection of the most widely-used SFR indicators will furnish an invaluable resource for the interpretation of more distant galaxies, *i.e.*, galaxies for which some or even nearly all such SFR metrics are inaccessible because of their relative faintness, so that a context exists in which to better understand the limited data available. Because the SFRS is fully representative of star-forming galaxies in the local Universe, it is an optimal benchmark for understanding star formation in the distant cosmos.

The interplay of various star formation and AGN indicators will be explored in future papers. Paper 2 will examine the relationship of UV SFR indicators to those obtained in the other bands. P. Bonfini et al. (2012, in preparation) will describe the methods whereby relatively faint AGNs in the sample are identified using structural decomposition. Y.-N. Zhu et al. (2012, in preparation) will examine a suite of narrow-band Hα imaging and compare the global Hα-derived SFRs to those in the other bands compiled for the SFRS. All the related photometry will be made public to facilitate investigations by others in the community.

The authors gratefully acknowledge the assistance of R. Brent Tully, who generously supplied quality distances for many of our sample galaxies. This research has made use of the NASA/IPAC Extragalactic Database (NED) which is operated by the Jet Propulsion Laboratory, California Institute of Technology, under contract with the National Aeronautics and Space Administration. This work is based in part on observations made with the Spitzer Space Telescope, which is operated by the Jet Propulsion Laboratory, California Institute of Technology under a contract with NASA. Support for this work was provided by NASA. The National Radio Astronomy Observatory is a facility of the National Science Foundation operated under cooperative agreement by Associated Universities, Inc. H. Wu is supported by NSFC grants 10833006, 10773014, and the 973 Program grant 2007CB815406. P. Barmby acknowledges research support through a Discovery Grant from the Natural Sciences and Engineering Research Council of Canada. S. Mahajan acknowledges support from a Smithsonian Institution Endowment Grant. A. Zezas and P. Bonfini acknowledge support from Marie-Curie IRG grant 224878 and European Union grant 206469. H. Smith acknowledges partial support from NASA grants NNX07AH49G and NNX10AD83G.

Facilities: VLA, *Spitzer*(IRAC, MIPS), *GALEX*, 2MASS, SDSS, NAOC.

REFERENCES

Abazajian, K. N., et al. 2009, ApJS, 182, 543
Armus, L., et al. 2009, PASP, 121, 559

Baldwin, J. A., Phillips, M. M., & Terlevich, R. 1981, PASP, 93, 5
Bell, E. F. 2003, ApJ, 586, 794
Bertin, E., & Arnouts, S. 1996, A&AS, 117, 393
Blanton, M. R., et al. 2001, AJ, 121, 2358
Bloom, J. S., Starr, D. L., Blake, C. H., Skrutskie, M. F., & Falco, E. E. 2006, Astronomical Data Analysis Software and Systems XV, 351, 751
Bonatto, C. J., & Pastoriza, M. G. 1997, ApJ, 486, 132
Boselli, A., et al. 2010, PASP, 122, 261
Buat, V., et al. 2005, ApJ, 619, L51
Buat, V., et al. 2010, MNRAS, 409, L1
Calzetti, D., et al. 2010, ApJ, 714, 1256
Calzetti, D. 2001, PASP, 113, 1449
Condon, J. J. 1992, ARA&A, 30, 575
Condon, J. J., Cotton, W. D., Greisen, E. W., Yin, Q. F., Perley, R. A., Taylor, G. B., & Broderick, J. J. 1998, AJ, 115, 1693
Condon, J. J., Cotton, W. D., Greisen, E. W., Yin, Q. F., Perley, R. A., Taylor, G. B., & Broderick, J. J. 2002, VizieR Online Data Catalog, 8065, 0
Dale, D. A., & Helou, G. 2002, ApJ, 576, 159
Dale, D. A., et al. 2005, ApJ, 633, 857
Dale, D. A., et al. 2007, ApJ, 655, 863
Dale, D. A., et al. 2009, ApJ, 703, 517
Devereux, N. A., & Eales, S. A. 1989, ApJ, 340, 708
Elbaz, D., et al. 2011, arXiv:1105.2537
Fabricant, D., Cheimets, P., Caldwell, N., & Geary, J. 1998, PASP, 110, 79
Fazio, G. G., et al. 2004, ApJS, 154, 10
Freedman, W. L., et al. 2001, ApJ, 553, 47
Impey, C. D., & Neugebauer, G. 1988, AJ, 95, 307
Helou, G., Soifer, B. T., & Rowan-Robinson, M. 1985, ApJ, 298, L7
Hogg, D. W., Tremonti, C. A., Blanton, M. R., Finkbeiner, D. P., Padmanabhan, N., Quintero, A. D., Schlegel, D. J., & Wherry, N. 2005, ApJ, 624, 162
Hopkins, A. M., & Beacom, J. F. 2006, ApJ, 651, 142
Ishihara, D. et al. 2010, A&A, 514, A1
Jeong, W.-S., et al. 2007, PASJ, 59, 429
Jester, S. et al. 2005, AJ, 130, 873
Karachentsev, I. D., Mitronova, S. N., Karachentseva, V. E., Kudrya, Y. N., & Jarrett, T. H. 2002, A&A, 396, 431
Karachentsev, I. D., Karachentseva, V. E., Huchtmeier, W. K., & Makarov, D. I. 2004, AJ, 127, 2031
Karachentsev, I. D., Kudrya, Y. N., Karachentseva, V. E., & Mitronova, S. N. 2006, Astrophysics, 49, 450
Kartaltepe, J. S., et al. 2010, ApJ, 709, 572
Kauffmann, G., et al. 2003, MNRAS, 346, 1055
Kawada, M., et al. 2007, PASJ, 59, S389
Kennicutt, R. C., Jr. 1998, ARA&A, 36, 189
Kennicutt, R. C., Jr., et al. 2003, PASP, 115, 928
Kewley, L. J., Dopita, M. A., Sutherland, R. S., Heisler, C. A., & Trevena, J. 2001, ApJ, 556, 121
Kewley, L. J., Geller, M. J., Jansen, R. A., & Dopita, M. A. 2002, AJ, 124, 3135
Kewley, L. J., Groves, B., Kauffmann, G., & Heckman, T. 2006, MNRAS, 372, 961
Kim, D.-C., Veilleux, S., & Sanders, D. B. 2002, ApJS, 143, 277
Kirby, E. M., Jerjen, H., Ryder, S. D., & Driver, S. P. 2008, AJ, 136, 1866
Laag, E., Croft, S., Canalizo, G., & Lacy, M. 2010, arXiv:1010.1704
Lada, C. J., Lombardi, M., & Alves, J. F. 2010, arXiv:1009.2985
Lamarre, J.-M., et al. 2010, A&A, 520, A9
Lilly, S. J., Le Fevre, O., Hammer, F., & Crampton, D. 1996, ApJ, 460, L1
Lupton, R., Gunn, J. E., Ivezić, Z., Knapp, G. R., & Kent, S. 2001, Astronomical Data Analysis Software and Systems X, 238, 269
Madden, S. C., Galliano, F., Jones, A. P., & Sauvage, M. 2006, A&A, 446, 877
Madau, P., Pozzetti, L., & Dickinson, M. 1998, ApJ, 498, 106
Martin, D. C., et al. 2005, ApJ, 619, L1
Mould, J. R., et al. 2000, ApJ, 529, 786
Mullaney, J. R., Alexander, D. M., Goulding, A. D., & Hickox, R. C. 2011, MNRAS, 414, 1082
Murakami, H., et al. 2007, PASJ, 59, S369
Netzer, H., et al. 2007, ApJ, 666, 806
Oconnell, R. W., Thuan, T. X., & Goldstein, S. J. 1978, ApJ, 226, L11
Parker, N. D., 1991, MNRAS, 251, 63
Poggianti, B. M., & Wu, H. 2000, ApJ, 529, 157
Rice, W., et al. 1988, ApJS, 68, 91
Rieke, G. H., Lebofsky, M. J., Thompson, R. I., Low, F. J., & Tokunaga, A. T. 1980, ApJ, 238, 24
Rieke, G. H., et al. 2004, ApJS, 154, 25
Sanders, D. B., Soifer, B. T., Elias, J. H., Neugebauer, G., & Matthews, K. 1988, ApJ, 328, L35
Sanders, D. B., Mazzarella, J. M., Kim, D.-C., Surace, J. A., & Soifer, B. T. 2003, AJ, 126, 1607
Saunders, W., et al. 2000, MNRAS, 317, 55
Schuster, M. T., Marengo, M., & Patten, B. M. 2006, Proc. SPIE, 6270, 65
Sobral, D., Best, P. N., Smail, I., Geach, J. E., Cirasuolo, M., Garn, T., & Dalton, G. B. 2011, MNRAS, 411, 675
Stern, D., et al. 2005, ApJ, 631, 163
Planck Collaboration 2011a, arXiv:1101.2022
Planck Collaboration 2011b, The Early Release Compact Source Catalog. arXiv:1101.2041
Planck Collaboration 2011c, arXiv:1101.2045
Schmidt, M. 1959, ApJ, 129, 243
Takeuchi, T. T., Buat, V., Heinis, S., Giovannoli, E., Yuan, F.-T., Iglesias-Páramo, J., Murata, K. L., & Burgarella, D. 2010, A&A, 514, A4
Tonry, J. L., Dressler, A., Blakeslee, J. P., Ajhar, E. A., Fletcher, A. B., Luppino, G. A., Metzger, M. R., & Moore, C. B. 2001, ApJ, 546, 681
Tully, R. B., & Fisher, J. R. 1977, A&A, 54, 661
Tully, R. B., Shaya, E. J., Karachentsev, I. D., Courtois, H. M., Kocevski, D. D., Rizzi, L., & Peel, A. 2008, ApJ, 676, 184
Wu, H., Cao, C., Hao, C.-N., Liu, F.-S., Wang, J.-L., Xia, X.-Y., Deng, Z.-G., & Young, C. K.-S. 2005, ApJ, 632, L79
Wuyts, S., et al. 2011, arXiv:1106.5502
Yun, M. S., Reddy, N. A., & Condon, J. J. 2001, ApJ, 554, 803

TABLE 2
BASIC GALAXY PARAMETERS FOR SFRS SAMPLE GALAXIES

SFRS	Name	Position[a] (J2000)		Distance[b] (Mpc)	$\log L_{60}$ ($L_\odot$)	F_{100}/F_{60}	$K_s - F_{60}$ (AB mag)	Weight	Axial Ratio	T Type	Extinction (B mag)
1	IC 486	8:00:20.98	26:36:48.7	114.4	9.55	1.53	3.51	1.5	0.76	1	0.20
2	IC 2217	8:00:49.73	27:30:01.7	76.1	9.57	1.96	4.92	13.2	0.81	20	0.25
3	NGC 2500	8:01:53.18	50:44:13.7	15.0	7.93	2.05	4.03	4.2	0.86	7	0.23
4	NGC 2512	8:03:07.85	23:23:30.6	69.3	9.67	1.92	4.31	7.4	0.76	3	0.30
5	MCG 6-18-009	8:03:28.94	33:27:44.5	164.3	10.11	1.87	4.45	1.5	0.83	···	0.27
6	MK 1212	8:07:05.52	27:07:33.7	173.3	10.21	1.80	5.33	7.4	0.94	···	0.25
7	IRAS 08072+1847	8:10:15.17	33:57:23.9	70.8	9.55	1.10	6.37	8.1	0.98	···	0.23
8	NGC 2532	8:10:07.01	18:38:18.1	77.6	9.75	2.86	4.13	5.0	0.87	5	0.30
9	UGC 4261	8:10:56.21	36:49:41.3	93.2	9.45	1.28	5.39	4.3	0.71	15	0.29
10	NGC 2535	8:11:13.08	25:12:15.3	61.6	9.30	2.80	4.16	5.5	0.56	5	0.26
11	NGC 2543	8:12:57.91	36:15:16.7	26.3±5.5	9.03	2.21	3.68	12.1	0.57	3	0.31
12	NGC 2537	8:13:14.74	45:59:21.9	15.0	7.82	1.85	3.52	3.2	0.74	9	0.23
13	IC 2233	8:13:58.82	45:44:43.7	13.7±2.8	7.47	1.58	4.14	1.0	0.16	7	0.23
14	IC 2239	8:14:06.79	23:51:58.9	88.5	9.78	1.80	4.56	13.2	0.84	···	0.27
15	UGC 4286	8:14:16.50	18:26:26.0	73.5	9.10	2.08	6.48	3.0	0.41	3	0.26
16	UGC 4306	8:17:36.60	35:26:50.7	36.0	9.12	1.89	4.74	8.3	0.64	20	0.33
17	NGC 2552	8:19:19.58	50:00:20.8	11.4±0.8	7.25	2.46	6.01	1.0	0.67	9	0.21
18	IC 2339	8:23:34.20	21:20:51.5	79.3	9.43	1.75	5.63	3.0	0.52	5	0.25
19	IRAS 08234+1054B	8:26:07.90	10:44:51.3	272.6	10.61	1.75	6.61	6.6	0.58	···	0.26
20	IRAS 08269+1514	8:29:45.19	15:04:39.4	134.5	9.60	2.87	5.18	3.0	0.46	···	0.24
21	NGC 2604	8:33:23.14	29:32:19.7	36.3±4.2	8.57	2.18	4.70	4.7	0.92	6	0.26
22	NGC 2608	8:35:39.96	46:29:28.1	36.3±4.2	8.83	2.60	3.37	12.1	0.66	3	0.26
23	MK 92	8:35:17.06	28:28:30.9	68.8	9.48	1.53	5.45	4.3	0.79	···	0.17
24	NGC 2623	8:38:24.00	25:45:16.3	81.6	10.62	1.16	6.95	15.5	0.45	···	0.20
25	CGCG 120-018	8:39:50.76	23:08:36.1	107.9	9.99	1.42	5.80	8.1	0.99	···	0.18
26	NGC 2644	8:41:31.85	4:58:49.2	25.0	8.49	2.37	3.91	4.6	0.44	15	0.22
27	UGC 4572	8:45:37.85	36:56:04.7	60.5	8.95	2.07	3.69	4.3	0.88	11	0.21
28	UGC 4653	8:53:54.62	35:08:44.2	234.0	10.54	2.13	4.51	1.0	0.70	3	0.19
29	IRAS 08512+2727	8:54:16.78	27:15:59.5	265.3	10.15	2.70	4.48	1.0	0.87	···	0.23
30	OJ 287	8:54:48.86	20:06:30.7	1258.8	11.75	1.45	4.46	1.0	1.00	···	0.13
31	IRAS 08538+4256	8:57:10.32	42:45:23.1	121.2	10.27	1.38	6.36	14.2	0.88	···	0.15
32	IRAS 08550+3908	8:58:13.75	38:56:31.9	367.8	10.72	1.25	5.19	1.5	0.55	···	0.14
33	NGC 2718	8:58:50.47	6:17:34.8	57.4	9.50	1.74	4.13	9.5	0.85	2	0.31
34	NGC 2712	8:59:30.48	44:54:50.0	30.9±6.4	8.72	2.42	3.08	12.1	0.54	3	0.14
35	NGC 2719	9:00:15.72	35:43:39.5	51.1	9.05	1.41	6.90	4.3	0.32	10	0.18
36	IRAS 08572+3915	9:00:25.37	39:03:53.7	244.3	11.13	0.61	8.31	15.5	0.89	···	0.14
37	IRAS 08579+3447	9:01:05.78	34:35:28.6	273.5	10.80	1.73	6.14	6.6	0.44	···	0.16
38	NGC 2731	9:02:08.40	8:18:06.0	35.0	9.04	1.67	4.81	6.9	0.72	20	0.34
39	NGC 2730	9:02:15.82	16:50:17.9	58.9	8.79	2.97	4.56	1.5	0.73	8	0.21
40	IC 2431	9:04:34.39	14:35:39.4	209.0	10.75	1.72	5.92	6.6	0.53	17	0.23
41	NGC 2750	9:05:47.93	25:26:15.0	37.0	9.22	1.95	4.58	8.3	0.72	5	0.19
42	IC 2434	9:07:16.06	37:12:55.3	104.5	9.69	2.02	3.89	7.4	0.59	20	0.13
43	NGC 2761	9:07:30.84	18:26:05.1	125.0	10.22	1.94	5.25	7.4	0.64	···	0.20
44	NGC 2773	9:09:44.16	7:10:25.7	80.4	9.66	1.85	4.63	13.2	0.74	···	0.30
45	NGC 2776	9:12:14.52	44:57:17.4	36.0	9.18	2.68	3.63	12.1	0.86	5	0.09
46	NGC 2789	9:14:59.66	29:43:48.9	93.6	9.70	2.31	3.76	3.8	0.77	0	0.15
47	IRAS 09121+3908	9:15:22.15	38:56:35.0	42.5	10.61	2.24	6.08	3.5	0.77	···	0.08
48	NGC 2824	9:19:02.23	26:16:11.9	37.0	8.70	1.63	3.26	2.3	0.63	-2	0.21
49	IRAS 09184+4356	9:21:38.74	43:43:34.1	170.1	10.03	2.14	5.09	4.7	0.58	···	0.09
50	CGCG 238-041	9:22:25.30	47:14:39.9	131.5	9.45	3.28	5.48	1.0	0.76	···	0.08
51	UGC 4985	9:22:37.39	21:57:26.8	143.4	9.68	2.79	4.65	3.0	0.43	···	0.19
52	NGC 2854	9:24:02.83	49:12:13.7	25.0	8.99	1.47	3.86	5.7	0.51	3	0.10
53	UGC 5046	9:28:06.65	17:11:47.4	64.9	9.48	1.69	4.82	6.9	0.53	20	0.14
54	UGC 5055	9:30:11.76	55:51:08.7	110.6	9.70	2.05	4.34	7.4	0.85	3	0.14
55	NGC 2893	9:30:16.97	29:32:23.9	24.0	8.72	1.51	4.33	5.7	0.90	1	0.12
56	MCG 3-24-062	9:30:22.99	19:28:09.3	66.2	9.11	2.81	4.10	5.5	0.69	···	0.17
57	CGCG 238-066	9:31:06.77	49:04:47.1	147.0	10.02	1.35	5.05	6.0	0.80	···	0.09
58	UGC 5097	9:34:10.63	0:14:31.9	72.5	9.55	1.70	5.34	8.1	0.71	15	0.34
59	CGCG 289-012	9:36:31.87	59:23:54.3	172.4	10.10	2.17	7.42	4.5	0.89	···	0.14
60	MCG 8-18-013	9:36:37.18	48:28:28.0	110.9	10.28	1.43	5.99	14.2	0.68	···	0.09
61	CGCG 181-068	9:37:19.22	33:49:25.8	100.6	9.49	2.74	4.19	5.5	0.39	···	0.07
62	NGC 2936	9:37:44.14	2:45:39.0	100.5	9.74	2.34	3.78	8.7	0.52	-5	0.27
63	NGC 2955	9:41:16.61	35:52:56.2	103.5	9.65	2.80	3.63	4.8	0.55	3	0.06
64	CGCG 182-010	9:45:15.22	34:42:44.2	175.1	10.22	1.76	5.11	7.4	0.72	···	0.07
65	UGC 5228	9:46:03.60	1:40:06.1	28.2±4.0	8.49	2.26	3.91	4.6	0.29	5	0.54
66	IRAS 09438+1141	9:46:32.57	11:27:19.5	203.0	10.13	2.49	5.63	4.5	0.87	···	0.21
67	NGC 3015	9:49:22.92	1:08:43.5	108.8	9.81	1.98	4.37	7.4	0.79	-2	0.39
68	MCG 2-25-039	9:49:36.98	9:00:18.8	77.6	9.32	2.23	4.72	4.7	0.44	···	0.20
69	NGC 3020	9:50:06.65	12:48:49.0	18.3±2.6	8.35	1.71	4.95	3.0	0.43	6	0.36
70	NGC 3049	9:54:49.56	9:16:15.9	18.3±2.6	8.52	1.60	4.43	5.7	0.65	2	0.23
71	NGC 3055	9:55:18.07	4:16:12.1	25.0	8.87	2.09	4.14	9.5	0.56	5	0.31
72	IC 2520	9:56:20.11	27:13:39.3	26.4±1.6	8.63	1.98	4.73	8.3	0.82	15	0.09
73	UGC 5403	10:02:35.54	19:10:36.9	33.0	8.85	1.58	4.45	5.7	0.54	0	0.15

TABLE 2 — *Continued*

SFRS	Name	Position[a] (J2000)		Distance[b] (Mpc)	log L_{60} ($L_\odot$)	F_{100}/F_{60}	$K_s - F_{60}$ (AB mag)	Weight	Axial Ratio	T Type	Extinction (B mag)
74	UGC 5459	10:08:10.08	53:05:01.5	25.8±1.7	8.40	2.30	3.71	5.0	0.20	5	0.07
75	MCG 5-24-022	10:10:03.38	32:04:12.9	92.1	9.31	2.68	6.88	2.3	0.67	···	0.17
76	IC 2551	10:10:40.32	24:24:50.9	94.9	9.94	1.10	5.28	9.8	0.79	···	0.20
77	IRAS 10106+2745	10:13:29.50	27:30:40.1	215.6	10.03	2.73	4.77	2.7	0.55	···	0.18
78	NGC 3162	10:13:31.58	22:44:15.2	26.4±1.6	8.52	2.21	3.86	14.5	0.82	4	0.15
79	IRAS 10120+1653	10:14:47.90	16:38:50.1	517.2	10.89	2.19	6.51	3.5	0.71	···	0.24
80	NGC 3190	10:18:05.66	21:49:56.1	26.4±1.6	8.59	2.95	1.80	22.2	0.37	1	0.20
81	IC 602	10:18:19.73	7:02:57.5	57.6	9.32	2.01	4.75	8.3	0.63	20	0.18
82	NGC 3191	10:19:05.14	46:27:14.8	134.0	9.91	2.24	4.79	8.7	0.79	4	0.08
83	NGC 3206	10:21:47.59	56:55:49.5	25.8±1.7	8.13	2.00	4.61	2.8	0.71	6	0.09
84	UGC 5613	10:23:32.54	52:20:31.3	139.8	10.35	1.97	5.40	8.4	0.72	8	0.06
85	UGC 5644	10:25:46.25	13:43:00.7	137.6	9.52	2.03	3.26	1.7	0.86	20	0.22
86	NGC 3245	10:27:18.41	28:30:26.6	20.9±2.1	8.49	1.60	1.62	2.0	0.53	-2	0.16
87	IRAS 10246+2042	10:27:25.87	20:26:51.4	84.2	9.64	1.50	5.07	9.8	0.87	···	0.19
88	MCG 7-22-012	10:30:11.42	43:21:38.1	66.0	9.16	2.63	7.19	2.3	0.45	···	0.09
89	IRAS 10276+1119	10:30:14.76	11:04:15.9	271.3	10.23	3.82	5.05	2.7	0.78	···	0.16
90	NGC 3265	10:31:06.77	28:47:48.0	21.8±1.6	8.58	1.54	4.33	5.7	0.82	-5	0.14
91	UGC 5713	10:31:38.90	25:59:02.1	95.0	9.31	1.24	3.49	2.3	0.36	4	0.16
92	NGC 3274	10:32:31.87	54:24:03.7	10.0	7.04	1.88	4.05	1.7	0.58	7	0.16
93	UGC 5720	10:32:17.23	27:40:07.7	20.0	8.94	1.15	5.35	4.3	0.66	10	0.09
94	KUG 1031+351	10:34:02.40	34:52:10.2	298.2	10.86	1.87	5.29	1.5	0.95	···	0.10
95	NGC 3306	10:37:10.22	12:39:09.3	46.6±8.9	9.11	1.82	4.59	8.3	0.66	9	0.16
96	NGC 3323	10:39:39.02	25:19:21.9	79.5	9.35	2.20	4.92	4.7	0.64	20	0.19
97	IC 2598	10:39:42.38	26:43:38.6	89.1	9.80	1.69	5.31	9.8	0.73	···	0.16
98	NGC 3338	10:42:07.54	13:44:49.2	21.4±4.0	8.50	3.01	2.73	13.2	0.49	5	0.19
99	NGC 3353	10:45:22.06	55:57:39.9	16.0	8.67	1.28	5.55	4.3	0.73	3	0.08
100	UGC 5881	10:46:42.53	25:55:53.6	93.0	9.57	1.39	4.41	4.8	0.54	1	0.20
101	NGC 3370	10:47:04.06	17:16:25.0	20.9±1.2	8.57	2.66	3.82	14.5	0.56	5	0.18
102	NGC 3381	10:48:24.82	34:42:41.1	25.7±5.3	8.48	2.82	4.15	2.3	0.87	20	0.11
103	UGC 5941	10:50:21.60	41:27:50.5	107.0	9.87	1.89	4.78	13.2	0.88	17	0.06
104	NGC 3413	10:51:20.74	32:45:59.0	16.2±1.6	7.27	1.90	3.87	1.7	0.59	-2	0.14
105	NGC 3408	10:52:11.69	58:26:17.3	138.0	9.67	1.70	3.76	1.5	0.79	5	0.08
106	NGC 3430	10:52:11.40	32:57:01.5	28.4	8.78	2.90	3.11	22.2	0.83	5	0.11
107	CGCG 95-055	10:52:50.74	16:59:07.6	25.7±5.3	10.52	0.91	5.32	1.5	0.53	···	0.20
108	IRAS 10565+2448	10:59:18.12	24:32:34.7	185.2	11.06	1.18	7.08	15.5	0.88	10	0.10
109	UGC 6074	10:59:58.25	50:54:10.6	38.0±7.1	9.28	1.34	5.03	6.9	0.79	15	0.09
110	NGC 3495	11:01:16.22	3:37:40.7	17.5±2.3	8.41	2.62	3.19	5.0	0.25	7	0.27
111	UGC 6103	11:01:58.99	45:13:40.9	91.7	9.71	1.67	4.77	9.8	0.78	···	0.06
112	MCG 7-23-019	11:03:54.31	40:51:00.1	150.6	10.57	1.76	6.41	6.6	0.70	10	0.09
113	UGC 6135	11:04:36.96	45:07:30.8	90.9	9.55	2.91	3.63	4.8	0.93	20	0.06
114	CGCG 241-078	11:06:37.37	46:02:19.6	110.9	9.88	1.40	5.54	8.1	0.56	···	0.06
115	IRAS 11069+2711	11:09:39.36	26:54:53.9	296.4	10.75	1.95	6.33	6.6	0.49	···	0.13
116	IC 676	11:12:39.82	9:03:21.0	26.9±2.2	8.54	1.56	4.08	5.7	0.71	-1	0.18
117	IRAS 11102+3026	11:12:57.36	30:10:28.6	129.6	10.00	1.78	6.02	7.0	0.66	20	0.11
118	IC 2637	11:13:49.75	9:35:10.7	128.2	9.91	1.75	4.28	7.4	0.94	-4	0.18
119	MCG 9-19-013	11:14:49.37	50:19:22.5	201.8	10.02	2.73	5.14	2.7	0.78	···	0.09
120	7ZW 384	11:16:54.41	59:31:50.8	340.4	10.53	2.43	5.31	1.5	0.62	···	0.07
121	IRAS 11167+5351	11:19:34.01	53:35:18.7	447.3	10.96	1.76	5.54	6.6	0.90	···	0.08
122	NGC 3633	11:20:26.21	3:35:08.2	30.0	9.05	1.76	4.05	9.5	0.49	1	0.30
123	NGC 3652	11:22:39.02	37:45:54.4	15.5±3.2	8.86	2.53	4.83	4.7	0.46	6	0.13
124	NGC 3656	11:23:38.64	53:50:31.7	37.0	9.12	2.28	3.27	12.1	0.84	90	0.09
125	NGC 3659	11:23:45.53	17:49:07.2	21.0±1.2	8.26	2.39	3.94	4.6	0.55	9	0.18
126	NGC 3664	11:24:24.26	3:19:31.0	26.9±2.2	7.99	2.06	5.41	2.0	0.92	9	0.27
127	NGC 3666	11:24:26.06	11:20:32.0	16.3±1.7	8.41	2.94	3.42	13.2	0.29	5	0.25
128	IC 691	11:26:44.30	59:09:19.5	16.0	8.70	1.33	5.34	6.9	0.75	11	0.07
129	NGC 3686	11:27:43.97	17:13:27.0	21.0±1.2	8.47	2.70	2.88	13.2	0.79	4	0.19
130	UGC 6469	11:28:17.71	2:39:14.3	102.6	9.62	1.73	6.14	7.0	0.44	4	0.24
131	IC 694	11:28:31.51	58:33:51.4	52.6	10.81	1.05	6.56	15.5	0.84	9	0.07
132	IC 698	11:29:03.84	9:06:43.4	96.8	9.92	1.90	4.61	13.2	0.61	-2	0.25
133	IRAS 11267+1558	11:29:24.70	15:41:41.3	736.6	11.18	2.72	6.80	1.5	0.89	···	0.22
134	NGC 3705	11:30:07.03	9:16:40.8	16.3±1.7	7.95	2.82	2.39	13.2	0.46	2	0.25
135	MCG 3-29-061	11:31:03.70	20:14:08.3	67.5	9.43	1.53	5.29	6.9	0.84	···	0.16
136	NGC 3720	11:32:21.60	0:48:14.4	89.8	9.68	2.40	6.58	4.0	0.88	1	0.23
137	NGC 3729	11:33:49.32	53:07:32.0	17.1±0.8	8.48	2.61	2.81	5.0	0.67	1	0.06
138	MCG 10-17-019	11:35:24.79	57:38:59.8	127.5	9.78	2.94	4.29	5.0	0.76	···	0.10
139	NGC 3758	11:36:28.94	21:35:46.5	131.6	9.80	1.70	3.87	4.8	0.91	···	0.14
140	UGC 6583	11:36:54.36	19:58:18.1	93.2	9.61	2.22	4.97	8.7	0.69	···	0.16
141	MCG 1-30-003	11:37:06.58	2:50:44.9	128.9	9.92	1.75	5.62	7.0	0.64	3	0.20
142	NGC 3769	11:37:44.11	47:53:35.1	17.1±0.8	8.05	2.67	3.30	5.0	0.37	3	0.13
143	NGC 3773	11:38:13.06	12:06:44.4	16.3±1.7	7.53	1.22	4.40	2.3	0.85	-2	0.26
144	NGC 3781	11:39:03.77	26:21:42.2	103.5	10.27	1.41	5.65	14.2	0.81	···	0.13
145	UGC 6625	11:39:47.54	19:56:00.2	158.2	9.91	2.73	4.27	5.0	0.93	20	0.16
146	NGC 3808A	11:40:44.64	22:26:49.0	107.2	9.90	2.17	5.52	4.0	0.60	5	0.17
147	NGC 3811	11:41:16.63	47:41:27.0	54.2	9.19	2.30	3.82	14.5	0.71	6	0.14

TABLE 2 — *Continued*

SFRS	Name	Position^{a} (J2000)		Distance^{b} (Mpc)	$\log L_{60}$ ($L_\odot$)	F_{100}/F_{60}	$K_s - F_{60}$ (AB mag)	Weight	Axial Ratio	T Type	Extinction (B mag)
148	NGC 3822	11:42:11.08	10:16:40.0	94.6	9.83	2.18	3.84	8.7	0.64	-2	0.40
149	UGC 6665	11:42:12.22	0:20:04.1	85.0	9.81	1.16	5.84	8.1	0.53	3	0.17
150	MCG 3-30-051	11:42:24.50	20:07:09.5	90.4	9.55	2.21	4.68	8.7	0.60	···	0.15
151	NGC 3839	11:43:54.34	10:47:04.9	91.3	9.91	1.84	5.29	13.2	0.65	8	0.40
152	UGC 6732	11:45:33.14	58:58:41.2	53.6	8.95	1.42	3.56	2.3	0.91	···	0.15
153	IC 730	11:45:35.26	3:13:54.6	93.1	9.82	1.81	4.66	13.2	0.65	···	0.14
154	IC 732	11:45:59.59	20:26:49.8	110.0	10.01	1.77	5.42	8.4	0.62	···	0.14
155	NGC 3912	11:50:04.46	26:28:45.3	22.5±3.2	8.95	1.93	4.34	9.5	0.47	3	0.16
156	NGC 3928	11:51:47.62	48:40:59.3	16.9±1.7	8.42	2.04	3.81	4.2	0.90	3	0.13
157	NGC 3934	11:52:12.65	16:51:06.7	61.6	9.26	1.60	4.41	5.7	0.75	···	0.19
158	UGC 6865	11:53:39.96	43:27:39.4	91.2	9.67	2.14	4.20	7.4	0.31	17	0.12
159	UGC 6901	11:55:38.35	43:02:45.1	107.6	9.77	2.55	4.38	8.7	0.78	20	0.12
160	CGCG 013-010	11:57:05.93	1:07:32.1	172.3	10.41	2.29	5.23	4.7	0.68	···	0.11
161	NGC 3991	11:57:30.96	32:20:13.3	55.6	9.22	1.89	5.06	8.3	0.30	10	0.11
162	NGC 4004	11:58:05.23	27:52:43.9	57.9	9.41	1.85	5.27	8.3	0.46	···	0.13
163	NGC 4014	11:58:35.83	16:10:38.1	62.6	9.32	2.53	3.53	12.1	0.59	0	0.27
164	NGC 4010	11:58:37.90	47:15:41.4	17.1±0.8	8.30	2.68	3.48	5.0	0.16	7	0.13
165	NGC 4018	11:58:40.78	25:18:58.9	72.6	9.44	2.92	4.49	5.5	0.33	2	0.12
166	NGC 4020	11:58:56.69	30:24:42.8	14.3±3.0	7.26	2.57	7.02	1.0	0.47	7	0.11
167	IRAS 11571+3003	11:59:42.60	29:47:12.5	218.6	10.06	2.19	5.57	4.5	0.82	···	0.10
168	UGC 7017	12:02:23.98	14:50:37.1	55.2	9.38	1.97	4.87	8.3	0.38	3	0.11
169	UGC 7016	12:02:22.51	29:51:42.4	110.3	9.64	2.37	3.51	3.8	0.34	2	0.25
170	MCG 3-31-030	12:03:35.95	16:03:19.9	13.1	7.11	2.75	3.83	1.0	0.62	···	0.25
171	NGC 4062	12:04:03.84	31:53:44.9	16.3±0.9	7.73	3.79	2.22	13.2	0.38	5	0.12
172	NGC 4064	12:04:11.10	18:26:38.1	8.5±1.53	7.80	2.07	3.03	3.2	0.43	1	0.25
173	UGC 7104	12:07:09.55	16:59:44.2	102.3	9.93	2.14	5.09	8.7	0.82	3	0.23
174	NGC 4116	12:07:36.82	2:41:32.3	16.0±2.1	8.18	2.94	4.32	2.3	0.51	8	0.15
175	NGC 4136	12:09:17.71	29:55:39.4	16.3±0.9	7.40	2.56	3.69	1.7	0.98	5	0.15
176	NGC 4150	12:10:33.67	30:24:05.8	13.7±1.4	6.26	1.98	2.23	1.0	0.66	-2	0.11
177	IRAS 12086+1441	12:11:14.38	14:24:35.2	13.1	8.04	1.41	6.18	5.3	0.70	···	0.18
178	NGC 4162	12:11:53.04	24:07:06.7	42.5±5.0	9.04	2.70	3.40	22.2	0.63	4	0.18
179	NGC 4178	12:12:46.92	10:52:08.6	16.8±0.8	8.54	2.36	4.03	14.5	0.31	8	0.14
180	IRAS 12112+0305	12:13:46.08	2:48:41.5	303.6	11.36	1.19	8.09	15.5	0.86	···	0.12
181	NGC 4189	12:13:47.26	13:25:29.3	16.8±0.8	8.46	2.64	3.51	5.0	0.81	6	0.18
182	NGC 4194	12:14:09.65	54:31:35.9	36.0	10.00	1.14	6.04	14.2	0.77	10	0.11
183	NGC 4204	12:15:14.45	20:39:30.9	10.0	7.26	2.02	5.15	1.0	0.40	8	0.21
184	NGC 4207	12:15:30.50	9:35:05.6	16.8±0.8	8.42	2.46	3.67	5.0	0.47	···	0.18
185	UGC 7286	12:15:59.26	27:26:31.9	115.4	9.47	1.79	6.79	3.0	0.41	2	0.19
186	NGC 4234	12:17:09.08	3:40:50.2	30.0	8.51	2.34	4.67	4.7	0.83	9	0.14
187	NGC 4237	12:17:11.42	15:19:26.3	16.8±0.8	8.39	3.27	2.78	13.2	0.60	4	0.23
188	NGC 4244	12:17:29.45	37:48:26.5	4.3±0.21	6.53	3.24	1.39	1.8	0.14	6	0.12
189	NGC 4253	12:18:26.52	29:48:46.5	64.9	9.57	1.05	4.39	4.8	0.83	1	0.20
190	MCG 3-32-005	12:20:47.23	17:00:57.9	13.1	8.38	1.92	5.24	2.8	0.72	···	0.16
191	NGC 4290	12:20:47.52	58:05:33.0	37.0	9.38	2.17	3.84	14.5	0.72	2	0.11
192	NGC 4294	12:21:17.81	11:30:27.0	16.8±0.8	8.38	2.02	4.11	4.2	0.46	6	0.19
193	NGC 4314	12:22:32.02	29:53:43.8	16.3±0.9	8.02	2.04	1.94	3.2	0.55	1	0.18
194	NGC 4385	12:25:42.79	0:34:21.4	29.0	9.17	1.32	4.59	6.9	0.56	-1	0.13
195	NGC 4395	12:25:48.86	33:32:48.7	4.7±0.24	6.79	3.53	4.60	1.8	0.73	9	0.11
196	NGC 4396	12:25:59.16	15:40:15.6	16.8±0.8	8.04	3.02	4.07	2.3	0.31	7	0.21
197	NGC 4412	12:26:36.07	3:57:52.9	30.6±6.4	9.02	1.97	4.01	9.5	0.91	3	0.15
198	NGC 4418	12:26:54.62	−0:52:39.4	29.0	10.06	0.77	7.27	14.2	0.50	1	0.14
199	NGC 4420	12:26:58.49	2:29:39.7	17.6±0.9	8.55	2.62	3.78	12.1	0.50	4	0.15
200	NGC 4424	12:27:11.62	9:25:14.4	6.0	8.40	1.90	3.37	3.2	0.50	1	0.19
201	NGC 4435	12:27:40.46	13:04:44.4	16.7±1.7	8.21	1.22	1.02	2.0	0.69	-2	0.20
202	NGC 4438	12:27:45.62	13:00:31.7	16.8±0.8	8.53	2.52	1.80	22.2	0.43	20	0.20
203	NGC 4448	12:28:15.46	28:37:13.1	16.3±0.9	7.33	3.11	1.33	2.0	0.36	2	0.16
204	3C 273	12:29:06.70	2:03:08.6	657.8	11.53	1.31	3.75	1.0	0.93	···	0.12
205	NGC 4470	12:29:37.78	7:49:27.1	16.8±0.8	8.21	2.43	3.83	4.6	0.64	1	0.18
206	IRAS 12274+0018	12:29:58.85	0:01:38.0	38.1	8.48	1.33	5.33	3.0	0.90	···	0.15
207	NGC 4491	12:30:57.12	11:29:00.7	16.8±0.8	8.36	1.25	4.06	2.3	0.53	1	0.19
208	NGC 4500	12:31:22.90	29:08:11.3	52.0	9.35	1.74	4.26	9.5	0.56	1	0.09
209	NGC 4495	12:31:22.15	57:57:52.5	74.2	9.59	2.22	4.43	8.7	0.53	2	0.14
210	IC 3476	12:32:41.88	14:03:01.6	16.8±0.8	8.05	2.42	4.60	1.0	0.62	10	0.24
211	NGC 4509	12:33:06.72	32:05:34.5	11.1	7.26	3.60	5.14	1.0	0.80	2	0.11
212	NGC 4519	12:33:30.26	8:39:17.1	16.8±0.8	8.51	1.74	4.37	9.5	0.75	7	0.19
213	NGC 4548	12:35:26.45	14:29:46.8	16.2±1.6	8.36	4.25	1.35	13.2	0.76	3	0.24
214	IRAS 12337+5044	12:36:06.70	50:28:18.7	172.5	10.06	2.17	5.55	4.5	0.53	···	0.13
215	IC 3581	12:36:38.06	24:25:43.6	106.1	10.02	1.27	5.23	6.0	0.71	···	0.09
216	NGC 4592	12:39:18.74	−0:31:55.0	11.1±1.2	8.29	2.18	4.00	4.6	0.30	8	0.22
217	NGC 4607	12:41:12.22	11:53:11.9	16.8±0.8	8.38	2.85	3.62	13.2	0.25	3	0.13
218	NGC 4625	12:41:52.73	41:16:26.3	9.2±0.57	7.37	3.12	3.17	1.8	0.79	9	0.15
219	NGC 4630	12:42:31.13	3:57:36.9	15.6±1.0	7.42	2.30	4.09	2.0	0.72	10	0.22
220	IC 3690	12:42:49.20	10:21:26.9	13.1	8.10	1.51	4.71	3.0	0.59	20	0.17
221	UGC 7905	12:43:47.93	54:53:45.2	78.7	9.43	1.39	7.46	4.3	0.58	17	0.12

TABLE 2 — *Continued*

SFRS	Name	Position[a] (J2000)		Distance[b] (Mpc)	$\log L_{60}$ ($L_\odot$)	F_{100}/F_{60}	$K_s - F_{60}$ (AB mag)	Weight	Axial Ratio	T Type	Extinction (*B* mag)
222	MCG 5-30-069	12:44:41.26	26:25:10.5	74.0	9.57	1.66	5.28	9.8	0.73	···	0.12
223	IC 3721	12:44:53.11	18:45:18.9	98.5	9.67	2.05	4.11	7.4	0.45	20	0.15
224	NGC 4670	12:45:17.26	27:07:32.2	14.3±1.1	8.29	1.64	4.53	2.3	0.55	15	0.12
225	NGC 4675	12:45:31.90	54:44:15.4	76.9	9.54	1.99	4.66	13.2	0.38	3	0.12
226	MCG 7-26-051	12:46:56.83	42:15:59.1	146.9	10.22	2.16	5.17	4.7	0.60	···	0.13
227	NGC 4689	12:47:46.51	4:20:09.8	16.8±0.8	8.37	3.72	2.51	13.2	0.81	4	0.19
228	NGC 4688	12:47:45.55	13:45:46.1	15.6±1.0	7.95	2.05	4.61	2.8	0.74	6	0.23
229	NGC 4704	12:48:46.44	41:55:16.5	122.8	9.81	1.36	4.47	4.8	0.87	4	0.14
230	NGC 4701	12:49:11.59	3:23:19.4	15.6±1.0	7.44	2.44	3.97	2.0	0.82	6	0.27
231	IRAS 12468+3436	12:49:17.16	34:19:43.0	498.3	10.87	2.41	7.19	3.5	0.78	···	0.10
232	IRAS 12470+1404	12:49:34.80	13:48:09.8	13.1	7.81	1.84	6.14	2.0	0.70	···	0.17
233	MCG 8-23-097	12:50:39.84	47:56:00.3	131.2	10.36	1.59	8.02	14.2	0.65	···	0.11
234	NGC 4747	12:51:45.60	25:46:30.1	14.3±1.1	8.20	1.99	4.06	4.2	0.72	6	0.08
235	UGC 8017	12:52:53.59	28:22:16.6	107.1	9.72	2.75	3.94	5.0	0.41	···	0.07
236	NGC 4765	12:53:14.57	4:27:47.7	15.6±1.0	7.39	1.87	4.75	1.0	0.67	···	0.27
237	VCC 2096	12:53:24.79	11:42:36.4	13.1	8.09	1.63	5.94	5.3	0.68	···	0.16
238	UGC 8041	12:55:12.65	0:06:59.9	23.0±1.6	7.86	2.47	4.99	1.0	0.48	7	0.18
239	UGC 8058	12:56:14.23	56:52:25.3	179.6	11.48	0.92	5.62	15.5	0.95	5	0.11
240	NGC 4837	12:56:48.31	48:17:48.9	132.5	9.94	2.19	4.21	8.7	0.46	···	0.13
241	UM 530	12:58:08.35	1:51:44.4	282.7	10.15	2.92	5.75	1.5	0.64	0	0.18
242	NGC 4861	12:59:01.92	34:51:21.4	18.5±1.1	7.78	1.20	6.88	5.3	0.53	9	0.09
243	NGC 4868	12:59:08.90	37:18:37.4	74.0	9.62	2.56	3.90	8.7	0.95	2	0.10
244	NGC 4922	13:01:25.27	29:18:49.5	107.2	10.27	1.07	4.96	6.0	0.87	90	0.07
245	UGC 8179	13:05:14.16	31:59:59.0	222.1	10.10	2.37	3.74	1.0	0.46	3	0.07
246	NGC 5001	13:09:33.12	53:29:39.4	134.8	10.11	2.32	4.53	2.7	0.56	20	0.14
247	IC 856	13:10:41.33	20:32:10.6	64.3	9.15	2.20	4.56	4.7	0.44	···	0.15
248	UGC 8269	13:11:15.12	46:42:02.3	124.1	10.06	2.06	5.63	8.4	0.44	20	0.10
249	NGC 5014	13:11:37.03	22:54:55.8	18.5±1.1	8.30	1.85	4.02	4.2	0.38	1	0.05
250	NGC 5012	13:11:31.22	36:16:55.7	40.2±6.2	9.02	2.79	2.94	22.2	0.54	5	0.08
251	IRAS 13116+4508	13:13:47.88	44:52:58.6	258.3	10.24	2.19	5.55	4.5	0.61	···	0.10
252	IC 860	13:15:03.50	24:37:07.8	54.5	10.02	1.06	6.74	14.2	0.66	···	0.06
253	IRAS 13144+4508	13:16:39.74	44:52:35.0	381.8	10.52	2.04	4.30	1.0	0.89	···	0.09
254	NGC 5060	13:17:16.22	6:02:14.8	97.4	9.83	2.25	4.67	8.7	0.68	3	0.31
255	UGC 8357	13:17:58.80	−0:18:42.0	146.9	10.14	1.83	5.06	7.4	0.49	17	0.32
256	UGC 8361	13:18:18.58	6:20:07.4	106.3	9.87	1.60	4.87	9.8	0.49	2	0.28
257	IC 883	13:20:35.40	34:08:21.6	104.7	10.60	1.61	6.87	15.5	0.84	10	0.06
258	NGC 5100	13:20:59.59	8:58:41.9	142.2	10.04	2.21	4.27	2.7	0.65	17	0.28
259	NGC 5104	13:21:23.09	0:20:32.7	87.8	10.08	1.82	4.87	7.4	0.56	1	0.32
260	NGC 5107	13:21:24.70	38:32:15.4	18.5±1.1	7.76	1.88	4.79	2.8	0.34	7	0.07
261	NGC 5112	13:21:56.40	38:44:05.0	18.5±1.1	8.22	2.46	4.38	4.6	0.62	6	0.07
262	NGC 5123	13:23:10.51	43:05:10.5	123.4	9.81	3.14	3.69	4.8	0.94	6	0.12
263	IRAS 13218+0552	13:24:19.90	5:37:04.7	850.4	11.54	0.80	5.28	1.0	0.96	···	0.25
264	IRAS 13232+1731	13:25:43.87	17:15:52.8	331.8	10.34	3.06	4.49	1.0	0.79	···	0.18
265	NGC 5147	13:26:19.73	2:06:03.1	18.0	8.40	2.34	4.10	4.6	0.75	8	0.22
266	NGC 5204	13:29:36.58	58:25:13.3	3.2±0.16	7.29	1.76	4.20	1.7	0.60	9	0.12
267	UGC 8502	13:30:39.36	31:17:02.6	149.9	9.97	1.74	6.26	7.0	0.53	17	0.09
268	UGC 8561	13:34:57.26	34:02:38.7	107.5	9.89	2.49	4.84	8.7	0.84	6	0.07
259	NGC 5230	13:35:31.87	13:40:34.2	105.6	9.62	3.17	3.57	4.8	0.93	5	0.17
270	IRAS 13349+2438	13:37:18.72	24:23:03.4	453.5	10.66	1.45	2.99	1.0	0.83	···	0.09
271	NGC 5256	13:38:23.47	6:53:15.6	125.2	10.47	1.68	5.27	6.0	0.58	···	0.10
272	UGC 8626	13:38:17.11	48:16:36.1	108.8	9.60	1.55	4.35	4.8	0.45	4	0.24
273	NGC 5263	13:39:55.66	28:24:02.7	77.5	9.69	2.03	4.58	13.2	0.33	20	0.10
274	MCG 1-35-028	13:40:27.19	4:46:25.8	105.1	9.85	1.54	4.89	9.8	0.74	···	0.24
275	IC 910	13:41:07.85	23:16:55.4	120.3	10.26	1.24	7.62	14.2	0.89	···	0.13
276	MK 268	13:41:11.14	30:22:41.3	173.7	10.06	1.25	4.35	1.7	0.65	···	0.12
277	NGC 5278	13:41:39.24	55:40:14.1	114.4	9.70	2.91	3.74	4.8	0.71	3	0.12
278	NGC 5273	13:42:08.38	35:39:15.5	16.5±1.6	7.83	1.40	1.55	2.0	0.91	-2	0.10
279	UGC 8685	13:43:08.83	30:20:15.9	152.6	10.14	2.25	4.85	4.7	0.78	4	0.11
280	UGC 8686	13:43:40.13	3:53:47.3	105.4	9.69	2.37	4.47	8.7	0.33	20	0.24
281	UGC 8696	13:44:42.17	55:53:13.6	163.0	11.23	0.94	7.32	15.5	0.45	···	0.12
282	NGC 5297	13:46:49.46	14:24:01.7	30.9±1.9	8.92	3.05	2.93	22.2	0.32	5	0.08
283	MK 796	13:46:23.66	43:52:20.4	98.5	9.85	1.72	5.34	7.0	0.88	···	0.15
284	IRAS 13446+1121	13:47:04.37	11:06:22.6	104.5	9.95	1.05	5.57	8.1	0.81	···	0.16
285	NGC 5303	13:47:45.00	38:18:16.7	23.0	8.61	2.10	4.46	9.5	0.57	15	0.12
286	NGC 5313	13:49:44.35	39:59:05.2	30.9±1.9	9.07	3.41	3.06	22.2	0.53	3	0.08
287	MCG 3-35-034	13:53:09.67	14:39:20.9	178.6	10.01	2.33	5.78	4.5	0.73	···	0.17
288	NGC 5347	13:53:17.78	33:29:27.1	39.0	8.69	1.88	3.16	4.3	0.78	2	0.12
289	NGC 5350	13:53:21.62	40:21:50.2	30.9±1.9	8.94	2.98	2.78	22.2	0.75	3	0.10
290	NGC 5368	13:54:31.18	15:02:38.9	74.6	9.23	2.08	3.56	4.3	0.76	2	0.12
291	UGC 8827	13:54:29.16	54:19:50.4	85.4	9.80	1.49	4.82	9.8	0.96	-2	0.12
292	UGC 8850	13:56:02.62	18:22:17.8	216.5	10.45	0.86	3.90	1.7	0.88	15	0.12
293	UGC 8856	13:56:07.90	30:04:52.9	137.9	9.99	2.15	5.44	4.0	0.48	17	0.11
294	NGC 5374	13:57:29.64	6:05:49.2	68.9	9.45	2.49	3.94	14.5	0.77	4	0.23
295	UGC 8902	13:59:02.81	15:33:56.7	114.4	9.60	2.59	3.24	3.8	0.39	3	0.11

TABLE 2 — *Continued*

SFRS	Name	Position^{a} (J2000)		Distance^{b} (Mpc)	$\log L_{60}$ ($L_{\odot}$)	F_{100}/F_{60}	$K_s - F_{60}$ (AB mag)	Weight	Axial Ratio	T Type	Extinction (B mag)
296	NGC 5403	13:59:50.76	38:10:56.2	37.0	9.11	3.68	4.68	1.5	0.32	3	0.10
297	MCG 7-29-036	14:00:57.84	42:51:20.4	144.6	10.13	1.72	6.10	8.4	0.45	···	0.07
298	NGC 5414	14:02:03.53	9:55:45.6	68.3	9.40	1.66	5.23	6.9	0.67	15	0.14
299	MCG 5-33-046	14:04:48.00	30:44:37.3	116.4	9.96	1.54	5.16	9.8	0.59	···	0.11
300	NGC 5474	14:05:01.42	53:39:44.4	5.6±0.43	7.32	2.45	3.70	1.7	0.58	6	0.13
301	NGC 5480	14:06:21.58	50:43:30.4	30.5±3.6	9.00	2.77	4.05	5.5	0.79	5	0.12
302	MCG 6-31-070	14:06:49.08	33:46:18.3	155.8	10.22	1.87	5.35	8.4	0.67	···	0.13
303	CGCG 74-129	14:10:41.35	13:33:28.8	76.5	9.67	0.81	5.86	8.1	0.74	···	0.12
304	NGC 5520	14:12:38.16	39:18:36.6	30.5±3.6	8.62	2.49	3.94	14.5	0.55	3	0.11
305	NGC 5515	14:12:22.80	50:20:54.4	114.1	9.76	2.67	3.58	3.8	0.60	2	0.10
306	NGC 5526	14:13:53.76	57:46:16.8	27.9±2.3	8.84	2.33	6.33	2.3	0.23	4	0.11
307	NGC 5522	14:14:50.38	15:08:48.8	72.1	9.36	2.08	3.71	4.3	0.31	3	0.12
308	NGC 5541	14:16:31.80	39:35:20.6	115.4	9.90	2.23	3.96	8.7	0.74	20	0.10
309	IC 4395	14:17:21.07	26:51:26.8	160.4	10.29	1.95	7.12	8.4	0.90	20	0.11
310	UGC 9165	14:18:47.78	24:56:25.9	81.3	9.66	2.32	4.51	8.7	0.37	20	0.15
311	MK 1490	14:19:43.22	49:14:11.9	116.2	10.33	1.35	6.27	14.2	0.92	···	0.13
312	NGC 5585	14:19:48.19	56:43:45.6	5.6±0.43	7.33	2.59	3.63	1.7	0.57	7	0.12
313	IC 4408	14:21:13.10	29:59:36.6	134.9	9.93	2.55	4.25	8.7	0.48	20	0.10
314	NGC 5584	14:22:23.76	−0:23:15.6	23.1±4.8	8.67	2.39	3.93	14.5	0.70	6	0.33
315	NGC 5633	14:27:28.39	46:08:47.5	36.5±7.6	9.02	2.94	3.67	22.2	0.67	3	0.16
316	NGC 5660	14:29:49.82	49:37:21.6	38.9±3.0	9.21	2.21	4.22	14.5	0.92	5	0.14
317	NGC 5656	14:30:25.51	35:19:15.7	53.7	9.13	1.73	3.95	22.2	0.83	3	0.10
318	NGC 5657	14:30:43.15	29:10:49.9	64.4	9.19	2.93	3.45	9.5	0.47	2	0.08
319	CGCG 133-083	14:31:54.10	21:56:18.3	190.6	10.34	1.79	5.94	8.4	0.85	···	0.24
320	MCG 7-30-028	14:33:48.36	40:05:38.9	116.1	9.79	2.68	4.76	8.7	0.95	···	0.10
321	MCG 6-32-070	14:35:18.38	35:07:07.2	127.0	10.07	2.03	4.88	7.4	0.94	···	0.07
322	UGC 9412	14:36:22.08	58:47:39.3	138.7	10.06	1.02	4.22	1.7	0.80	11	0.11
323	NGC 5698	14:37:14.69	38:27:15.4	60.9	8.99	2.06	3.73	4.3	0.53	3	0.08
324	NGC 5691	14:37:53.33	−0:23:55.9	19.8±1.0	8.90	1.92	4.37	9.5	0.69	1	0.33
325	MCG 9-24-035	14:45:45.12	51:34:50.9	137.4	10.19	1.30	4.82	6.0	0.70	···	0.13
326	MCG 9-24-038	14:46:37.08	56:13:58.7	166.6	10.01	2.40	4.73	4.7	0.60	···	0.11
327	UGC 9560	14:50:56.57	35:34:19.6	23.0	7.85	2.06	5.55	2.0	0.54	···	0.10
328	IC 1076	14:54:59.62	18:02:14.4	92.5	9.51	2.14	4.57	8.7	0.60	···	0.20
329	IRAS 14538+1730	14:56:08.54	17:18:34.4	432.9	10.92	2.04	5.82	6.6	0.61	···	0.17
330	NGC 5795	14:56:19.34	49:23:55.4	38.2±7.9	9.02	2.64	3.94	14.5	0.26	20	0.16
331	UGC 9618	14:57:00.79	24:37:02.2	145.8	10.55	2.41	5.28	1.5	0.54	17	0.21
332	UGC 9639	14:58:36.00	44:53:01.0	157.7	10.21	2.12	4.52	1.5	0.82	2	0.14
333	MCG 6-33-022	15:08:05.98	34:23:27.2	194.5	10.43	2.03	5.76	8.4	0.58	···	0.13
334	NGC 5879	15:09:46.78	57:00:00.8	15.5±0.9	8.37	2.76	3.11	13.2	0.38	4	0.12
335	MCG 9-25-036	15:12:52.33	51:23:55.0	160.1	9.65	2.94	5.68	2.0	0.64	···	0.16
336	NGC 5899	15:15:03.22	42:02:59.5	43.5±4.4	9.09	3.60	2.87	22.2	0.34	5	0.16
337	NGC 5905	15:15:23.33	55:31:02.3	58.7	9.32	2.39	3.71	12.1	0.79	3	0.11
338	MK 848	15:18:06.14	42:44:45.1	173.9	10.89	1.09	7.02	15.5	0.61	-2	0.16
339	IC 4553	15:34:57.22	23:30:13.2	83.5	11.21	1.13	7.94	15.5	0.86	15	0.26
340	UGC 9922	15:35:53.88	38:40:31.8	86.7	9.61	1.86	5.26	13.2	0.53	17	0.13
341	IC 4567	15:37:13.27	43:17:53.9	88.6	9.61	2.89	3.89	5.0	0.71	6	0.17
342	MCG 4-37-016	15:39:27.50	24:56:51.4	102.9	9.76	1.27	6.60	8.1	0.74	···	0.28
343	NGC 5975	15:39:57.96	21:28:14.3	69.3	9.60	1.87	4.41	7.4	0.51	20	0.29
344	NGC 5980	15:41:30.43	15:47:15.6	65.2	9.47	2.58	3.75	12.1	0.41	20	0.22
345	NGC 5992	15:44:21.50	41:05:10.9	140.2	9.89	2.85	5.00	3.0	0.90	20	0.16
346	NGC 5996	15:46:58.87	17:53:03.0	54.0	9.37	1.85	5.15	8.3	0.80	···	0.21
347	IRAS 15519+3537	15:53:48.86	35:28:02.2	354.1	10.53	2.26	5.72	3.5	0.76	···	0.17
348	UGC 10099	15:56:36.41	41:52:50.5	152.2	10.06	1.85	5.31	7.4	0.97	11	0.13
349	MCG 5-38-006	15:58:43.70	26:49:05.3	69.6	9.51	1.00	4.94	9.8	0.87	···	0.27
350	UGC 10120	15:59:11.18	20:45:16.8	138.9	9.50	2.09	3.63	1.7	0.82	3	0.17
351	NGC 6027A	15:59:09.62	35:01:47.5	70.6	9.04	2.14	3.65	4.3	0.69	1	0.27
352	NGC 6040A	16:04:26.52	17:44:31.2	177.0	9.81	1.74	3.69	1.7	0.54	5	0.29
353	UGC 10200	16:05:45.89	41:20:41.1	31.2±6.5	8.55	1.27	5.03	6.9	0.88	···	0.12
354	IRAS 16052+5334	16:06:33.00	53:26:32.1	366.1	10.52	2.96	5.38	1.5	0.76	···	0.11
355	IRAS 16053+1836	16:07:38.52	18:28:48.3	161.4	10.16	1.57	5.12	6.0	0.89	···	0.26
356	NGC 6090	16:11:40.32	52:27:23.1	131.2	10.47	1.54	6.16	14.2	0.69	17	0.17
357	UGC 10273	16:12:44.69	28:17:10.0	111.3	9.73	2.46	5.76	4.0	0.23	15	0.26
358	IRAS 16150+2233	16:17:08.95	22:26:28.0	278.1	10.14	7.02	5.38	1.5	0.62	0	0.37
359	UGC 10322	16:18:07.85	22:13:32.3	69.1	9.30	2.85	4.29	5.5	0.36	20	0.37
360	NGC 6120	16:19:48.12	37:46:27.7	134.9	10.28	2.06	4.98	7.4	0.83	···	0.12
361	MCG 3-42-004	16:24:15.17	20:11:00.8	171.9	10.02	2.19	4.63	4.7	0.87	···	0.34
362	UGC 10407	16:28:27.89	41:13:03.5	124.7	9.84	1.80	5.65	7.0	0.79	···	0.10
363	IRAS 16320+3922	16:33:49.63	39:15:47.5	139.4	9.53	2.96	6.18	2.0	0.98	···	0.08
364	NGC 6186	16:34:25.49	21:32:27.2	162.8	10.31	2.15	3.83	2.7	0.56	1	0.30
365	MCG 9-27-053	16:35:15.41	52:46:49.9	129.2	9.99	2.30	5.34	4.0	0.45	···	0.22
366	UGC 10514	16:42:23.66	25:05:11.5	100.5	9.81	1.69	5.74	8.1	0.41	8	0.32
367	IRAS 16435+2154	16:45:40.68	21:49:19.0	142.3	10.04	1.84	5.88	8.4	0.52	···	0.34
368	IC 4623	16:51:05.33	22:31:38.6	138.5	9.90	2.18	4.67	8.7	0.62	···	0.36
369	IRAS 16516+3030	16:53:37.18	30:26:09.7	306.1	10.66	1.97	5.34	1.5	0.85	···	0.26

TABLE 2 — *Continued*

SFRS	Name	Position[a] (J2000)	Distance[b] (Mpc)	$\log L_{60}$ ($L_\odot$)	F_{100}/F_{60}	$K_s - F_{60}$ (AB mag)	Weight	Axial Ratio	T Type	Extinction (B mag)

Note. — Morphological T types and B-band Milky Way extinction (in magnitudes, estimated from the 100 μm dust maps) were taken from the PSCz catalog (Saunders et al. 2000), except as noted. Axial ratios were measured directly from the IRAC mosaics using SExtractor and are estimated to be accurate to 0.05 (1σ). L_{60} is a monochromatic 60 μm luminosity calculated for purposes of sample selection. The more useful L(TIR) is given in Table 7. Weights are the ratio of the total number of PSCz galaxies within a given bin to the number of SFRS sample galaxies taken from that same bin, subject to the area restrictions noted in Sec. 2.

[a] Coordinates are based on IRAC imaging.

[b] Quality distances from R. B. Tully (priv. comm.) are given with 1σ error estimates. All other distances are derived from the PSCz velocities after correcting for local bulk flow as described in Sec. 3.1.

TABLE 4
Spitzer/IRAC Photometry for SFRS Galaxies

SFRS	Name	3.6 μm	4.5 μm	5.8 μm	8.0 μm
1	IC 486	12.58	12.71	12.37	11.81
2	IC 2217	13.06	13.44	11.95	10.78
3	NGC 2500	11.78	12.25	11.48	10.95
4	NGC 2512	12.25	12.64	11.67	10.63
5	MCG 6-18-009	13.14	13.50	12.80	11.51
6	MK 1212	13.65	13.90	12.85	11.37
7	IRAS 08072+1847	13.81	13.35	12.11	10.94
8	NGC 2532	···	12.22	···	9.97
9	UGC 4261	14.07	14.48	13.31	12.17
10	NGC 2535	12.52	12.94	11.94	10.96
11	NGC 2543	11.92	12.32	11.67	10.72
12	NGC 2537	12.09	12.57	12.07	11.48
13	IC 2233	13.09	13.48	13.49	13.54
14	IC 2239	12.82	13.27	12.58	11.53
15	UGC 4286	13.27	13.69	12.68	11.63
16	UGC 4306	12.51	12.91	11.50	10.40
17	NGC 2552	12.78	13.27	14.01±0.04	12.83
18	IC 2339	13.61	14.01	13.17	12.24
19	IRAS 08234+1054B	14.83	15.04	14.44	12.72
20	IRAS 08269+1514	14.51	14.82	13.52	12.19
21	NGC 2604	12.87	13.23	12.83	11.76
22	NGC 2608	11.89	12.31	11.70	10.74
23	MK 92	13.86	14.22	12.73	11.56
24	NGC 2623	12.69	12.78	11.72	10.70
25	CGCG 120-018	13.68	13.99	12.73	11.48
26	NGC 2644	12.66	13.08	12.23	11.42
27	UGC 4572	13.04	13.52	12.70	11.73
28	UGC 4653	13.75	14.20	13.91	12.67
29	IRAS 08512+2727	14.03	14.38	13.81	11.80
30	OJ 287	12.04	11.76	11.35	10.95
31	IRAS 08538+4256	13.85	14.13	12.92	11.67
32	IRAS 08550+3908	14.19	14.18	13.64	12.68
33	NGC 2718	11.90	12.37	11.48	10.55
34	NGC 2712	11.69	12.12	11.44	10.64
35	NGC 2719	13.99	14.41	13.76	12.98
36	IRAS 08572+3915	12.26	11.16	10.13	9.49
37	IRAS 08579+3447	14.21	14.44	13.87	12.15
38	NGC 2731	12.74	13.13	11.71	10.64
39	NGC 2730	13.10	13.55	12.78	11.73
40	IC 2431	13.81	14.16	13.36	11.88
41	NGC 2750	12.00	12.37	11.56	10.49
42	IC 2434	12.71	13.13	12.51	11.58
43	NGC 2761	12.86	13.18	11.85	10.56
44	NGC 2773	12.68	13.07	11.74	10.56
45	NGC 2776	11.65	11.98	11.09	10.05
46	NGC 2789	12.24	12.67	11.93	11.01
47	IRAS 09121+3908	14.94	15.03	14.44	12.50
48	NGC 2824	12.66	13.14	12.89	12.45
49	IRAS 09184+4356	13.77	14.09	13.02	11.54
50	CGCG 238-041	14.89	15.21	13.76	12.46
51	UGC 4985	13.92	14.27	13.06	11.87
52	NGC 2854	12.45	12.87	11.83	10.89
53	UGC 5046	12.84	13.22	11.92	10.79
54	UGC 5055	13.05	13.50	12.68	11.61
55	NGC 2893	12.65	13.12	12.18	11.15
56	MCG 3-24-062	13.05	13.46	12.21	11.11
57	CGCG 238-066	13.50	13.61	12.77	11.66
58	UGC 5097	13.18	13.56	12.08	10.96
59	CGCG 289-012	13.73	14.12	12.95	11.45
60	MCG 8-18-013	13.08	13.35	11.97	10.33
61	CGCG 181-068	13.20	13.60	12.57	11.48
62	NGC 2936	12.24	12.67	11.99	11.03
63	NGC 2955	12.40	12.82	11.93	10.88
64	CGCG 182-010	13.49	13.72	12.71	11.28
65	UGC 5228	12.62	13.00	12.14	11.30
66	IRAS 09438+1141	14.45	14.83	13.93	12.25
67	NGC 3015	12.76	13.16	11.95	10.73
68	MCG 2-25-039	13.32	13.71	12.30	11.12
69	NGC 3020	13.03	13.50	12.77	12.06
70	NGC 3049	12.38	12.84	11.92	11.16
71	NGC 3055	11.90	12.33	11.18	10.26
72	IC 2520	12.44	12.83	11.23	10.13
73	UGC 5403	12.68	13.10	11.99	10.94
74	UGC 5459	12.12	12.51	11.76	11.04

TABLE 4 — *Continued*

SFRS	Name	3.6 μm	4.5 μm	5.8 μm	8.0 μm
75	MCG 5-24-022	13.12	13.57	12.85	11.81
76	IC 2551	12.90	13.29	11.89	10.74
77	IRAS 10106+2745	14.06	14.40	13.51	11.77
78	NGC 3162	11.79	12.27	11.26	10.33
79	IRAS 10120+1653	15.98	16.06	15.72±0.04	13.81
80	NGC 3190	10.10	10.60	10.50	10.20
81	IC 602	12.78	13.19	11.85	10.79
82	NGC 3191	13.30	13.66	12.46	11.21
83	NGC 3206	12.96	13.41	13.40±0.04	12.62
84	UGC 5613	12.62	12.35	13.02	10.64
85	UGC 5644	13.02	13.48	12.98	12.07
86	NGC 3245	10.54	11.07	11.18	11.37
87	IRAS 10246+2042	13.22	13.62	12.33	11.15
88	MCG 7-22-012	13.05	13.44	12.19	11.11
89	IRAS 10276+1119	14.31	14.48	13.95	12.24
90	NGC 3265	12.82	13.27	12.20	11.18
91	UGC 5713	12.82	12.85	12.26	11.73
92	NGC 3274	13.16	13.58	13.32	13.03
93	UGC 5720	12.86	13.19	12.02	11.03
94	KUG 1031+351	13.24	13.56	12.81	10.67
95	NGC 3306	12.63	13.05	11.67	10.58
96	NGC 3323	13.41	13.83	12.47	11.40
97	IC 2598	13.04	13.39	11.80	10.58
98	NGC 3338	10.91	11.39	10.67	9.81
99	NGC 3353	12.77	13.10	11.99	10.99
100	UGC 5881	12.88	13.18	12.48	11.60
101	NGC 3370	11.75	12.20	11.04	10.13
102	NGC 3381	12.55	12.97	11.99	11.17
103	UGC 5941	13.05	13.34	12.40	11.28
104	NGC 3413	12.24	12.67	12.24	11.80
105	NGC 3408	13.19	13.60	12.83	11.76
106	NGC 3430	13.96	14.06	13.58	12.64
107	CGCG 95-055	10.53	10.98	10.08	9.17
108	IRAS 10565+2448W	13.20	13.21	12.03	10.51
109	UGC 6074	12.97	13.38	12.52	11.47
110	NGC 3495	11.42	11.81	11.27	10.33
111	UGC 6103	12.95	13.30	12.06	10.92
112	MCG 7-23-019	13.37	13.63	12.29	10.92
113	UGC 6135	12.41	12.89	11.93	10.79
114	CGCG 241-078	13.67	13.90	12.74	11.60
115	IRAS 11069+2711	15.60	15.94	15.26±0.04	13.10
116	IC 676	12.19	12.64	11.83	10.99
117	IRAS 11102+3026	14.23	14.48	13.42	12.23
118	IC 2637	12.64	12.96	11.94	10.86
119	MCG 9-19-013	14.17	14.48	13.40	11.77
120	7ZW 384	14.52	14.77	14.31	12.43
121	IRAS 11167+5351	13.60	13.31	12.82	11.91
122	NGC 3633	12.14	12.58	11.43	10.37
123	NGC 3652	12.68	13.08	12.05	11.22
124	NGC 3656	11.78	12.22	11.90	11.18
125	NGC 3659	12.61	13.03	11.97	11.07
126	NGC 3664	13.44	13.85	13.54±0.04	12.84
127	NGC 3666	11.68	12.19	11.31	10.47
128	IC 691	12.72	12.82	11.84	10.84
129	NGC 3686	11.08	11.58	10.72	9.81
130	UGC 6469	13.44	13.83	12.61	11.41
131	NGC 3690	10.38	10.42	9.38	8.33
132	IC 698	12.42	12.82	11.50	10.33
133	IRAS 11267+1558	16.15	16.07	15.75±0.04	13.70
134	NGC 3705	10.50	10.99	10.49	9.84
135	MCG 3-29-061	13.40	13.78	12.58	11.49
136	NGC 3720	15.11	15.62	15.62±0.04	15.16
137	NGC 3729	11.11	11.49	11.28	10.43
138	MCG 10-17-019	13.10	13.49	12.20	10.94
139	NGC 3758	12.03	12.06	11.54	10.92
140	UGC 6583	13.24	13.64	12.17	11.00
141	MCG 1-30-003	13.84	14.16	12.72	11.41
142	NGC 3769	11.68	12.13	11.37	10.59
143	NGC 3773	13.04	13.51	12.86	12.13
144	NGC 3781	12.85	13.12	12.24	11.22
145	UGC 6625	13.28	13.68	12.60	11.26
146	NGC 3808	13.44	13.78	12.41	11.22
147	NGC 3811	12.12	12.57	11.65	10.72
148	NGC 3822	11.87	12.23	11.23	10.12
149	UGC 6665	13.30	13.58	12.37	11.38
150	MCG 3-30-051	13.11	13.50	12.10	10.90

TABLE 4 — *Continued*

SFRS	Name	3.6 μm	4.5 μm	5.8 μm	8.0 μm
151	NGC 3839	12.75	13.10	11.53	10.33
152	UGC 6732	12.33	12.52	12.11	11.50
153	IC 730	12.63	13.02	11.80	10.62
154	IC 732	13.77	14.12	12.91	11.71
155	NGC 3912	12.32	12.73	11.60	10.69
156	NGC 3928	12.11	12.53	11.68	10.73
157	NGC 3934	12.77	13.15	12.22	11.22
158	UGC 6865	12.45	···	11.70	10.67
159	UGC 6901	12.78	13.18	11.86	10.67
160	CGCG 013-010	13.11	13.43	12.32	10.88
161	NGC 3991	12.30	12.65	11.58	10.70
162	NGC 4004	12.91	13.27	11.90	10.91
163	NGC 4014	11.95	12.38	11.41	10.41
164	NGC 4010	11.83	12.22	11.46	10.65
165	NGC 4018	12.65	13.04	11.72	10.66
166	NGC 4020	12.70	13.14	12.53	11.80
167	IRAS 11571+3003	14.83	15.19	14.53	12.93
168	UGC 7017	12.49	12.87	11.37	10.25
169	UGC 7016	12.49	12.92	12.34	11.32
170	MCG 3-31-030	13.53	13.96	12.87	11.88
171	NGC 4062	10.69	11.19	10.55	9.84
172	NGC 4064	11.13	11.59	11.21	10.62
173	CGCG 098-059	12.86	13.13	11.84	10.65
174	NGC 4116	12.22	12.65	11.98	11.00
175	NGC 4136	11.78	12.28	11.65	10.97
176	NGC 4150	11.37	11.85	11.88	11.79
177	IRAS 12086+1441	14.68	14.97	13.78	12.12
178	NGC 4162	11.81	12.28	11.48	10.53
179	NGC 4178	11.33	11.76	11.00	10.32
180	IRAS 12112+0305	14.28	14.43	13.57	11.88
181	NGC 4189	11.53	12.01	11.23	10.20
182	NGC 4194	11.42	11.64	10.12	8.83
183	NGC 4204	13.47	13.63	14.34±0.05	12.47
184	NGC 4207	11.86	12.26	11.31	10.41
185	UGC 7286	13.39	13.85	13.21	12.21
186	NGC 4234	12.70	13.13	12.24	11.22
187	NGC 4237	11.18	11.64	11.15	10.26
188	NGC 4244	10.31	10.72	10.66	10.48
189	NGC 4253	12.35	12.23	11.68	11.03
190	MCG 3-32-005	13.15	13.48	11.95	10.67
191	NGC 4290	11.65	12.08	11.49	10.64
192	NGC 4294	12.13	12.54	11.79	11.12
193	NGC 4314	10.26	10.79	10.87	10.83
194	NGC 4385	12.26	12.69	11.83	10.79
195	NGC 4395	10.13±0.05	10.51±0.05	10.28±0.05	9.94±0.05
196	NGC 4396	12.46	12.91	12.09	11.37
197	NGC 4412	12.16	12.60	11.72	10.78
198	NGC 4418	12.64	12.52	10.69	9.87
199	NGC 4420	12.03	12.43	11.40	10.48
200	NGC 4424	11.46	11.90	11.44	10.88
201	NGC 4435	10.36	11.06	11.18	11.26
202	NGC 4438	9.91	10.43	10.46	10.42
203	NGC 4448	10.42	11.01	11.01	10.77
204	3C 273	10.69	10.51	10.21	10.02
205	NGC 4470	12.56	13.04±0.04	11.87	11.02
206	IRAS 12274+0018	14.57	14.90	13.40	12.24
207	NGC 4491	12.42	···	12.69	···
208	NGC 4500	12.10	12.47	11.49	10.54
209	NGC 4495	12.40	12.77	11.57	10.57
210	IC 3476	12.70	···	10.38	···
211	NGC 4509	14.63	15.01	14.92±0.04	14.34
212	NGC 4519	12.09	12.51	11.96	10.71
213	NGC 4548	9.99	10.49	10.32	9.82
214	IRAS 12337+5044	13.93	14.24	13.04	11.58
215	IC 3581	13.08	13.45	12.45	11.28
216	NGC 4592	12.19	12.63	12.36	11.54
217	NGC 4607	11.87	12.25	11.31	10.48
218	NGC 4625	12.40	12.87	12.11	11.22
219	NGC 4630	12.18	12.61	11.76	10.84
220	IC 3690	13.73	14.11	13.28	12.17
221	UGC 7905	13.77	14.14	12.86	11.81
222	MCG 5-30-069	13.27	13.64	12.29	11.15
223	IC 3721	12.69	13.10	12.18	11.07
224	NGC 4670	12.62	13.11	12.54	11.77
225	NGC 4675	12.96	13.35	12.37	11.34
226	MCG 7-26-051	12.99	13.29	11.98	10.64

TABLE 4 — *Continued*

SFRS	Name	3.6 μm	4.5 μm	5.8 μm	8.0 μm
227	NGC 4689	10.93	11.36	10.71	9.84
228	NGC 4688	13.27	13.54	13.82±0.04	12.53
229	NGC 4704	13.12	13.48	12.84	11.80
230	NGC 4701	12.24	12.66	11.66	10.75
231	IRAS 12468+3436	15.88	15.94	15.47	13.18
232	IRAS 12470+1404	· · ·	15.42	· · ·	13.02
233	MCG 8-23-097	13.30	13.61	12.57	11.36
234	NGC 4747	12.92	13.32	12.53	11.73
235	UGC 8017	12.52	12.95	11.80	10.66
236	NGC 4765	13.10	13.50	12.62	11.76
237	VCC 2096	14.02	14.29	13.69	11.81
238	UGC 8041	12.66	13.04	13.29±0.04	11.94
239	UGC 8058	9.81	9.52	9.06	8.45
240	NGC 4837	12.96	13.32	12.27	11.18
241	UM 530	15.24	15.45	14.83±0.04	12.91
242	NGC 4861	13.00±0.05	13.35±0.05	12.08±0.05	12.75±0.05
243	NGC 4868	11.89	12.33	11.31	10.33
244	NGC 4922	12.79	12.59	11.72	10.81
245	UGC 8179	13.13	13.54	12.88	11.58
246	NGC 5001	12.69	13.07	11.98	10.74
247	IC 856	13.20	13.60	12.31	11.24
248	UGC 8269	13.64	13.95	12.99	11.86
249	NGC 5014	12.48	12.91	11.92	10.99
250	NGC 5012	11.28	11.77	10.97	10.12
251	IRAS 13116+4508	14.84	15.17	14.68±0.04	12.75
252	IC 860	13.07	13.53	12.98	12.13
253	IRAS 13144+4508	· · ·	12.03	· · ·	10.96
254	NGC 5060	12.60	13.01	12.09	11.00
255	UGC 8357	13.12	13.48	12.27	10.98
256	UGC 8361	13.01	13.39	12.26	11.08
257	IC 883	12.75	12.88	11.38	10.20
258	NGC 5100	12.69	12.93	12.03	10.92
259	NGC 5104	12.10	12.45	11.49	10.46
260	NGC 5107	13.53	13.97	13.81±0.04	13.39
261	NGC 5112	12.11	12.61	11.96	11.22
262	NGC 5123	12.46	12.89	11.93	10.82
263	IRAS 13218+0552	11.90	11.44	10.85	10.29
264	IRAS 13232+1731	14.07	14.42	13.96	11.83
265	NGC 5147	11.98	12.41	11.43	10.68
266	NGC 5204	11.97	12.39	12.21	11.70
267	UGC 8502	13.97	14.28	13.10	11.78
268	UGC 8561	12.77	13.16	11.81	10.69
269	NGC 5230	12.25	12.70	12.00	10.86
270	IRAS 13349+2438	· · ·	11.51	10.59	10.12
271	NGC 5256	12.62	12.86	11.85	10.74
272	UGC 8626	13.24	13.66	12.87	11.76
273	NGC 5263	12.40	12.80	11.50	10.40
274	MCG 1-35-028	13.08	13.43	12.46	11.34
275	IC 910	13.34	13.48	12.40	11.23
276	MK 268	13.24	13.20	12.61	11.97
277	NGC 5278	12.56	13.00	12.42	11.45
278	NGC 5273	11.26	11.73	11.91	12.22
279	UGC 8685	13.13	13.49	12.69	11.53
280	UGC 8686	12.99	13.35	12.35	11.22
281	UGC 8696	12.69	12.37	11.40	10.49
282	NGC 5297	11.37	11.82	11.10	10.36
283	MK 796	12.67	12.56	11.82	10.93
284	IRAS 13446+1121	12.76	12.66	11.89	10.96
285	NGC 5303	12.45	12.85	11.43	10.35
286	NGC 5313	11.33	11.77	10.91	9.99
287	MCG 3-35-034	13.25	13.62	12.89	11.62
288	NGC 5347	12.64	12.71	12.11	11.39
289	NGC 5350	11.07	11.42	11.07	10.24
290	NGC 5368	12.67	13.15	12.55	11.57
291	UGC 8827	12.59	12.93	11.96	10.89
292	UGC 8850	10.80	10.48	10.09	9.72
293	UGC 8856	13.61	13.93	12.47	11.19
294	NGC 5374	12.22	12.60	11.62	10.58
295	UGC 8902	12.45	12.91	12.38	11.46
296	NGC 5403	11.50	11.91	11.16	10.40
297	MCG 7-29-036	13.97	14.30	13.27	11.98
298	NGC 5414	13.19	13.55	12.30	11.23
299	MCG 5-33-046	13.35	13.70	12.72	11.61
300	NGC 5474	12.16	12.62	12.46	12.05
301	NGC 5480	11.03	11.45	10.19	9.21
302	MCG 6-31-070	13.40	13.72	12.54	11.23

TABLE 4 — *Continued*

SFRS	Name	3.6 μm	4.5 μm	5.8 μm	8.0 μm
303	CGCG 074-129	13.37	13.29	12.27	11.34
304	NGC 5520	12.33	12.75	11.75	10.72
305	NGC 5515	12.29	12.69	11.85	10.80
306	NGC 5526	12.63	13.03	11.94	10.94
307	NGC 5522	12.33	12.78	12.03	11.04
308	NGC 5541	12.69	13.10	11.96	10.80
309	IC 4395	12.80	13.20	12.36	11.13
310	UGC 9165	12.49	12.86	11.57	10.44
311	MK 1490	13.35	13.58	12.27	10.94
312	NGC 5585	11.75	12.29	12.04	11.71
313	IC 4408	12.78	13.17	12.12	10.86
314	NGC 5584	11.83	12.25	11.54	10.75
315	NGC 5633	11.95	12.37	11.25	10.26
316	NGC 5660	11.80	12.22	11.33	10.25
317	NGC 5656	11.75	12.21	11.31	10.43
318	NGC 5657	···	13.25	···	11.33
319	CGCG 133-083	13.95	14.19	13.01	11.44
320	MCG 7-30-028	13.24	13.66	12.44	11.21
321	MCG 6-32-070	12.86	13.24	11.78	10.52
322	UGC 9412	10.93	10.71	10.36	9.62
323	NGC 5698	12.60	13.04	12.42	11.52
324	NGC 5691	12.18	12.65	11.61	10.74
325	MCG 9-24-035	13.00	13.43	12.79	11.72
326	MCG 9-24-038	13.46	13.80	12.63	11.20
327	UGC 9560	15.83	15.23	15.92	14.07
328	IC 1076	13.15	13.53	12.21	11.09
329	IRAS 14538+1730	14.56	14.68	14.29	12.20
330	NGC 5795	12.21	12.64	11.52	10.47
331	UGC 9618	12.31	12.57	11.38	10.09
332	UGC 9639	12.69	12.96	12.00	10.67
333	MCG 6-33-022	13.42	13.71	12.62	11.10
334	NGC 5879	11.19	11.66	10.84	10.08
335	MCG 9-25-036	14.10	14.52	13.54	12.22
336	NGC 5899	11.12	11.50	10.75	9.89
337	NGC 5905	10.89	11.34	10.59	9.66
338	MK 848	13.31	13.44	12.20	10.69
339	IC 4553	12.11	12.25	11.08	10.07
340	UGC 9922	13.41	13.79	12.28	11.14
341	IC 4567	12.38	12.79	11.72	10.62
342	MCG 4-37-016	13.61	13.96	13.09	12.03
343	NGC 5975	12.30	12.73	11.79	10.75
344	NGC 5980	11.81	12.22	11.20	10.22
345	NGC 5992	13.45	13.79	12.38	11.08
346	NGC 5996	12.33	12.72	11.61	10.65
347	IRAS 15519+3537	14.55	14.86	14.28	12.00
348	UGC 10099	13.59	13.94	12.66	11.32
349	MCG 5-38-006	12.93	13.37	12.24	11.15
350	UGC 10120	12.55	12.51	12.13	11.61
351	NGC 6027A	12.72	13.18	13.06	12.54
352	NGC 6040	13.12	13.52	13.32	12.36
353	UGC 10200	13.81	14.10	13.15	12.35
354	IRAS 16052+5334	14.43	14.63	14.10	11.84
355	IRAS 16053+1836	13.40	13.73	12.60	11.21
356	NGC 6090	12.84	13.14	11.62	10.34
357	UGC 10273	13.88	14.24	12.93	11.81
358	IRAS 16150+2233	14.75	14.55	13.91	12.77
359	UGC 10322	12.70	13.11	11.78	10.67
360	NGC 6120	12.62	12.98	11.64	10.31
361	MCG 3-42-004	13.43	13.79	13.02	11.65
362	UGC 10407	13.78	14.13	12.73	11.55
363	IRAS 16320+3922	13.40	13.86	13.20	12.15
364	NGC 6186	12.00	12.43	11.73	10.78
365	MCG 9-27-053	13.71	14.05	13.10	11.94
366	UGC 10514	13.36	13.74	12.27	11.10
367	IRAS 16435+2154	14.00	14.33	12.94	11.61
368	IC 4623	13.36	13.74	12.69	11.43
369	IRAS 16516+3030	13.91	14.18	13.60	11.48

NOTE. — Table 4 is published in its entirety in the electronic edition of *Publications of the Astronomical Society of the Pacific*. All magnitudes are expressed on the AB system. Where uncertainties are not given, they are dominated by the uncertainty in the cryogenic IRAC absolute flux calibration (3%, 1σ).

TABLE 5
1.4 GHz Flux Measurements for SFRS Galaxies

SFRS	Name	Position[a] (J2000)	Offset[b] (arcsec)	F(1.4 GHz) (mJy)	References[c]	Remarks[d]
1	IC 486	08:00:20.98 +26:36:50.2	1.5	10.2±0.5	1	
2	IC 2217	08:00:49.89 +27:30:01.9	2.2	18.8±0.7	1	
3	NGC 2500	08:01:52.41 +50:44:25.6	14.0	14.7±3.2	1	E*
4	NGC 2512	08:03:07.86 +23:23:31.6	1.1	18.6±0.7	1	
5	MCG 6-18-009	08:03:28.82 +33:27:44.4	1.5	17.9±0.7	1	
6	MK 1212	08:07:05.61 +27:07:33.8	1.2	12.4±0.6	1	
7	IRAS 08072+1847	08:10:07.18 +18:38:17.8	2.4	6.8±0.4	1	
8	NGC 2532	08:10:15.43 +33:57:25.9	3.9	46.5±2.1	1	
9	UGC 4261	08:10:56.46 +36:49:47.3	6.7	8.2±0.5	1	
10	NGC 2535	08:11:13.63 +25:12:27.1	13.9	18.2±1.9	1,2	E*
11	NGC 2543	08:12:57.84 +36:15:15.2	1.7	12.2±0.9	1	
12	NGC 2537	08:13:14.03 +45:59:37.3	17.1	10.5±1.7	1	E*
13	IC 2233	08:13:58.82 +45:44:43.7	· · ·	<2.0	2	
14	IC 2239	08:14:07.01 +23:51:59.7	3.1	12.5±0.6	1	
15	UGC 4286	08:14:16.50 +18:26:26.0	· · ·	3.9±0.6	3	D
16	UGC 4306	08:17:36.83 +35:26:45.0	6.4	27.1±0.9	1	
17	NGC 2552	08:19:19.58 +50:00:20.8	· · ·	<0.4	3	
18	IC 2339	08:23:33.04 +21:20:27.0	29.4	6.0±0.9	2	D,E*
19	IRAS 08234+1054B	08:26:07.73 +10:44:52.5	2.8	8.9±0.5	1	
20	IRAS 08269+1514	08:29:45.30 +15:04:38.1	2.1	6.5±0.5	1	
21	NGC 2604	08:33:22.54 +29:32:14.9	9.1	9.4±1.0	1	
22	NGC 2608	08:35:17.19 +28:28:23.2	7.8	15.2±1.4	1	
23	MK 92	08:35:40.17 +46:29:33.8	6.1	24.3±1.1	1	
24	NGC 2623	08:38:24.10 +25:45:16.3	1.3	95.7±2.9	1	
25	CGCG 120-018	08:39:50.61 +23:08:37.5	2.5	12.3±0.5	1	
26	NGC 2644	08:41:32.07 +04:58:53.3	5.3	11.8±1.0	1	
27	UGC 4572	08:45:37.83 +36:56:04.4	0.5	8.1±0.5	1	
28	UGC 4653	08:53:54.40 +35:08:56.4	12.6	38.0±1.5	1	
29	IRAS 08512+2727	08:54:16.83 +27:16:01.0	1.7	8.1±0.5	1	
30	OJ 287	08:54:48.87 +20:06:30.7	0.1	1511.8±5.4	1	
31	IRAS 08538+4256	08:57:10.48 +42:45:24.2	2.1	21.0±0.7	1	
32	IRAS 08550+3908	08:58:13.98 +38:56:30.8	2.9	24.0±0.8	1	
33	NGC 2718	08:58:50.63 +06:17:33.7	2.7	29.6±1.6	1	
34	NGC 2712	08:59:30.62 +44:54:48.9	1.9	12.4±1.0	1	
35	NGC 2719	09:00:15.72 +35:43:28.6	10.8	29.7±1.6	1	B
36	IRAS 08572+3915	09:00:25.58 +39:03:52.8	2.6	4.3±0.4	1	
37	IRAS 08579+3447	09:01:05.81 +34:35:28.5	0.3	24.4±0.8	1	
38	NGC 2731	09:02:08.38 +08:18:02.7	3.3	23.9±1.1	1	
39	NGC 2730	09:02:15.80 +16:50:15.4	2.5	8.9±1.3	1	
40	IC 2431	09:04:34.84 +14:35:38.8	6.6	104.1±3.7	1	
41	NGC 2750	09:05:47.77 +25:26:21.2	6.6	25.0±1.7	1	
42	IC 2434	09:07:15.96 +37:12:55.8	1.3	21.2±1.0	1	
43	NGC 2761	09:07:30.91 +18:26:04.7	1.1	28.0±0.9	1	
44	NGC 2773	09:09:44.15 +07:10:25.6	0.1	22.6±0.8	1	
45	NGC 2776	09:12:14.26 +44:57:22.8	6.0	31.1±2.5	1	
46	NGC 2789	09:14:59.62 +29:43:49.1	0.7	18.3±0.7	1	
47	IRAS 09121+3908	09:15:22.15 +38:56:35.0	· · ·	5.4±0.7	2	D*
48	NGC 2824	09:19:02.27 +26:16:12.7	0.9	8.9±0.5	1	
49	IRAS 09184+4356	09:21:38.62 +43:43:36.0	2.2	9.8±0.5	1	
50	CGCG 238-041	09:22:25.58 +47:14:40.8	3.0	8.4±0.9	1	
51	UGC 4985	09:22:37.65 +21:57:28.9	4.2	6.1±0.5	1	
52	NGC 2854	09:24:02.92 +49:12:13.4	0.9	18.8±1.0	1	
53	UGC 5046	09:28:06.54 +17:11:46.8	1.7	22.1±0.8	1	
54	UGC 5055	09:30:11.76 +55:51:09.9	1.2	11.4±0.5	1	
55	NGC 2893	09:30:17.00 +29:32:25.6	1.7	7.4±0.5	1	
56	MCG 3-24-062	09:30:23.02 +19:28:11.7	2.5	11.5±0.5	1	
57	CGCG 238-066	09:31:06.67 +49:04:48.5	1.7	8.9±0.5	1	
58	UGC 5097	09:34:10.68 +00:14:31.9	0.8	27.7±1.2	1	
59	CGCG 289-012	09:36:31.92 +59:23:53.8	0.6	13.6±0.6	1	
60	MCG 8-18-013	09:36:36.98 +48:28:21.2	7.1	34.1±1.5	1	
61	CGCG 181-068	09:37:19.34 +33:49:27.2	2.0	12.6±0.6	1	
62	NGC 2936	09:37:44.02 +02:45:33.4	5.8	29.2±1.5	1	
63	NGC 2955	09:41:16.78 +35:52:58.1	2.9	12.9±0.6	1	
64	CGCG 182-010	09:45:15.06 +34:42:46.5	3.0	12.1±0.5	1	
65	UGC 5228	09:46:03.60 +01:40:06.1	· · ·	13.7±2.1	2	D,E*
66	IRAS 09438+1141	09:46:32.33 +11:27:20.5	3.6	9.6±1.1	1	
67	NGC 3015	09:49:22.97 +01:08:43.4	0.7	20.5±0.8	1	
68	MCG 2-25-039	09:49:37.05 +09:00:18.2	1.1	14.7±0.6	1	
69	NGC 3020	09:50:06.65 +12:48:49.0	· · ·	44.0±4.0	2	E
70	NGC 3049	09:54:49.49 +09:16:13.6	2.6	9.1±1.1	1	
71	NGC 3055	09:55:17.99 +04:16:11.2	1.6	36.6±1.8	1	
72	IC 2520	09:56:20.22 +27:13:39.9	1.6	24.1±1.4	1	
73	UGC 5403	10:02:35.57 +19:10:36.7	0.4	11.8±0.5	1	

TABLE 5 — *Continued*

SFRS	Name	Position[a] (J2000)	Offset[b] (arcsec)	F(1.4 GHz) (mJy)	References[c]	Remarks[d]
74	UGC 5459	10:08:08.87 +53:05:12.2	15.3	16.6±2.0	1,2	E*
75	MCG 5-24-022	10:10:02.78 +32:04:09.1	8.6	5.6±0.4	1	
76	IC 2551	10:10:40.30 +24:24:50.0	1.0	25.8±0.9	1	
77	IRAS 10106+2745	10:13:29.51 +27:30:41.0	0.9	8.1±0.5	1	
78	NGC 3162	10:13:31.68 +22:44:17.4	2.5	18.0±1.9	1	
79	IRAS 10120+1653	10:14:47.95 +16:38:48.6	1.6	9.7±0.5	1	
80	NGC 3190	10:18:06.60 +21:49:27.4	···	5.0±2.0	2	D,E*
81	IC 602	10:18:19.75 +07:02:55.0	2.6	29.7±1.5	1	
82	NGC 3191	10:19:05.05 +46:27:16.9	2.3	12.8±0.6	1	
83	NGC 3206	10:21:43.30 +56:55:16.0	···	0.8±0.2	3	E*
84	UGC 5613	10:23:32.53 +52:20:31.5	0.2	49.6±1.5	1	
85	UGC 5644	10:25:46.10 +13:43:04.1	4.0	13.1±0.9	1	
86	NGC 3245	10:27:18.18 +28:30:27.2	3.1	6.7±0.5	1	
87	IRAS 10246+2042	10:27:25.76 +20:26:54.8	3.7	12.3±0.9	1	
88	MCG 7-22-012	10:30:11.16 +43:21:37.9	2.9	12.1±0.5	1	
89	IRAS 10276+1119	10:30:14.81 +11:04:11.8	4.1	5.8±0.4	1	
90	NGC 3265	10:31:06.87 +28:47:51.9	4.2	10.1±0.9	1	
91	UGC 5713	10:31:41.38 +25:59:16.6	···	<1.0	2	D
92	NGC 3274	10:32:17.49 +27:40:10.5	4.4	4.3±0.7	1	
93	UGC 5720	10:32:31.98 +54:24:02.4	1.6	16.6±0.6	1	
94	KUG 1031+351	10:34:02.44 +34:52:10.0	0.6	38.3±1.5	1	
95	NGC 3306	10:37:10.26 +12:39:08.8	0.7	23.3±0.8	1	
96	NGC 3323	10:39:39.05 +25:19:20.3	1.6	13.4±0.6	1	
97	IC 2598	10:39:42.38 +26:43:38.4	0.2	27.2±0.9	1	
98	NGC 3338	10:42:06.58 +13:44:47.5	···	42.7±4.0	2	D,E*
99	NGC 3353	10:45:22.26 +55:57:40.9	2.0	15.5±0.9	1	
100	UGC 5881	10:46:42.55 +25:55:52.7	0.9	10.7±0.5	1	
101	NGC 3370	10:47:04.14 +17:16:30.3	5.3	24.9±1.9	1	
102	NGC 3381	10:48:24.96 +34:42:30.4	10.8	7.6±0.6	2	E*
103	UGC 5941	10:50:21.60 +41:27:50.5	···	12.5±1.0	2	D,E*
104	NGC 3413	10:51:20.48 +32:46:01.7	4.2	5.1±0.5	1	
105	NGC 3408	10:52:11.96 +58:26:18.4	2.4	6.1±0.5	1	
106	NGC 3430	10:52:11.18 +32:57:02.2	2.8	32.7±2.2	1	*
107	CGCG 95-055	10:52:50.51 +16:59:07.6	3.3	10.5±0.5	1	D*
108	IRAS 10565+2448W	10:59:18.20 +24:32:35.0	1.1	57.0±2.1	1	E
109	UGC 6074	10:59:58.17 +50:54:11.7	1.3	8.8±0.5	1	
110	NGC 3495	11:01:16.05 +03:37:42.6	···	25.8±2.0	2	E*
111	UGC 6103	11:01:58.92 +45:13:43.3	2.5	14.6±0.6	1	
112	MCG 7-23-019	11:03:53.89 +40:50:59.9	4.7	36.4±1.2	1	
113	UGC 6135	11:04:36.82 +45:07:31.4	1.6	17.4±1.0	1	
114	CGCG 241-078	11:06:37.37 +46:02:19.2	0.4	16.3±0.6	1	
115	IRAS 11069+2711	11:09:38.90 +26:54:56.0	···	2.4±0.8	2	D*
116	IC 676	11:12:39.82 +09:03:22.5	1.5	9.7±0.5	1	
117	IRAS 11102+3026	11:12:57.50 +30:10:30.0	2.3	10.5±0.5	1	
118	IC 2637	11:13:49.71 +09:35:10.5	0.7	42.2±1.3	1	
119	MCG 9-19-013	11:14:49.37 +50:19:22.5	···	6.2±1.2	2	D*
120	7ZW 384	11:16:54.03 +59:31:48.7	···	17.8±1.8	2	D*
121	IRAS 11167+5351	11:19:34.31 +53:35:18.3	2.7	16.1±0.6	1	
122	NGC 3633	11:20:26.27 +03:35:08.5	1.0	19.4±1.0	1	
123	NGC 3652	11:22:38.66 +37:45:55.3	4.4	22.9±1.5	1	
124	NGC 3656	11:23:38.43 +53:50:32.9	2.3	19.8±0.7	1	
125	NGC 3659	11:23:45.45 +17:49:03.2	4.1	12.8±1.4	1	
126	NGC 3664	11:24:25.16 +03:19:32.8	13.5	9.4±1.9	2	E*
127	NGC 3666	11:24:26.28 +11:20:27.9	5.2	16.8±1.7	1	
128	IC 691	11:26:44.48 +59:09:00.2	19.4	37.8±1.8	1	B,E*
129	NGC 3686	11:27:43.99 +17:13:29.5	2.5	15.8±2.0	1	
130	UGC 6469	11:28:17.77 +02:39:14.7	1.0	18.1±1.0	1	
131	NGC 3690	11:28:32.61 +58:33:46.8	9.8	677.1±5.4	1	
132	IC 698	11:29:03.78 +09:06:42.7	1.1	31.1±1.0	1	
133	IRAS 11267+1558	11:29:24.80 +15:41:41.9	1.6	3.1±0.4	1	
134	NGC 3705	11:30:08.19 +09:16:26.4	···	20.6±0.7	2	E*
135	MCG 3-29-061	11:31:03.67 +20:14:08.3	0.4	8.2±0.5	1	
136	NGC 3720	11:32:21.76 +00:48:14.9	2.5	11.1±0.6	1	
137	NGC 3729	11:33:49.36 +53:07:33.5	1.6	21.0±1.5	1	
138	MCG 10-17-019	11:35:24.67 +57:38:59.7	1.0	14.1±0.6	1	
139	NGC 3758	11:36:29.17 +21:35:49.1	4.1	10.0±0.5	1	
140	UGC 6583	11:36:54.25 +19:58:19.4	2.0	18.6±0.7	1	
141	MCG 1-30-003	11:37:06.84 +02:50:44.7	···	9.7±0.5	2	D*
142	NGC 3769	11:37:44.27 +47:53:27.9	7.4	19.7±1.9	1	
143	NGC 3773	11:38:12.90 +12:06:45.5	2.6	5.8±0.5	1	
144	NGC 3781	11:39:03.72 +26:21:43.0	1.0	50.1±1.6	1	
145	UGC 6625	11:39:47.55 +19:55:58.5	1.8	17.4±1.3	1	
146	NGC 3808	11:40:44.53 +22:26:42.9	6.3	25.5±1.3	1	
147	NGC 3811	11:41:13.17 +47:41:45.7	···	16.0±2.0	2	D,E*

TABLE 5 — *Continued*

SFRS	Name	Position[a] (J2000)	Offset[b] (arcsec)	F(1.4 GHz) (mJy)	References[c]	Remarks[d]
148	NGC 3822	11:42:11.12 +10:16:39.0	1.2	34.0±1.1	1	
149	UGC 6665	11:42:12.34 +00:20:03.2	2.1	32.6±1.4	1	
150	MCG 3-30-051	11:42:24.49 +20:07:11.8	2.3	12.2±0.6	1	
151	NGC 3839	11:43:54.33 +10:47:04.7	0.1	47.4±1.8	1	
152	UGC 6732	11:45:32.92 +58:58:42.1	2.0	5.1±0.5	1	
153	IC 730	11:45:35.24 +03:13:54.6	0.2	22.8±0.8	1	
154	IC 732	11:45:59.83 +20:26:28.7	21.4	18.8±1.0	1	B*
155	NGC 3912	11:50:04.40 +26:28:44.7	1.0	21.3±1.1	1	
156	NGC 3928	11:51:47.44 +48:41:01.3	2.7	12.2±0.6	1	
157	NGC 3934	11:52:12.70 +16:51:01.8	4.9	28.0±1.3	1	
158	UGC 6865	11:53:40.08 +43:27:37.3	2.4	19.4±1.1	1	
159	UGC 6901	11:55:38.36 +43:02:44.4	0.7	16.9±0.7	1	
160	CGCG 013-010	11:57:06.01 +01:07:32.1	1.2	39.0±1.2	1	
161	NGC 3991	11:57:31.08 +32:20:16.0	3.1	34.4±1.5	1	
162	NGC 4004	11:58:05.10 +27:52:41.7	2.8	29.2±1.6	1	
163	NGC 4014	11:58:35.82 +16:10:38.3	0.3	20.0±1.0	1	
164	NGC 4010	11:58:36.54 +47:15:33.0	16.1	20.3±2.3	1	E*
165	NGC 4018	11:58:40.51 +25:19:02.3	5.0	29.9±1.3	1	
166	NGC 4020	11:58:58.26 +30:24:55.2	23.8	6.8±1.7	1	B,E*
167	IRAS 11571+3003	11:59:42.72 +29:47:17.6	···	1.4±0.2	3	*
168	UGC 7017	12:02:22.37 +29:51:43.0	2.0	35.6±1.5	1	
169	UGC 7016	12:02:24.11 +14:50:36.5	2.0	11.9±0.6	1	
170	MCG 3-31-030	12:03:35.71 +16:03:15.6	5.6	2.7±0.5	1	
171	NGC 4062	12:04:02.42 +31:53:41.6	18.4	7.3±1.5	1	E*
172	NGC 4064	12:04:10.95 +18:26:40.6	3.3	9.5±0.5	1	
173	CGCG 098-059	12:07:09.52 +16:59:42.2	2.0	18.3±1.0	1	
174	NGC 4116	12:07:36.88 +02:41:30.4	2.1	17.3±2.7	1	
175	NGC 4136	12:09:17.71 +29:55:39.4	···	14.6±1.7	2	E
176	NGC 4150	12:10:33.71 +30:24:55.2	···	<2.0	2	B
177	IRAS 12086+1441	12:11:14.43 +14:24:41.6	6.4	6.3±0.4	1	
178	NGC 4162	12:11:53.50 +24:07:09.7	6.9	34.2±1.9	1	
179	NGC 4178	12:12:46.13 +10:52:06.2	11.8	30.3±2.7	4	E*
180	IRAS 12112+0305	12:13:45.94 +02:48:40.8	2.2	23.3±0.8	1	
181	NGC 4189	12:13:48.85 +13:25:30.2	23.2	17.8±2.0	4	E*
182	NGC 4194	12:14:09.67 +54:31:35.9	0.2	100.7±3.0	1	
183	NGC 4204	12:15:14.45 +20:39:30.9	···	<0.4	3	
184	NGC 4207	12:15:30.42 +09:35:05.4	1.3	18.7±1.4	1	
185	UGC 7286	12:15:59.03 +27:26:35.1	4.3	2.9±0.4	1	
186	NGC 4234	12:17:08.89 +03:40:55.2	5.7	4.9±0.4	1	E*
187	NGC 4237	12:17:11.51 +15:19:21.4	5.1	6.0±0.5	1	
188	NGC 4244	12:17:27.57 +37:47:45.6	···	27.7±2.8	2	E*
189	NGC 4253	12:18:26.43 +29:48:47.3	1.4	38.1±1.2	1	
190	MCG 3-32-005	12:20:47.22 +17:00:57.4	0.5	25.4±0.9	1	
191	NGC 4290	12:20:47.33 +58:05:34.0	1.8	18.9±1.3	1	
192	NGC 4294	12:21:17.68 +11:30:41.0	14.1	21.1±1.6	1	E*
193	NGC 4314	12:22:31.94 +29:53:45.2	1.7	13.1±1.0	1	
194	NGC 4385	12:25:42.83 +00:34:23.4	2.1	13.1±0.6	1	
195	NGC 4395	12:25:48.86 +33:32:48.7	···	78.0±8.0	2	E*
196	NGC 4396	12:25:58.94 +15:40:12.7	4.3	20.3±2.1	1	
197	NGC 4412	12:26:36.09 +03:57:52.8	0.3	14.6±0.6	1	
198	NGC 4418	12:26:54.54 -00:52:38.8	1.4	40.8±1.3	1	
199	NGC 4420	12:26:58.50 +02:29:40.0	···	<4.0	2,3	*
200	NGC 4424	12:27:10.53 +09:25:02.8	19.8	3.9±0.6	1	*
201	NGC 4435	12:27:40.46 +13:04:44.4	···	<1.5	2	
202	NGC 4438	12:27:45.56 +13:00:31.0	1.2	63.3±2.7	1	
203	NGC 4448	12:28:15.46 +28:37:13.1	···	5.1±0.8	2	E*
204	3C 273	12:29:06.41 +02:03:05.1	5.5	54991.2±1900.3	1	
205	NGC 4470	12:29:38.01 +07:49:18.4	9.4	15.5±1.6	1	
206	IRAS 12274+0018	12:29:58.80 +00:01:38.0	···	<0.9	3	*
207	NGC 4491	12:30:57.10 +11:29:01.0	···	<4.5	3	*
208	NGC 4500	12:31:22.14 +57:57:52.9	0.5	28.2±1.2	4	
209	NGC 4495	12:31:22.82 +29:08:11.4	0.9	30.1±1.0	1	
210	IC 3476	12:32:41.64 +14:03:03.1	3.8	7.5±1.1	1	
211	NGC 4509	12:33:06.21 +32:05:27.0	9.9	2.9±0.4	1	
212	NGC 4519	12:33:30.62 +08:39:11.2	···	25.6±1.6	2	
213	NGC 4548	12:35:26.45 +14:29:46.8	···	5.0±2.0	2	E
214	IRAS 12337+5044	12:36:06.96 +50:28:16.8	3.1	13.0±0.5	1	
215	IC 3581	12:36:37.93 +24:25:44.1	1.9	13.9±0.6	1	
216	NGC 4592	12:39:18.68 -00:31:53.1	2.1	6.7±1.4	1	
217	NGC 4607	12:41:12.75 +11:53:12.1	7.8	22.9±1.6	1	
218	NGC 4625	12:41:52.73 +41:16:26.2	···	5.6±2.0	2	D,E*
219	NGC 4630	12:42:31.98 +03:57:39.6	13.1	12.6±1.2	1	E*
220	IC 3690	12:42:49.29 +10:21:22.3	4.8	6.9±0.5	1	
221	UGC 7905	12:43:47.88 +54:53:48.0	2.8	16.9±0.6	1	

TABLE 5 — *Continued*

SFRS	Name	Position[a] (J2000)	Offset[b] (arcsec)	F(1.4 GHz) (mJy)	References[c]	Remarks[d]
222	MCG 5-30-069	12:44:41.27 +26:25:10.7	0.3	9.8±0.5	1	
223	IC 3721	12:44:53.16 +18:45:18.4	0.9	23.5±1.1	1	
224	NGC 4670	12:45:17.11 +27:07:30.4	2.6	13.7±1.0	1	
225	NGC 4675	12:45:32.02 +54:44:15.4	1.1	14.2±0.6	1	
226	MCG 7-26-051	12:46:56.70 +42:16:00.4	2.0	31.3±1.0	1	
227	NGC 4689	12:47:44.61 +13:45:44.1	13.9	12.5±1.8	1	E
228	NGC 4688	12:47:44.35 +04:19:04.4	···	<2.6	2	*
229	NGC 4704	12:48:46.57 +41:55:17.7	1.9	9.8±0.9	1	
230	NGC 4701	12:49:11.68 +03:23:21.5	2.5	18.5±1.6	1	
231	IRAS 12468+3436	12:49:17.27 +34:19:52.1	···	5.1±0.2	1,3	*
232	IRAS 12470+1404	12:49:34.78 +13:48:11.4	···	2.3±0.2	1,3	*
233	MCG 8-23-097	12:50:39.80 +47:56:00.6	0.5	29.7±1.0	1	
234	NGC 4747	12:51:45.59 +25:46:26.1	4.0	7.4±0.5	1	
235	UGC 8017	12:52:53.59 +28:22:16.1	0.5	28.9±1.2	1	
236	NGC 4765	12:53:14.43 +04:27:50.8	3.7	17.6±1.3	1	
237	VCC 2096	12:53:24.79 +11:42:38.1	1.7	19.9±0.7	1	
238	UGC 8041	12:55:12.60 +00:07:00.0	···	<1.5	3	E
239	UGC 8058	12:56:14.13 +56:52:23.8	1.8	308.9±2.1	1	
240	NGC 4837	12:56:48.30 +48:17:50.7	1.7	25.5±1.1	1	
241	UM 530	12:58:08.45 +01:51:43.1	···	4.3±0.5	3	A*
242	NGC 4861	12:59:00.25 +34:50:48.3	···	14.4±1.4	2	D,E*
243	NGC 4868	12:59:08.92 +37:18:36.8	0.7	26.5±1.4	1	
244	NGC 4922	13:01:25.23 +29:18:50.3	1.0	38.8±1.2	1	
245	UGC 8179	13:05:14.13 +31:59:58.0	1.1	16.6±1.0	1	
246	NGC 5001	13:09:33.47 +53:29:39.2	3.1	24.6±1.1	1	
247	IC 856	13:10:41.67 +20:32:13.5	5.6	12.6±0.6	1	
248	UGC 8269	13:11:15.11 +46:42:00.6	1.8	18.7±0.7	1	
249	NGC 5014	13:11:31.16 +36:16:55.1	1.0	11.4±0.5	1	
250	NGC 5012	13:11:37.05 +22:54:53.0	2.8	29.7±1.9	1	
251	IRAS 13116+4508	13:13:47.90 +44:52:59.0	···	<0.5	3	
252	IC 860	13:15:03.47 +24:37:07.2	0.7	30.8±1.0	1	
253	IRAS 13144+4508	13:16:39.64 +44:52:35.1	1.2	5.9±0.4	1	
254	NGC 5060	13:17:16.29 +06:02:14.0	1.2	16.2±0.6	1	
255	UGC 8357	13:17:58.74 -00:18:42.5	1.0	20.4±1.0	1	
256	UGC 8361	13:18:18.60 +06:20:06.4	1.0	17.3±0.7	1	
257	IC 883	13:20:35.38 +34:08:22.6	1.1	104.4±3.2	1	
258	NGC 5100	13:20:59.58 +08:58:41.5	0.5	102.3±3.1	1	
259	NGC 5104	13:21:23.16 +00:20:33.4	1.3	39.9±1.3	1	
260	NGC 5107	13:21:23.40 +38:32:18.5	15.5	4.5±0.5	1	*
261	NGC 5112	13:21:59.25 +38:44:17.0	···	22.4±3.0	2	E*
262	NGC 5123	13:23:10.45 +43:05:13.0	2.6	18.7±1.3	1	
263	IRAS 13218+0552	13:24:19.96 +05:37:01.2	···	2.8±0.2	3	*
264	IRAS 13232+1731	13:25:43.79 +17:15:53.2	1.3	11.2±0.5	1	
265	NGC 5147	13:26:20.29 +02:06:02.9	8.4	25.2±2.6	1	
266	NGC 5204	13:29:36.38 +58:24:46.2	···	18.8±4.4	2	E
267	UGC 8502	13:30:38.79 +31:17:06.7	8.3	7.7±0.5	1	
268	UGC 8561	13:34:57.16 +34:02:38.9	1.3	29.3±1.5	1	
269	NGC 5230	13:35:31.05 +13:40:33.4	12.0	14.5±1.7	1	*
270	IRAS 13349+2438	13:37:18.73 +24:23:02.8	0.6	19.6±0.7	1	
271	NGC 5256	13:38:17.60 +48:16:38.4	5.3	126.3±4.5	1	
272	UGC 8626	13:38:23.52 +06:53:14.7	1.2	6.3±0.4	1	
273	NGC 5263	13:39:55.53 +28:23:59.4	3.7	38.0±1.8	1	
274	MCG 1-35-028	13:40:27.31 +04:46:27.8	2.7	15.8±0.6	1	
275	IC 910	13:41:07.85 +23:16:56.2	0.8	38.7±1.2	1	
276	MK 268	13:41:11.09 +30:22:41.3	0.6	42.5±1.3	1	
277	NGC 5278	13:41:39.81 +55:40:14.7	4.8	23.1±1.1	1	
278	NGC 5273	13:42:08.92 +35:39:12.4	7.3	3.5±0.4	1	
279	UGC 8685	13:43:08.76 +30:20:14.7	1.5	15.4±0.6	1	
280	UGC 8686	13:43:40.34 +03:53:48.5	3.4	14.7±0.6	1	
281	UGC 8696	13:44:42.21 +55:53:13.1	0.6	158.8±6.9	2,4	E
282	NGC 5297	13:46:23.79 +43:52:08.7	11.8	23.0±2.4	1	E*
283	MK 796	13:46:49.47 +14:24:03.1	1.5	190.6±6.7	1	
284	IRAS 13446+1121	13:47:04.43 +11:06:22.9	0.9	20.4±0.7	1	
285	NGC 5303	13:47:45.07 +38:18:19.6	3.0	24.9±1.5	1	
286	NGC 5313	13:49:44.15 +39:59:05.7	2.3	44.3±2.0	1	
287	MCG 3-35-034	13:53:09.52 +14:39:22.2	2.5	20.8±0.7	1	
288	NGC 5347	13:53:18.04 +33:29:25.6	3.6	5.6±0.5	1	
289	NGC 5350	13:53:21.28 +40:21:48.5	4.3	16.8±1.7	1	
290	NGC 5368	13:54:29.31 +54:19:50.3	1.3	9.1±0.5	1	
291	UGC 8827	13:54:31.24 +15:02:39.1	1.0	23.0±1.1	1	
292	UGC 8850	13:56:02.86 +18:22:19.0	3.6	380.5±1.4	1	
293	UGC 8856	13:56:07.83 +30:04:52.3	1.0	21.7±0.8	1	
294	NGC 5374	13:57:29.73 +06:05:49.7	1.5	24.2±1.4	1	
295	UGC 8902	13:59:02.80 +15:33:54.7	1.9	12.4±1.0	1	

TABLE 5 — *Continued*

SFRS	Name	Position[a] (J2000)	Offset[b] (arcsec)	F(1.4 GHz) (mJy)	References[c]	Remarks[d]
296	NGC 5403	13:59:51.04 +38:10:56.3	3.3	37.4±1.8	1	
297	MCG 7-29-036	14:00:57.84 +42:51:20.4	· · ·	5.2±0.6	2	D*
298	NGC 5414	14:02:03.42 +09:55:44.2	2.1	19.6±1.3	1	
299	MCG 5-33-046	14:04:47.88 +30:44:36.2	1.8	10.4±0.5	1	
300	NGC 5474	14:05:01.42 +53:39:44.4	· · ·	13.0±3.0	2	E*
301	NGC 5480	14:06:21.86 +50:43:31.0	2.8	29.0±1.5	1	
302	MCG 6-31-070	14:06:48.99 +33:46:16.2	2.4	18.1±0.7	1	
303	CGCG 074-129	14:10:41.42 +13:33:26.1	2.9	7.6±0.5	1	
304	NGC 5520	14:12:22.87 +50:20:54.2	0.7	14.8±0.6	1	
305	NGC 5515	14:12:38.17 +39:18:36.3	0.4	28.8±1.0	1	
306	NGC 5526	14:13:53.78 +57:46:17.5	0.7	15.9±0.9	1	
307	NGC 5522	14:14:50.33 +15:08:52.6	3.9	17.6±1.0	1	
308	NGC 5541	14:16:31.88 +39:35:23.3	2.9	33.0±1.4	1	
309	IC 4395	14:17:21.09 +26:51:28.4	1.6	22.6±0.8	1	
310	UGC 9165	14:18:47.66 +24:56:24.9	2.0	30.6±1.3	1	
311	MK 1490	14:19:43.28 +49:14:12.3	0.7	20.2±0.7	1	
312	NGC 5585	14:19:48.19 +56:43:45.6	· · ·	18.7±2.9	2	E*
313	IC 4408	14:21:12.96 +29:59:36.2	2.0	20.1±0.7	1	
314	NGC 5584	14:22:25.36 -00:23:31.2	· · ·	19.4±2.1	4	E
315	NGC 5633	14:27:28.39 +46:08:49.3	1.7	27.9±1.5	1	
316	NGC 5660	14:29:49.79 +49:37:25.5	3.9	33.4±2.1	1	
317	NGC 5656	14:30:25.35 +35:19:16.2	2.1	20.8±1.3	1	
318	NGC 5657	14:30:43.68 +29:10:47.5	7.3	10.3±0.9	1,2	
319	CGCG 133-083	14:31:54.03 +21:56:20.2	2.1	11.1±0.5	1	*
320	MCG 7-30-028	14:33:48.36 +40:05:38.9	· · ·	12.6±0.5	2	D
321	MCG 6-32-070	14:35:18.28 +35:07:08.5	1.8	22.0±0.8	1	
322	UGC 9412	14:36:22.07 +58:47:41.6	2.3	11.2±0.5	1	
323	NGC 5698	14:37:14.47 +38:27:18.1	3.8	4.9±0.5	1	
324	NGC 5691	14:37:53.36 -00:23:54.2	1.8	19.0±1.3	1	
325	MCG 9-24-035	14:45:45.04 +51:34:50.0	1.2	11.5±0.5	1	
326	MCG 9-24-038	14:46:37.29 +56:14:00.8	2.8	13.8±0.6	1	
327	UGC 9560	14:50:56.18 +35:34:13.9	7.4	5.9±0.5	1	
328	IC 1076	14:54:59.56 +18:02:14.3	0.8	20.7±0.7	1	
329	IRAS 14538+1730	14:56:08.47 +17:18:35.4	1.4	12.2±0.5	1	*
330	NGC 5795	14:56:19.35 +49:23:56.1	0.7	18.3±1.0	1,2	E
331	UGC 9618	14:57:00.69 +24:37:01.8	1.4	93.1±3.3	1	
332	UGC 9639	14:58:36.00 +44:53:02.2	1.1	35.7±1.1	1	
333	MCG 6-33-022	15:08:05.64 +34:23:23.2	5.8	133.1±4.0	1	
334	NGC 5879	15:09:46.73 +56:59:56.5	4.2	19.5±1.6	1	
335	MCG 9-25-036	15:12:52.33 +51:23:55.0	· · ·	5.0±0.5	2	D*
336	NGC 5899	15:15:03.60 +42:03:05.1	7.0	41.9±2.0	1	
337	NGC 5905	15:15:23.30 +55:31:00.6	1.7	20.1±1.5	1	
338	MK 848	15:18:06.20 +42:44:42.5	2.6	50.3±1.6	1	
339	IC 4553	15:34:57.26 +23:30:11.1	2.2	326.3±9.8	1	
340	UGC 9922	15:35:54.00 +38:40:29.8	2.4	22.0±1.0	1	
341	IC 4567	15:37:13.42 +43:17:55.9	2.5	23.9±1.3	1	
342	MCG 4-37-016	15:39:26.77 +24:56:45.6	11.6	20.1±1.0	1	B*
343	NGC 5975	15:39:57.99 +21:28:13.2	1.2	22.1±0.8	1	
344	NGC 5980	15:41:30.44 +15:47:16.5	0.9	25.3±1.2	1	
345	NGC 5992	15:44:21.63 +41:05:10.3	1.5	16.0±0.6	1	
346	NGC 5996	15:46:58.87 +17:53:04.1	1.0	29.6±1.6	1	
347	IRAS 15519+3537	15:53:48.80 +35:28:10.4	8.2	11.4±0.8	1	
348	UGC 10099	15:56:36.40 +41:52:50.6	0.1	14.8±0.6	1	
349	MCG 5-38-006	15:58:43.54 +26:49:04.1	2.5	10.8±0.5	1	
350	UGC 10120	15:59:10.07 +35:01:45.6	5.8	5.5±0.4	1	
351	NGC 6027A	15:59:11.18 +20:45:16.8	· · ·	11.3±1.0	2	E*
352	NGC 6040	16:04:26.52 +17:44:33.3	2.1	95.9±2.9	1	
353	UGC 10200	16:05:45.61 +41:20:43.8	4.2	11.2±0.9	1	
354	IRAS 16052+5334	16:06:32.84 +53:26:32.3	1.4	10.2±0.5	1	
355	IRAS 16053+1836	16:07:38.39 +18:28:46.9	2.3	14.0±0.6	1	
356	NGC 6090	16:11:40.75 +52:27:26.5	5.3	48.0±1.5	1	
357	UGC 10273	16:12:44.93 +28:17:11.5	3.6	22.2±1.1	1	
358	IRAS 16150+2233	16:17:08.79 +22:26:28.4	· · ·	3.9±0.3	1,3	*
359	UGC 10322	16:18:08.10 +22:13:32.0	3.5	24.4±1.1	1	
360	NGC 6120	16:19:48.16 +37:46:28.6	1.0	33.7±1.1	1	
361	MCG 3-42-004	16:24:15.13 +20:10:59.0	1.8	10.3±0.5	1	
362	UGC 10407	16:28:28.19 +41:13:04.6	3.7	18.4±0.7	1	
363	IRAS 16320+3922	16:33:49.62 +39:15:49.0	· · ·	6.5±0.5	1,3	*
364	NGC 6186	16:34:25.49 +21:32:27.2	· · ·	17.4±1.1	2	D,E*
365	MCG 9-27-053	16:35:15.46 +52:46:49.8	0.4	20.0±0.7	1	
366	UGC 10514	16:42:23.66 +25:05:10.7	0.8	31.9±1.3	1	
367	IRAS 16435+2154	16:45:40.71 +21:49:18.4	0.7	11.6±0.5	1	
368	IC 4623	16:51:05.29 +22:31:40.9	2.3	11.0±0.5	1	
369	IRAS 16516+3030	16:53:37.34 +30:26:09.7	2.2	13.1±0.6	1	

TABLE 5 — *Continued*

SFRS	Name	Position[a] (J2000)	Offset[b] (arcsec)	F(1.4 GHz) (mJy)	References[c]	Remarks[d]

Note. — Table 5 is published in its entirety in the electronic edition of *Publications of the Astronomical Society of the Pacific*. A portion is shown here for guidance regarding its form and content.

[a] Coordinates correspond to the centroids measured in the NVSS or AA319 images.

[b] Offset measured relative to the IRAC position.

[c] References. 1. NVSS query; 2. NVSS image; 3. AA319 data; 4. Condon et al. (2002).

[d] Remarks. A = Radio source double or triple; B = likely blended; D= deconvolved blend; E = extended source. Further details for individual sources marked with an asterisk (*): **3.** high integral, 110″×105″ at 30° position angle (PA); **10.** 55″×43″ at 29° PA, excludes 4.4 mJy point source at 08:11:16.1 +25:10:55; **12.** extended with off-center bright spot, 58″×43″ at 51° PA; **18.** 58″×40″ blended with IC 2338 (6.9 mJy); **47.** blended with 5.2 mJy source at 09:15:22.4 +38:55:42; **65.** blended with $z = 0.22$ QSO (7.8 mJy at 09:46:03.94 +01:39:23.7), cf. 9.4 mJy for this galaxy in reference 4; **74.** needle galaxy in IR, 101″× <38″ at −47° PA; **80.** two point sources 16 mJy plus 6 mJy diffuse attributed to galaxy; **83.** radio source is star-forming region in galaxy outskirts; **98.** 179″×111″ at 106° PA, flux excludes 4.4 mJy point source at 10:42:02.5 +13:45:04; **102.** 41″×34″ at 153° PA; **103.** excludes two point sources (23, 37 mJy at 30–50″ separation); **106.** 88″×46″ at 35° PA; **107.** excludes 9.4 mJy source 1′ distant; **110.** 183″×46″ at 24° PA, cf. 19.4 mJy in reference 4; **115.** excludes 22 mJy source at 11:09:37.4 +26:55:16, flux uncertain; **119.** excludes >4.6 mJy, possibly extended, source to S; **120.** excludes 8.9 mJy point source at 11:16:52.4, +59:30:56; **126.** extended >60″, position uncertainty 11″; **128.** galaxy compact with bright nucleus in IR, radio 53″×21″ at −4° PA and offset from galaxy; **134.** 107″×47″ at 134° PA; **141.** excludes UGC 6587 (4.0 mJy at 11:37:09.53 +02:50:20.4); **147.** 57″×40″ at 144° PA, excludes 19.2 mJy source 50″ to NW; **154.** two galaxies blended, IRAS flux is sum; **164.** needle galaxy in reference 1, 118″×36″ at 62° PA, high integral; **166.** major axis >75″, radio offset from IR; **167.** cf. 2.8±0.5 mJy in reference 1; **171.** major axis >60″; **179.** 126″×53″ at 43° PA, radio image shows four point sources plus diffuse emission; **181.** 86″×42″ at 72° PA, off-nuclear star-forming regions; **186.** radio diameter <36″, clumpy and extended in IR; **188.** needle galaxy >11′, measured flux in polygon; **192.** 60″×29″ at −34° PA, clumpy in IR; **195.** clumpy in IR and in radio image (reference 2); **199.** noise affected by 3C 273 sidelobes; **200.** high integral, radio image shows linear artifacts (reference 2); **203.** 76″×49″ at 125° PA; **206.** cf. 2.6±0.4 in reference 1, noise mildly affected by 3C273 sidelobes; **207.** noise affected by M87 sidelobes; **218.** assumed Gaussian diameter 40″; **219.** major axis 56″; **228.** 56″×56″ high integral; **231.** cf. 4.8±0.4 in reference 1; **232.** cf. 2.3±0.4 in reference 1; **241.** lobes 41, 9.4 mJy; cf. 6.4±0.6 in reference 1; **242.** elongated galaxy, radio flux includes 10.5 mJy point source (12:59:00.4, 34:50:44); **260.** radio diameter <70″, clumpy in IR; **261.** measured in polygon, cf. 17.3 mJy in reference 4; **263.** cf. 4.9±0.5 in reference 1; **269.** 59″×44″ at 71° PA, excludes 5 mJy point source 1′ to NE; **283.** 107″×53″ at −45° PA, high integral, excludes 5 mJy point source to NW; **297.** excludes 5.7 mJy point source at 14:00:58.77 +42:50:42.4; **300.** position is brightest visible/IR clump, radio flux measured in circle based on IR image; **312.** galaxy clumpy and extended in IR, radio flux measured in circle based on IR image; **319.** excludes 6.5 mJy point source UGC 9376 at 14:33:46.83 +40:04:51.3; **329.** major axis 27″, flux includes 1 mJy H II reg at 14:56:22.42 +49:24:06.4; **335.** excludes 0.8 mJy point source galaxy at 15:12:50.66 +51:23:28.9; **342.** includes companion 24″ SW, *IRAS* flux is sum; **351.** 48″×24″ at 17° PA, excludes 6.7 mJy point source at 15:59:10.2 +20:46:22; cf. 9.3±1.0 mJy in reference 1; **358.** cf. 3.1±0.4 mJy in reference 1; **363.** cf. 9.4±0.6 mJy in reference 1; **364.** 58″×48″ at 45° PA, excludes 7.1 mJy point source at 16:34:28.7 +21:32:15.

TABLE 7
Far-Infrared Photometry for SFRS Galaxies

SFRS	Name	L(TIR) ($L_{\odot}$)	MIPS F(24)[a] (Jy)	IRAS F(60) (Jy)	IRAS F(100) (Jy)	Planck F(350) (Jy)	Planck F(550) (Jy)	Planck (F850) (Jy)
1	IC 486	10.90	0.44[b]	0.99	<1.51	···	···	···
2	IC 2217	10.74	<0.32	2.46	4.81	···	···	···
3	NGC 2500	9.34	0.22	2.81	5.75	3.02±0.14	···	···
4	NGC 2512	10.88	0.66[b]	3.80	7.31	···	···	···
5	MCG 6-18-009	11.25	<0.27	1.65	3.09	···	···	···
6	MK 1212	11.35	<0.33	1.87	3.36	···	···	···
7	IRAS 08072+1847	10.72	0.74[b]	2.79	3.08	···	···	···
8	NGC 2532	11.09	0.63	3.61	10.34	4.02±0.21	1.43±0.08	···
9	UGC 4261	10.65	<0.35	1.22	1.56	···	···	···
10	NGC 2535	10.62	0.28	2.13	5.97	···	···	···
11	NGC 2543	9.90	0.33[b]	2.78	6.14	3.04±0.31	···	···
12	NGC 2537	9.36	0.27	3.12	5.78	···	···	···
13	IC 2233	8.62	0.037	0.93	1.47	···	···	···
14	IC 2239	10.98	<0.57	2.94	5.30	···	···	···
15	UGC 4286	10.63	<0.59	0.87	1.81	···	···	···
16	UGC 4306	10.20	<0.36	3.59	6.77	···	···	···
17	NGC 2552	8.53	0.056	0.61	1.50	···	···	···
18	IC 2339	10.51	0.15	1.65	2.88	···	0.85±0.13	···
19	IRAS 08234+1054B	11.73	<0.32	1.82	3.19	···	···	···
20	IRAS 08269+1514	11.05	<0.32	0.80	2.30	···	···	···
21	NGC 2604	10.00	<0.40	1.31	2.85	···	···	···
22	NGC 2608	10.15	0.25[b]	2.30	5.97	2.19±0.14	···	···
23	MK 92	10.59	0.35[b]	2.53	3.88	···	···	···
24	NGC 2623	11.49	1.35	24.33	28.24	···	···	···
25	CGCG 120-018	10.99	0.28[b]	3.18	4.51	···	···	···
26	NGC 2644	9.69	<0.31	1.53	3.62	···	···	···
27	UGC 4572	10.29	<0.27	1.01	2.09	···	···	···
28	UGC 4653	11.69	<0.30	2.14	4.55	1.58±0.20	···	···
29	IRAS 08512+2727	11.59	<0.32	0.67	1.81	···	···	···
30	OJ 287[c]	13.19	<0.71	0.94	1.31	2.62±0.15	3.62±0.10	3.92±0.11
31	IRAS 08538+4256	11.24	0.39[b]	4.65	6.44	···	···	···
32	IRAS 08550+3908	11.80	<0.30	1.23	1.54	···	···	···
33	NGC 2718	10.68	0.58[b]	4.03	7.01	···	···	···
34	NGC 2712	9.98	0.30[b]	2.19	5.29	2.26±0.11	0.69±0.09	···
35	NGC 2719	10.02	0.08	1.85	2.61	···	···	···
36	IRAS 08572+3915	12.02	1.44	7.53	4.59	···	···	···
37	IRAS 08579+3447	11.82	<0.27	2.78	4.82	···	···	···
38	NGC 2731	10.16	<0.55	3.11	5.20	···	···	···
39	NGC 2730	10.34	<0.34	0.74	2.20	···	···	···
40	IC 2431	11.82	0.54[b]	4.43	7.63	···	···	···
41	NGC 2750	10.33	0.59[b]	3.93	7.68	2.66±0.15	0.86±0.08	···
42	IC 2434	10.88	<0.25	1.70	3.44	···	···	···
43	NGC 2761	11.36	0.46[b]	3.97	7.70	1.61±0.11	···	···
44	NGC 2773	10.84	0.39[b]	2.84	5.26	···	···	···
45	NGC 2776	10.31	0.32[b]	3.42	9.17	3.72±0.13	1.20±0.11	···
46	NGC 2789	10.95	<0.33	2.23	5.16	1.57±0.12	···	···
47	IRAS 09121+3908	10.03	<0.25	1.18	2.64	···	···	···
48	NGC 2824	9.87	<0.33	1.12	1.83	···	···	···
49	IRAS 09184+4356	11.25	<0.25	1.32	2.83	···	···	···
50	CGCG 238-041	10.99	<0.31	0.60	1.97	···	···	···
51	UGC 4985	11.12	<0.33	0.84	2.34	···	···	···
52	NGC 2854	9.54	0.20	2.00	2.93	2.57±0.24	···	···
53	UGC 5046	10.67	<0.49	3.01	5.09	···	···	···
54	UGC 5055	10.95	<0.33	1.53	3.14	···	···	···
55	NGC 2893	9.78	0.59[b]	2.54	3.83	···	···	···
56	MCG 3-24-062	10.52	<0.29	1.24	3.49	···	···	···
57	CGCG 238-066	11.20	0.46[b]	1.75	2.36	···	···	···
58	UGC 5097	10.68	0.31[b]	2.83	4.81	···	···	···
59	CGCG 289-012	11.31	<0.26	1.49	3.24	···	···	···
60	MCG 8-18-013	11.29	0.56	5.87	8.40	···	···	···
61	CGCG 181-068	10.86	<0.28	1.19	3.26	···	···	···
62	NGC 2936	10.95	0.20	2.15	5.03	···	···	···
63	NGC 2955	10.99	<0.31	1.61	4.51	1.10±0.10	···	···
64	CGCG 182-010	11.40	0.40[b]	1.94	3.41	···	···	···
65	UGC 5228	9.78	<0.27	1.63	3.69	···	···	···
66	IRAS 09438+1141	11.46	<0.32	1.16	2.89	···	···	···
67	NGC 3015	11.02	<0.33	2.16	4.28	···	···	···
68	MCG 2-25-039	10.64	<0.30	1.45	3.23	···	···	···
69	NGC 3020	9.37	0.28[b]	1.98	3.38	···	···	···
70	NGC 3049	9.50	0.42	2.71	4.34	1.91±0.17	1.06±0.11	···
71	NGC 3055	10.04	0.64[b]	4.05	8.48	···	···	···

TABLE 7 — *Continued*

SFRS	Name	L(TIR) (L$_{\odot}$)	MIPS F(24)^{a} (Jy)	IRAS F(60) (Jy)	IRAS F(100) (Jy)	Planck F(350) (Jy)	Planck F(550) (Jy)	Planck (F850) (Jy)
72	IC 2520	9.97	0.48^{b}	3.42	6.77	···	···	···
73	UGC 5403	10.00	0.39^{b}	2.71	4.28	···	···	···
74	UGC 5459	9.79	0.27^{b}	2.17	5.00	2.95±0.16	1.02±0.10	···
75	MCG 5-24-022	10.71	<0.26	0.97	2.60	···	···	···
76	IC 2551	11.06	0.82^{b}	3.84	4.24	···	···	···
77	IRAS 10106+2745	11.41	<0.26	0.81	2.21	2.18±0.28	···	···
78	NGC 3162	9.98	0.52^{b}	2.93	6.48	2.69±0.13	1.08±0.08	···
79	IRAS 10120+1653	12.21	<0.37	0.86	1.88	···	···	···
80	NGC 3190	10.05	0.25	3.33	9.84	4.45±0.28	1.52±0.12	···
81	IC 602	10.55	<0.33	2.84	5.71	1.29±0.12	···	···
82	NGC 3191	11.15	<0.29	1.70	3.81	1.00±0.14	···	···
83	NGC 3206	9.40	<0.10	1.07	2.14	···	···	···
84	UGC 5613	11.44	0.32	4.20	8.27	···	···	···
85	UGC 5644	10.67	0.07	0.66	1.34	···	···	···
86	NGC 3245	9.40	0.18^{b}	1.98	3.17	···	···	···
87	IRAS 10246+2042	10.78	<0.39	2.58	3.86	···	···	···
88	MCG 7-22-012	10.41	0.07	1.43	3.76	0.86±0.11	···	···
89	IRAS 10276+1119	11.83	<0.51	0.79	<3.02	···	···	···
90	NGC 3265	9.52	0.28	2.21	3.40	···	···	···
91	UGC 5713	10.66	<0.39	0.91	1.13	···	···	···
92	NGC 3274	8.48	0.06	0.99	1.86	···	···	···
93	UGC 5720	9.76	0.84	4.79	5.49	···	···	···
94	KUG 1031+351	11.93	0.31^{b}	2.68	5.02	1.06±0.10	···	···
95	NGC 3306	10.37	0.41^{b}	2.89	5.26	···	···	···
96	NGC 3323	10.65	<0.27	1.50	3.30	···	···	···
97	IC 2598	10.92	0.35^{b}	3.24	5.49	···	···	···
98	NGC 3338	9.91	0.37	3.43	10.32	6.21±0.23	2.55±0.14	0.55±0.06
99	NGC 3353	9.63	0.91	5.18	6.65	1.20±0.11	···	···
100	UGC 5881	10.71	<0.30	1.76	2.45	···	···	···
101	NGC 3370	9.85	0.38	3.43	9.13	3.73±0.16	1.41±0.09	···
102	NGC 3381	9.71	<0.25	1.40	3.95	1.48±0.11	···	···
103	UGC 5941	11.02	<0.31	2.52	4.76	···	···	···
104	NGC 3413	8.92	0.06	1.03	1.96	···	···	···
105	NGC 3408	9.41	0.12	0.91	1.55	0.81±0.10	···	···
106	NGC 3430	11.40	0.17	2.87	8.32	5.99±0.55	1.60±0.20	···
107	CGCG 95-055	9.42	0.22	1.88	1.72	···	···	···
108	IRAS 10565+2448	11.95	0.95	12.17	14.34	1.84±0.10	···	···
109	UGC 6074	10.28	0.78^{b}	3.48	4.68	···	···	···
110	NGC 3495	9.74	0.60^{b}	3.36	8.80	4.99±0.26	1.80±0.12	···
111	UGC 6103	10.88	0.38^{b}	2.47	4.12	···	···	···
112	MCG 7-23-019	11.57	0.25	6.06	10.66	0.91±0.14	···	···
113	UGC 6135	10.89	<0.25	1.73	5.04	1.01±0.09	···	···
114	CGCG 241-078	10.93	<0.28	2.42	3.38	···	···	···
115	IRAS 11069+2711	11.76	0.11	2.14	4.18	···	···	···
116	IC 676	9.90	0.52	3.05	4.76	···	···	···
117	IRAS 11102+3026	11.02	0.10	2.27	4.04	···	···	···
118	IC 2637	11.00	0.17	1.95	3.42	···	···	···
119	MCG 9-19-013	11.37	<0.25	0.90	2.46	···	···	···
120	7ZW 384	11.66	0.09	0.94	2.28	···	···	···
121	IRAS 11167+5351	11.95	0.13	1.39	2.44	···	···	···
122	NGC 3633	10.09	0.70^{b}	3.04	5.36	···	···	···
123	NGC 3652	9.39	0.19	2.38	6.03	1.60±0.15	···	···
124	NGC 3656	10.08	0.15	2.39	5.45	1.50±0.12	···	···
125	NGC 3659	9.47	0.13	1.65	3.95	1.55±0.12	···	···
126	NGC 3664	9.37	0.08	0.90	1.85	2.83±0.54	1.66±0.25	···
127	NGC 3666	9.57	0.22	2.92	8.59	2.84±0.12	0.99±0.07	···
128	IC 691	9.42	0.46	3.61	4.79	···	···	···
129	NGC 3686	9.92	0.48	3.82	10.31	4.09±0.12	1.06±0.10	···
130	UGC 6469	10.71	0.12	1.66	2.88	···	···	···
131	IC 694	11.91	17.32	105.80	111.20	9.62±0.17	2.56±0.09	0.64±0.06
132	IC 698	11.07	0.32	3.74	7.11	···	···	···
133	IRAS 11267+1558	12.25	0.039	0.76	<2.07	···	···	···
134	NGC 3705	9.68	0.38	3.69	10.42	5.83±0.31	2.08±0.13	···
135	MCG 3-29-061	10.54	0.26	2.64	4.05	···	···	···
136	NGC 3720	10.91	0.18	2.55	6.11	1.67±0.17	···	···
137	NGC 3729	9.62	0.40	2.85	7.44	2.32±0.13	0.60±0.07	···
138	MCG 10-17-019	11.05	0.12	1.39	4.08	1.17±0.11	···	···
139	NGC 3758	10.97	0.24	1.43	2.43	···	···	···
140	UGC 6583	10.97	<0.51	1.98	4.39	1.14±0.10	···	···
141	MCG 1-30-003	11.05	0.24	1.97	3.45	···	···	···
142	NGC 3769	9.52	0.22	2.53	6.76	3.03±0.11	1.05±0.07	···
143	NGC 3773	8.97	0.14	1.51	1.84	···	···	···
144	NGC 3781	11.31	0.71	7.07	9.99	1.85±0.19	0.55±0.08	···

TABLE 7 — *Continued*

SFRS	Name	L(TIR) ($L_\odot$)	MIPS F(24)[a] (Jy)	IRAS F(60) (Jy)	IRAS F(100) (Jy)	Planck F(350) (Jy)	Planck F(550) (Jy)	Planck (F850) (Jy)
145	UGC 6625	11.16	0.12	1.23	3.36	···	···	···
146	NGC 3808A	11.06	0.20	2.78	6.02	1.15±0.17	···	···
147	NGC 3811	10.45	0.20	2.49	5.73	1.92±0.11	0.71±0.09	···
148	NGC 3822	11.03	0.28	3.19	6.97	3.39±0.39	···	···
149	UGC 6665	10.91	0.62	3.89	4.51	···	···	···
150	MCG 3-30-051	10.77	0.18	1.82	4.02	···	···	···
151	NGC 3839	11.04	0.31	4.18	7.68	···	···	···
152	UGC 6732	10.16	0.27	1.41	2.00	···	···	···
153	IC 730	10.93	0.23	3.24	5.86	···	···	···
154	IC 732	11.13	0.33[b]	3.43	6.08	1.63±0.12	0.78±0.08	···
155	NGC 3912	9.75	0.26	3.40	6.56	1.49±0.08	···	···
156	NGC 3928	9.47	0.31	2.67	5.46	···	···	···
157	NGC 3934	10.33	0.11	2.25	3.60	···	···	···
158	UGC 6865	10.86	0.21	2.31	4.94	1.52±0.12	···	···
159	UGC 6901	11.00	0.17	2.01	5.13	1.15±0.11	···	···
160	CGCG 013-010	11.57	<0.25	3.29	7.53	1.45±0.11	···	···
161	NGC 3991	10.43	0.24	2.56	4.84	3.56±0.17	1.10±0.07	···
162	NGC 4004	10.61	0.36	3.63	6.71	1.84±0.11	0.62±0.08	···
163	NGC 4014	10.62	0.23	2.46	6.22	···	···	···
164	NGC 4010	9.50	0.21	2.40	6.42	4.08±0.24	1.53±0.11	0.38±0.05
165	NGC 4018	10.77	0.17	2.35	6.87	1.16±0.09	···	···
166	NGC 4020	8.94	0.09	0.96	2.47	1.10±0.09	···	···
167	IRAS 11571+3003	11.16	0.050	0.86	1.88	···	···	···
168	UGC 7017	10.59	0.29	3.78	7.46	1.59±0.11	···	···
169	UGC 7016	10.85	0.12	1.46	3.46	···	···	···
170	MCG 3-31-030	8.72	0.054	0.67	1.84	···	···	···
171	NGC 4062	9.67	0.35	2.68	10.16	5.91±0.14	1.76±0.09	0.39±0.06
172	NGC 4064	8.95	0.34	3.29	6.81	···	···	···
173	CGCG 098-059	11.14	0.34	3.41	7.31	···	···	···
174	NGC 4116	9.38	0.18	1.89	5.56	3.33±0.14	1.28±0.10	···
175	NGC 4136	9.36	0.12	2.12	5.42	3.13±0.10	1.12±0.08	0.59±0.07
176	NGC 4150	8.87	0.07	1.24	2.46	···	···	···
177	IRAS 12086+1441	9.06	<0.47	1.26	1.78	···	···	···
178	NGC 4162	10.31	0.23	2.45	6.61	3.61±0.35	1.05±0.18	···
179	NGC 4178	9.67	0.39	4.02	9.47	6.19±0.15	1.75±0.11	···
180	IRAS 12112+0305	12.15	0.34	8.36	9.91	···	···	···
181	NGC 4189	9.65	0.39	3.29	8.70	3.05±0.16	···	···
182	NGC 4194	10.94	3.83	22.79	25.94	2.02±0.11	···	···
183	NGC 4204	8.54	0.08	1.01	2.04	2.01±0.21	···	···
184	NGC 4207	9.54	0.21	3.03	7.46	1.41±0.11	···	···
185	UGC 7286	10.55	0.06	0.90	1.61	···	···	···
186	NGC 4234	9.77	0.14	1.66	3.88	0.96±0.13	···	···
187	NGC 4237	9.64	0.28	2.81	9.19	4.08±0.15	0.81±0.08	···
188	NGC 4244[d]	8.69	0.40	4.20	16.06	7.92±0.53	3.54±0.19	0.90±0.09
189	NGC 4253	10.83	1.19	4.06	4.25	···	···	···
190	MCG 3-32-005	9.21	0.24	2.78	5.35	···	···	···
191	NGC 4290	10.33	0.45	3.90	8.46	2.62±0.17	0.80±0.08	···
192	NGC 4294	9.43	0.21	2.75	5.56	2.22±0.21	0.96±0.10	···
193	NGC 4314	9.51	0.29	3.44	7.02	1.93±0.23	···	···
194	NGC 4385	10.14	0.96	4.66	6.13	1.91±0.13	···	···
195	NGC 4395	8.71	0.51[e]	4.21	12.90	6.20±0.34	2.87±0.19	0.81±0.10
196	NGC 4396	9.27	0.13	1.27	3.84	2.58±0.13	···	···
197	NGC 4412	10.03	0.37	3.00	5.90	···	···	···
198	NGC 4418	11.02	9.57[b]	43.86	33.78	3.33±0.16	1.24±0.11	···
199	NGC 4420	9.57	0.23	2.70	7.08	2.12±0.18	···	···
200	NGC 4424	8.56	0.30	2.89	5.48	···	···	···
201	NGC 4435	9.03	0.11	1.88	2.29	4.56±0.26	1.07±0.13	···
202	NGC 4438[d]	9.73	0.23	4.28	12.05	4.56±0.26	1.07±0.13	···
203	NGC 4448	9.36	0.18	1.60	4.97	3.20±0.17	0.82±0.11	···
204	3C 273	12.56	0.52	2.22	2.91	4.07±0.13	6.94±0.17	8.60±0.16
205	NGC 4470	9.32	0.14	1.85	4.49	1.18±0.17	···	···
206	IRAS 12274+0018	9.44	0.06	0.81	1.08	···	···	···
207	NGC 4491	9.29	0.30	2.64	3.31	···	···	···
208	NGC 4500	10.55	0.45	3.92	6.84	0.97±0.13	···	···
209	NGC 4495	10.82	0.26	3.16	7.00	1.84±0.13	···	···
210	IC 3476	9.20	0.14	1.30	3.15	···	···	···
211	NGC 4509	8.65	0.06	0.60	<2.16	···	···	···
212	NGC 4519	9.58	0.51	3.76	6.56	2.85±0.14	1.10±0.10	···
213	NGC 4548	9.73	0.48	2.61	11.10	6.46±0.25	2.01±0.11	···
214	IRAS 12337+5044	11.19	0.11	1.41	3.06	···	···	···
215	IC 3581	10.99	0.29	3.80	4.82	1.33±0.17	···	···
216	NGC 4592	8.97	0.12	2.18	4.76	2.32±0.13	1.08±0.12	···
217	NGC 4607	9.57	0.25	2.75	7.84	2.79±0.31	···	···
218	NGC 4625	8.75	0.12	1.22	3.81	···	···	···

TABLE 7 — *Continued*

SFRS	Name	L(TIR) ($L_\odot$)	MIPS F(24)[a] (Jy)	IRAS F(60) (Jy)	IRAS F(100) (Jy)	Planck F(350) (Jy)	Planck F(550) (Jy)	Planck (F850) (Jy)
219	NGC 4630	9.39	0.26	2.42	5.56	2.19±0.12	⋯	⋯
220	IC 3690	8.83	0.13	1.44	2.17	⋯	⋯	⋯
221	UGC 7905	10.45	0.15	1.82	2.53	⋯	⋯	⋯
222	MCG 5-30-069	10.70	0.27	3.04	5.05	⋯	⋯	⋯
223	IC 3721	10.85	0.18	2.02	4.14	⋯	⋯	⋯
224	NGC 4670	9.19	0.25	2.44	4.01	⋯	⋯	⋯
225	NGC 4675	10.71	0.22	2.50	4.98	1.07±0.14	⋯	⋯
226	MCG 7-26-051	11.35	0.20	2.89	6.23	1.07±0.19	⋯	⋯
227	NGC 4689	9.71	0.40	2.69	10.02	⋯	⋯	⋯
228	NGC 4688	8.97	0.12	1.00	2.05	1.71±0.14	⋯	⋯
229	NGC 4704	10.96	0.33	1.70	2.32	⋯	⋯	⋯
230	NGC 4701	9.43	0.21	2.68	6.54	2.04±0.13	⋯	⋯
231	IRAS 12468+3436	11.92	0.037	0.90	2.17	⋯	⋯	⋯
232	IRAS 12470+1404	8.66	0.09	0.74	<1.36	⋯	⋯	⋯
233	MCG 8-23-097	11.36	0.29	5.08	8.10	1.37±0.11	⋯	⋯
234	NGC 4747	9.24	0.30[b]	2.16	4.29	1.86±0.11	⋯	⋯
235	UGC 8017	11.01	0.17	1.90	5.22	1.18±0.11	⋯	⋯
236	NGC 4765	9.24	0.17	2.23	4.18	⋯	⋯	⋯
237	VCC 2096	8.83	0.11	1.40	2.28	⋯	⋯	⋯
238	UGC 8041	9.33	0.07	1.01	2.49	1.89±0.11	1.00±0.11	⋯
239	UGC 8058	12.57	8.52[b]	33.60	30.89	1.87±0.08	⋯	⋯
240	NGC 4837	11.10	0.16	1.92	4.20	0.99±0.13	⋯	⋯
241	UM 530	11.40	0.07	0.61	<1.78	⋯	⋯	⋯
242	NGC 4861	9.32	0.34	1.98	2.38	⋯	⋯	⋯
243	NGC 4868	10.92	0.33	3.41	8.72	2.49±0.13	0.68±0.08	⋯
244	NGC 4922	11.34	1.16	6.61	7.08	0.90±0.17	⋯	⋯
245	UGC 8179	11.25	0.07	0.92	2.18	0.89±0.11	⋯	⋯
246	NGC 5001	11.28	0.22	2.67	6.19	⋯	⋯	⋯
247	IC 856	10.40	0.13	1.62	3.56	⋯	⋯	⋯
248	UGC 8269	11.13	0.08	2.88	5.93	2.03±0.19	0.87±0.09	⋯
249	NGC 5014	9.44	<0.27	2.28	4.21	0.88±0.14	⋯	⋯
250	NGC 5012	10.36	0.30	2.89	8.06	3.81±0.10	⋯	⋯
251	IRAS 13116+4508	11.29	0.03	0.90	<1.97	⋯	⋯	⋯
252	IC 860	10.95	0.89	17.60	18.70	2.05±0.16	⋯	⋯
253	IRAS 13144+4508	11.89	0.36	0.72	1.47	⋯	⋯	⋯
254	NGC 5060	11.06	0.29	3.06	6.87	1.52±0.16	⋯	⋯
255	UGC 8357	11.25	0.23	2.52	4.62	1.42±0.19	⋯	⋯
256	UGC 8361	10.95	0.23	2.79	4.46	⋯	⋯	⋯
257	IC 883	11.66	1.06	15.10	24.38	2.55±0.15	⋯	⋯
258	NGC 5100	11.21	0.17	2.12	4.68	1.43±0.17	⋯	⋯
259	NGC 5104	11.23	0.56	6.99	12.74	1.57±0.13	⋯	⋯
260	NGC 5107	8.97	0.06	0.88	1.65	⋯	⋯	⋯
261	NGC 5112	9.53	0.16	2.46	6.06	2.25±0.16	0.63±0.10	⋯
262	NGC 5123	11.14	0.17	1.68	5.28	1.77±0.12	⋯	⋯
263	IRAS 13218+0552	12.37	0.23	1.25	<1.00	⋯	⋯	⋯
264	IRAS 13232+1731	11.59	0.07	0.66	2.02	1.23±0.18	⋯	⋯
265	NGC 5147	9.57	0.23	2.88	6.74	2.62±0.13	0.90±0.14	⋯
266	NGC 5204	7.95	0.18	2.86	5.02	2.50±0.13	1.05±0.07	0.32±0.05
267	UGC 8502	11.09	0.19	1.61	2.80	⋯	⋯	⋯
268	UGC 8561	11.14	0.25	2.78	6.92	⋯	⋯	⋯
259	NGC 5230	10.99	0.19	1.56	4.95	1.50±0.18	⋯	⋯
270	IRAS 13349+2438	12.29	0.87	0.69	<1.00	⋯	⋯	⋯
271	NGC 5256	11.58	0.86	7.29	12.25	⋯	⋯	⋯
272	UGC 8626	10.66	0.11	1.41	2.18	⋯	⋯	⋯
273	NGC 5263	10.88	0.30	3.65	7.40	1.88±0.09	⋯	⋯
274	MCG 1-35-028	10.98	0.35	2.71	4.17	⋯	⋯	⋯
275	IC 910	11.24	0.47	5.05	6.28	⋯	⋯	⋯
276	MK 268	11.13	0.24	1.43	1.79	⋯	⋯	⋯
277	NGC 5278	10.97	0.11	1.51	4.39	1.46±0.13	⋯	⋯
278	NGC 5273	8.81	0.10	0.81	1.13	⋯	⋯	⋯
279	UGC 8685	11.31	0.18	2.30	5.17	0.90±0.12	⋯	⋯
280	UGC 8686	10.94	0.18	1.88	4.45	1.13±0.13	⋯	⋯
281	UGC 8696	12.10	2.33[b]	23.70	22.31	1.56±0.12	⋯	⋯
282	NGC 5297	10.08	0.23	2.43	7.40	3.62±0.14	1.13±0.09	0.45±0.07
283	MK 796	11.09	0.58	3.17	5.44	⋯	⋯	⋯
284	IRAS 13446+1121	11.02	0.57	3.43	3.59	⋯	⋯	⋯
285	NGC 5303	9.78	0.28	3.09	6.50	⋯	⋯	⋯
286	NGC 5313	10.24	0.33	3.09	10.53	3.11±0.13	0.93±0.09	⋯
287	MCG 3-35-034	11.16	0.08	1.20	2.80	⋯	⋯	⋯
288	NGC 5347	10.24	0.84	1.44	2.71	1.18±0.17	⋯	⋯
289	NGC 5350	10.16	0.39	2.72	8.11	⋯	⋯	⋯
290	NGC 5368	10.43	0.12	1.32	2.74	⋯	⋯	⋯
291	UGC 8827	10.94	0.49	3.90	5.82	⋯	⋯	⋯
292	UGC 8850	11.85	1.39	2.18	1.87	⋯	⋯	⋯

TABLE 7 — *Continued*

SFRS	Name	L(TIR) $(L_\odot)$	MIPS F(24)[a] (Jy)	IRAS F(60) (Jy)	IRAS F(100) (Jy)	Planck F(350) (Jy)	Planck F(550) (Jy)	Planck (F850) (Jy)
293	UGC 8856	11.14	0.14	2.02	4.35	···	···	···
294	NGC 5374	10.77	0.29	2.81	6.99	1.34±0.16	···	···
295	UGC 8902	10.86	0.11	1.26	3.26	1.13±0.14	···	···
296	NGC 5403	10.36	0.18	2.88	10.60	3.95±0.15	1.03±0.10	···
297	MCG 7-29-036	11.19	0.19	2.47	4.25	1.14±0.11	···	···
298	NGC 5414	10.56	0.24	2.55	4.23	···	···	···
299	MCG 5-33-046	11.02	0.26	2.71	4.16	···	···	···
300	NGC 5474	8.44	0.14	2.22	5.45	3.01±0.20	1.31±0.08	···
301	NGC 5480	10.21	0.37	3.66	10.13	2.85±0.18	0.86±0.10	···
302	MCG 6-31-070	11.31	0.21	2.61	4.89	0.86±0.10	···	···
303	CGCG 74-129	10.81	0.83	3.69	2.98	···	···	···
304	NGC 5520	9.95	0.19	2.31	5.75	1.39±0.11	···	···
305	NGC 5515	11.02	0.16	1.79	4.78	···	···	···
306	NGC 5526	9.82	0.17	2.16	5.04	1.69±0.14	···	···
307	NGC 5522	10.57	0.15	2.06	4.28	1.80±0.12	···	···
308	NGC 5541	11.09	0.22	2.39	5.34	1.60±0.21	···	···
309	IC 4395	11.39	0.22	2.87	5.59	···	···	···
310	UGC 9165	10.90	0.23	3.10	7.18	1.41±0.14	···	···
311	MK 1490	11.36	0.70	6.21	8.39	1.63±0.18	···	···
312	NGC 5585	8.35	0.12	1.70	4.40	2.63±0.12	0.96±0.09	···
313	IC 4408	11.17	0.17	1.83	4.67	1.16±0.10	···	···
314	NGC 5584	9.77	0.28	2.56	6.11	3.31±0.17	1.04±0.12	···
315	NGC 5633	10.26	0.27	2.67	7.84	1.76±0.09	···	···
316	NGC 5660	10.37	0.34	4.14	9.16	3.07±0.18	0.96±0.11	···
317	NGC 5656	10.22	0.24	1.54	2.66	···	···	···
318	NGC 5657	10.76	0.29[b]	2.70	7.92	2.72±0.15	1.00±0.09	···
319	CGCG 133-083	11.41	0.19	2.25	4.03	···	···	···
320	MCG 7-30-028	11.04	0.14	1.82	4.88	0.99±0.10	···	···
321	MCG 6-32-070	11.21	0.25	2.86	5.81	1.00±0.11	···	···
322	UGC 9412	11.34	0.92	2.24	2.28	···	···	···
323	NGC 5698	10.33	0.24	1.27	2.61	0.82±0.10	···	···
324	NGC 5691	9.65	0.28	3.43	6.60	···	···	···
325	MCG 9-24-035	11.18	0.32	3.13	4.07	···	···	···
326	MCG 9-24-038	11.17	0.10	1.34	3.21	···	···	···
327	UGC 9560	9.19	0.10	0.71	1.46	···	···	···
328	IC 1076	10.73	0.15	1.66	3.56	···	···	···
329	IRAS 14538+1730	11.93	0.08	1.39	2.84	···	···	···
330	NGC 5795	10.23	0.22	2.65	6.99	1.43±0.12	···	···
331	UGC 9618	11.73	0.40	6.45	15.52	3.08±0.17	0.84±0.10	···
332	UGC 9639	11.40	0.32	2.47	5.23	1.19±0.14	···	···
333	MCG 6-33-022	11.50	0.15	2.58	5.25	1.05±0.12	···	···
334	NGC 5879	9.58	0.33	3.30	9.11	···	···	0.28±0.04
335	MCG 9-25-036	10.86	0.013	0.65	1.91	···	···	···
336	NGC 5899	10.61	0.55	3.20	11.53	4.59±0.23	1.28±0.11	···
337	NGC 5905	10.63	0.33	2.82	6.73	2.78±0.10	0.82±0.07	0.26±0.04
338	MK 848	11.85	1.19	9.39	10.26	···	···	···
339	IC 4553	12.12	5.42	104.10	117.70	13.94±0.20	3.64±0.12	0.94±0.08
340	UGC 9922	10.76	0.20	2.31	4.30	···	···	···
341	IC 4567	10.93	0.21	2.18	6.29	1.73±0.20	···	···
342	MCG 4-37-016	10.91	0.45	2.27	2.88	···	···	···
343	NGC 5975	10.77	0.29	3.86	7.23	···	···	···
344	NGC 5980	10.80	0.32	3.33	8.60	2.31±0.11	···	···
345	NGC 5992	11.19	0.21	1.50	<4.27	···	···	···
346	NGC 5996	10.63	0.47	4.10	7.60	···	···	···
347	IRAS 15519+3537	11.60	0.049	0.88	1.99	···	···	···
348	UGC 10099	11.15	0.16	1.86	3.45	···	···	···
349	MCG 5-38-006	10.64	0.58	3.06	3.07	···	···	···
350	UGC 10120	10.79	0.15	0.64	1.34	···	···	···
351	NGC 6027A	10.21	0.033	1.03	2.20	···	···	···
352	NGC 6039	11.11	<0.25	0.77	1.34	···	···	···
353	UGC 10200	9.62	0.21	1.46	1.86	···	···	···
354	IRAS 16052+5334	11.70	0.044	0.80	2.37	···	···	···
355	IRAS 16053+1836	11.19	0.18	2.11	3.32	···	···	···
356	NGC 6090	11.57	0.93	6.49	9.98	···	···	···
357	UGC 10273	10.97	0.16	1.77	4.36	2.26±0.26	···	···
358	IRAS 16150+2233	11.76	0.12	0.61	4.28[d]	···	···	···
359	UGC 10322	10.66	0.19	1.96	5.58	···	···	···
360	NGC 6120	11.39	0.27	4.01	8.26	1.31±0.18	···	···
361	MCG 3-42-004	11.18	0.12	1.34	2.94	···	···	···
362	UGC 10407	10.93	0.15	1.74	3.13	···	···	···
363	IRAS 16320+3922	10.75	0.014	0.67	1.98	···	···	···
364	NGC 6186	11.46	0.26	2.92	6.27	···	···	···
365	MCG 9-27-053	11.10	0.07	2.22	5.10	···	···	···
366	UGC 10514	10.90	0.22	2.65	4.47	···	···	···

TABLE 7 — *Continued*

SFRS	Name	L(TIR) ($L_\odot$)	MIPS F(24)[a] (Jy)	IRAS F(60) (Jy)	IRAS F(100) (Jy)	Planck F(350) (Jy)	Planck F(550) (Jy)	Planck (F850) (Jy)
367	IRAS 16435+2154	11.09	0.11	2.07	3.81	...	...	...
368	IC 4623	11.07	0.14	1.62	3.53	...	...	...
369	IRAS 16516+3030	11.71	0.12	1.63	3.21	...	...	...

Note. —

[a] The MIPS 24 μm photometry has been aperture corrected using the correction factors listed in Table 8. The uncertainties in total 24 μm flux densities are dominated by the uncertainty in the absolute calibration, which is estimated as 4–8% according to the MIPS Instrument Handbook, version 2. Where upper limits are given, the photometry is from IRAS with quality flag = 1.

[b] IRAS flux density (MIPS not available). Typical uncertainties are 10–20%.

[c] OJ 287 is highly variable. Flux densities here are from *IRAS* survey coadds (Impey & Neugebauer 1988), but many more measurements exist in the literature.

[d] IRAS flux densities taken from Rice et al. 1988.

[e] Measurement taken from Dale et al. 2005.

TABLE 8
Spitzer/MIPS Aperture Correction Factors for SFRS Galaxies

SFRS	Name	Factor
24	NGC 2623	1.01
35	NGC 2719	1.01
36	IRAS 08572+3915	1.04
52	NGC 2854	1.05
60	MCG 8-18-013	1.05
70	NGC 3049	1.01
85	UGC 5644	1.07
90	NGC 3265	1.03
93	UGC 5720	1.03
104	NGC 3413	1.07
106	CGCG 95-055	1.08
108	IRAS 10565+2448	1.05
112	MCG 7-23-019	1.07
115	IRAS 11069+2711	1.02
116	IC 676	1.06
117	IRAS 11102+3026	1.08
118	IC 2637	1.08
120	7ZW 384	1.06
121	IRAS 11167+5351	1.07
124	NGC 3656	1.11
125	NGC 3659	1.02
128	IC 691	1.06
130	UGC 6469	1.05
132	IC 698	1.06
133	IRAS 11267+1558	1.12
135	MCG 3-29-061	1.07
136	NGC 3720	1.08
138	MCG 10-17-019	1.07
139	NGC 3758	1.07
143	NGC 3773	1.05
144	NGC 3781	1.05
145	UGC 6625	1.05
146	NGC 3808A	1.09
148	NGC 3822	1.06
150	MCG 3-30-051	1.06
151	NGC 3839	1.04
152	UGC 6732	1.05
153	IC 730	1.08
155	NGC 3912	1.03
156	NGC 3928	1.05
157	NGC 3934	1.05
158	UGC 6865	1.01
159	UGC 6901	1.04
162	NGC 4004	1.02
163	NGC 4014	1.03
165	NGC 4018	1.03
167	IRAS 11571+3003	1.07
168	UGC 7017	1.05
169	UGC 7016	1.04
170	MCG 3-31-030	1.08
176	NGC 4150	1.07
180	IRAS 12112+0305	1.02
184	NGC 4207	1.01
185	UGC 7286	1.09
186	NGC 4234	1.04
190	MCG 3-32-005	1.07
191	NGC 4290	1.02
193	NGC 4314	1.04
194	NGC 4385	1.05
197	NGC 4412	1.04
206	IRAS 12265+0219	1.07
206	IRAS 12274+0018	1.11
207	NGC 4491	1.04
208	NGC 4500	1.04
209	NGC 4495	1.06
211	NGC 4509	1.08
214	IRAS 12337+5044	1.06
215	IC 3581	1.05
219	NGC 4630	1.02
221	UGC 7905	1.02
222	MCG 5-30-069	1.07
223	IC 3721	1.08
224	NGC 4670	1.05
229	NGC 4704	1.04

TABLE 8 — *Continued*

SFRS	Name	Factor
230	NGC 4701	1.01
231	IRAS 12468+3436	1.05
232	IRAS 12470+1404	1.08
233	MCG 8-23-097	1.06
235	UGC 8017	1.04
236	NGC 4765	1.05
237	VCC2096	1.01
239	UGC 8058	1.02
240	NGC 4837	1.05
241	UM 530	1.10
242	NGC 4861	1.01
243	NGC 4868	1.04
244	NGC 4922	1.05
245	UGC 8179	1.05
246	NGC 5001	1.06
247	IC 856	1.07
248	UGC 8269	1.09
251	IRAS 13116+4508	1.10
252	IC 860	1.05
253	IRAS 13144+4508	1.04
254	NGC 5060	1.06
255	UGC 8357	1.07
256	UGC 8361	1.08
257	IC 883	1.06
258	NGC 5100	1.04
259	NGC 5104	1.07
262	NGC 5123	1.03
263	IRAS 13218+0552	1.08
264	IRAS 13232+1731	1.06
267	UGC 8502	1.06
268	UGC 8561	1.05
271	NGC 5256	1.02
272	UGC 8626	1.08
273	NGC 5263	1.03
274	MCG 1-35-028	1.05
275	IC 910	1.05
276	MK 268	1.05
277	NGC 5278	1.05
278	NGC 5273	1.07
279	UGC 8685	1.06
283	MK 796	1.02
284	IRAS 13446+1121	1.04
285	NGC 5303	1.04
287	MCG 3-35-034	1.07
290	NGC 5368	1.04
291	UGC 8827	1.04
293	UGC 8856	1.08
294	NGC 5374	1.03
295	UGC 8902	1.03
298	NGC 5414	1.07
299	MCG 5-33-046	1.06
301	NGC 5480	1.01
302	MCG 6-31-070	1.07
303	CGCG 74-129	1.05
304	NGC 5520	1.03
305	NGC 5515	1.06
306	NGC 5526	1.02
307	NGC 5522	1.04
308	NGC 5541	1.05
309	IC 4395	1.06
310	UGC 9165	1.04
311	MK 1490	1.06
312	IC 4408	1.01
315	NGC 5633	1.03
317	NGC 5656	1.02
319	CGCG 133-083	1.08
321	MCG 6-32-070	1.05
322	UGC 9412	1.04
323	NGC 5698	1.04
324	NGC 5691	1.03
325	MCG 9-24-035	1.07
326	MCG 9-24-038	1.06
327	UGC 9560	1.07
328	IC 1076	1.05
329	IRAS 14538+1730	1.11
330	NGC 5795	1.03

TABLE 8 — *Continued*

SFRS	Name	Factor
332	UGC 9639	1.05
333	MCG 6-33-022	1.05
335	MCG 9-25-036	1.10
338	MK 848	1.02
340	UGC 9922	1.05
341	IC 4567	1.03
342	MCG 4-37-016	1.03
343	NGC 5975	1.06
344	NGC 5980	1.01
345	NGC 5992	1.07
347	IRAS 15519+3537	1.10
348	UGC 10099	1.06
349	MCG 5-38-006	1.05
350	UGC 10120	1.08
351	NGC 6027A	1.03
353	UGC 10200	1.03
355	IRAS 16053+1836	1.07
356	NGC 6090	1.02
357	UGC 10273	1.01
358	IRAS 16150+2233	1.10
359	UGC 10322	1.05
360	NGC 6120	1.05
361	MCG 3-42-004	1.08
362	UGC 10407	1.04
363	IRAS 16320+3922	1.10
364	NGC 6186	1.03
365	MCG 9-27-053	1.08
366	UGC 10514	1.06
367	IRAS 16435+2154	1.08
368	IC 4623	1.02
369	IRAS 16516+3030	1.06

NOTE. — MIPS 24 μm aperture correction factors based on Version 2 of the MIPS Instrument Handbook, page 94. These factors have been applied to the photometry presented in Table 7. When not given, the correction factor was taken to be unity.

TABLE 9
Visible and Near-Infrared Photometry for SFRS Galaxies

SFRS			SDSS				2MASS	
	u	g	r	i	z	J	H	K_s
1	15.838±0.015	14.095±0.002	13.370±0.004	13.009±0.002	12.807±0.005	12.38±0.02	12.18±0.02	12.34±0.03
2	15.387±0.025	14.100±0.010	13.683±0.018	13.407±0.023	13.289±0.023	12.70±0.02	12.54±0.03	12.74±0.04
3	15.796±0.049	13.236±0.008	12.769±0.006	12.985±0.017	13.718±0.032	11.66±0.02	11.52±0.03	11.12±0.07
4	15.413±0.018	13.567±0.004	12.873±0.003	12.531±0.003	12.321±0.005	11.73±0.02	11.47±0.03	11.66±0.03
5	15.966±0.019	14.575±0.003	13.883±0.004	13.486±0.003	13.239±0.005	12.67±0.03	12.49±0.03	12.60±0.04
6	16.531±0.015	15.256±0.027	14.641±0.033	14.277±0.025	14.062±0.025	13.46±0.03	13.35±0.03	13.43±0.04
7	18.184±0.043	16.437±0.005	15.549±0.003	15.117±0.004	14.790±0.008	14.14±0.04	14.04±0.06	14.03±0.06
8	15.073±0.025	13.432±0.007	12.865±0.004	12.500±0.005	12.571±0.009	11.54±0.02	11.36±0.03	11.45±0.04
9	16.282±0.034	15.343±0.022	15.027±0.025	14.781±0.022	14.631±0.022	13.76±0.04	13.65±0.06	13.87±0.07
10	15.622±0.045	13.769±0.019	13.273±0.017	13.002±0.018	13.477±0.053	11.86±0.03	11.70±0.03	11.96±0.04
11	15.379±0.033	13.209±0.009	12.554±0.011	12.164±0.011	12.081±0.013	11.40±0.02	11.11±0.03	11.27±0.03
12	13.899±0.016	12.392±0.005	12.296±0.015	12.141±0.014	11.548±0.006	10.82±0.02	10.72±0.03	10.97±0.03
13	15.123±0.795	13.483±0.104	13.208±0.130	13.192±0.237	13.428±1.629	12.33±0.03	12.31±0.04	12.59±0.06
14	15.865±0.017	14.325±0.132	13.508±0.025	13.083±0.014	12.803±0.007	12.23±0.02	12.05±0.03	12.18±0.03
15	15.990±0.030	14.387±0.005	13.788±0.020	13.420±0.002	13.337±0.018	12.77±0.03	12.46±0.03	12.71±0.04
16	17.051±0.125	16.092±0.139	15.167±0.133	14.548±0.115	14.597±0.205	12.32±0.02	12.02±0.02	12.17±0.03
17[a]	13.17±0.2	15.010±0.101	14.438±0.072	13.937±0.011	14.318±0.042	15.39±0.09	15.21±0.12	15.45±0.15
18	15.759±0.018	14.404±0.003	13.916±0.003	13.610±0.003	13.530±0.009	13.11±0.04	12.93±0.04	13.21±0.05
19	18.932±0.184	16.922±0.029	16.673±0.055	16.446±0.062	15.747±0.044	14.80±0.09	14.41±0.09	14.62±0.17
20	17.733±0.061	16.293±0.010	15.617±0.010	15.261±0.012	14.977±0.018	13.74±0.05	13.44±0.05	13.77±0.08
21	15.230±0.032	13.700±0.008	13.279±0.007	13.174±0.010	13.480±0.022	12.91±0.04	12.78±0.05	12.88±0.06
22	15.558±0.082	13.520±0.021	12.853±0.017	12.575±0.024	12.565±0.040	11.17±0.02	10.97±0.02	11.17±0.03
23	16.070±0.020	15.179±0.016	14.604±0.015	14.470±0.016	14.244±0.017	13.36±0.07	13.16±0.07	13.31±0.05
24	16.040±0.022	14.313±0.005	13.682±0.004	13.329±0.004	13.187±0.006	12.44±0.02	12.16±0.03	12.27±0.03
25	17.069±0.039	15.448±0.003	14.675±0.002	14.276±0.002	13.969±0.006	13.45±0.03	13.16±0.04	13.33±0.05
26	15.084±0.027	13.722±0.019	13.127±0.021	12.825±0.024	12.700±0.023	12.10±0.03	12.01±0.04	12.20±0.06
27	15.368±0.009	13.983±0.002	13.356±0.001	13.055±0.002	12.841±0.003	12.42±0.02	12.25±0.02	12.49±0.04
28	17.186±0.066	14.997±0.019	14.367±0.019	13.991±0.024	13.831±0.029	14.74±0.05	14.56±0.07	14.37±0.05
29	16.708±0.020	15.432±0.005	14.814±0.004	14.550±0.005	14.342±0.008	13.82±0.04	13.75±0.07	13.76±0.07
30	16.619±0.006	16.008±0.002	15.484±0.002	15.098±0.002	14.778±0.003	14.42±0.02	13.97±0.04	13.63±0.03
31	17.066±0.041	15.478±0.006	14.820±0.010	14.398±0.007	14.168±0.011	13.69±0.05	13.29±0.06	13.47±0.06
32	19.894±0.697	16.680±0.035	15.660±0.013	15.294±0.025	15.319±0.074	14.20±0.06	13.90±0.07	13.71±0.06
33	14.732±0.021	13.187±0.003	12.508±0.005	12.221±0.004	12.210±0.013	11.43±0.02	11.21±0.03	11.35±0.03
34	14.887±0.024	12.959±0.017	12.246±0.006	11.932±0.014	11.835±0.008	10.88±0.02	10.72±0.02	10.94±0.03
35	15.191±0.012	14.392±0.024	14.123±0.020	13.946±0.021	13.913±0.028	13.36±0.03	13.55±0.05	13.67±0.07
36	18.985±0.188	17.292±0.062	16.793±0.055	16.516±0.064	16.260±0.052	15.84±0.12	15.10±0.10	14.92±0.09
37	17.601±0.052	16.322±0.015	15.710±0.027	15.250±0.028	15.041±0.037	14.13±0.04	13.80±0.05	13.86±0.06
38	14.908±0.214	13.756±0.081	13.202±0.024	12.946±0.021	12.829±0.035	12.32±0.03	12.17±0.04	12.33±0.05
39	15.409±0.058	13.898±0.132	13.457±0.112	13.343±0.146	13.591±0.050	13.34±0.03	13.24±0.06	13.66±0.08
40	16.549±0.073	15.675±0.098	15.487±0.128	15.131±0.137	15.213±0.160	13.17±0.05	13.13±0.08	12.88±0.05
41	15.294±0.017	14.332±0.004	13.673±0.003	13.350±0.005	13.052±0.013	11.35±0.03	11.41±0.05	11.51±0.06
42	15.750±0.019	14.044±0.005	13.323±0.004	12.937±0.005	12.742±0.005	12.15±0.01	11.93±0.01	12.08±0.09
43	17.080±0.083	15.103±0.020	14.108±0.007	13.695±0.006	13.431±0.007	12.78±0.03	12.53±0.04	12.58±0.04
44	16.244±0.028	14.715±0.017	13.804±0.012	13.385±0.011	13.216±0.009	12.44±0.02	12.19±0.03	12.34±0.03
45	14.538±0.018	12.741±0.008	12.137±0.008	11.799±0.006	11.856±0.005	10.92±0.02	10.80±0.02	10.97±0.04
46	15.178±0.011	13.536±0.007	12.836±0.007	12.475±0.007	12.253±0.005	11.73±0.02	11.47±0.02	11.69±0.03
47	19.163±0.110	17.512±0.010	16.651±0.008	16.115±0.007	15.808±0.016	15.04±0.07	14.93±0.10	14.71±0.09
48	15.647±0.012	13.957±0.005	13.151±0.005	12.744±0.004	12.463±0.004	11.95±0.02	11.76±0.02	11.97±0.03
49	17.383±0.038	15.730±0.019	14.967±0.017	14.537±0.014	14.291±0.010	13.77±0.04	13.41±0.04	13.60±0.05
50	16.451±0.022	15.669±0.019	15.411±0.008	15.254±0.008	15.105±0.015	14.81±0.06	14.93±0.11	14.81±0.11
51	17.576±0.067	16.064±0.006	15.260±0.005	14.824±0.004	14.530±0.016	13.92±0.04	13.63±0.06	13.66±0.05
52	15.054±0.013	13.610±0.005	12.975±0.005	12.636±0.004	12.447±0.007	11.92±0.03	11.69±0.03	11.93±0.03
53	15.659±0.018	14.315±0.011	13.647±0.011	13.305±0.012	13.117±0.010	12.61±0.03	12.34±0.03	12.46±0.03
54	15.990±0.041	14.495±0.054	13.819±0.038	13.479±0.036	13.309±0.029	12.72±0.03	12.50±0.03	12.64±0.04
55	14.790±0.009	13.542±0.015	12.952±0.015	12.656±0.015	12.507±0.006	12.10±0.02	11.87±0.02	12.15±0.02
56	16.374±0.025	14.933±0.005	14.141±0.003	13.744±0.003	13.537±0.010	12.95±0.03	12.64±0.03	12.64±0.04
57	16.543±0.020	15.034±0.002	14.350±0.002	13.994±0.002	13.780±0.007	13.29±0.03	13.07±0.04	13.25±0.04
58	15.120±0.028	14.184±0.014	13.778±0.012	13.579±0.009	13.439±0.012	12.88±0.03	12.79±0.04	13.02±0.06
59	16.153±0.025	15.036±0.010	14.520±0.007	14.170±0.006	14.047±0.009	13.50±0.03	13.43±0.06	13.49±0.05
60	17.470±1.411	14.456±0.022	13.819±0.118	13.550±0.025	12.678±0.114	13.00±0.03	12.79±0.04	12.91±0.04
61	17.281±0.051	15.551±0.008	14.677±0.036	14.185±0.006	13.848±0.009	13.16±0.04	12.83±0.04	12.83±0.04
62	16.061±0.031	14.634±0.012	13.735±0.007	13.291±0.006	13.032±0.012	11.74±0.02	11.50±0.03	11.69±0.04
63	15.235±0.023	13.589±0.042	13.001±0.008	12.633±0.004	12.536±0.011	11.86±0.02	11.65±0.03	11.88±0.03
64	17.083±0.046	15.370±0.009	14.586±0.005	14.183±0.003	13.954±0.006	13.36±0.03	13.13±0.03	13.21±0.04
65	15.985±0.110	13.779±0.010	13.130±0.021	12.855±0.004	12.955±0.042	12.10±0.04	11.94±0.04	12.01±0.06
66	17.146±0.021	15.905±0.003	15.304±0.004	14.940±0.011	14.746±0.022	14.36±0.07	14.04±0.07	14.27±0.11
67	15.579±0.011	14.256±0.003	13.595±0.002	13.235±0.003	12.961±0.003	12.49±0.02	12.20±0.02	12.41±0.03
68	16.114±0.021	14.827±0.035	14.202±0.033	13.898±0.033	13.674±0.022	13.24±0.04	12.88±0.04	13.14±0.06
69	14.917±0.018	13.988±0.009	13.676±0.005	13.561±0.006	13.657±0.012	12.35±0.04	12.32±0.06	12.52±0.08
70	14.924±0.016	13.599±0.005	12.951±0.002	12.736±0.004	12.903±0.009	11.80±0.04	11.65±0.04	11.80±0.06
71	14.100±0.015	12.801±0.004	12.258±0.003	12.035±0.005	12.049±0.014	11.28±0.03	11.07±0.03	11.33±0.04
72	15.196±0.017	13.897±0.004	13.247±0.004	12.966±0.004	12.765±0.005	12.26±0.02	12.02±0.02	12.22±0.03
73	15.797±0.024	14.138±0.009	13.377±0.007	12.992±0.007	12.764±0.004	12.24±0.02	11.97±0.02	12.18±0.03
74	15.131±0.879	13.174±0.242	12.714±0.210	12.484±0.136	12.375±0.280	11.31±0.03	11.34±0.04	11.49±0.05

TABLE 9 — *Continued*

SFRS			SDSS				2MASS	
	u	g	r	i	z	J	H	K_s
75	16.423±0.019	14.735±0.008	13.944±0.008	13.543±0.008	13.222±0.007	15.50±0.18	15.20±0.15	15.55±0.32
76	15.590±0.013	14.365±0.011	13.674±0.011	13.366±0.011	13.142±0.010	12.57±0.03	12.43±0.03	12.58±0.04
77	17.913±0.057	16.305±0.019	15.531±0.015	15.051±0.015	14.804±0.013	14.18±0.05	13.90±0.06	13.80±0.06
78	14.281±0.013	12.955±0.003	12.566±0.004	12.125±0.004	12.113±0.008	11.08±0.02	10.97±0.02	11.31±0.04
79	19.633±0.166	18.305±0.017	17.493±0.013	16.979±0.012	16.684±0.032	16.23±0.11	15.81±0.13	15.30±0.13
80	14.632±0.039	12.364±0.024	11.370±0.020	10.777±0.022	10.344±0.020	9.37±0.02	9.12±0.02	9.30±0.02
81	14.678±0.012	13.666±0.007	13.119±0.005	12.923±0.007	12.766±0.007	12.26±0.03	12.20±0.04	12.39±0.05
82	15.098±0.013	14.011±0.005	13.620±0.004	13.374±0.003	13.287±0.006	12.95±0.03	12.75±0.05	12.99±0.05
83	15.094±0.050	13.866±0.018	13.349±0.005	13.205±0.023	13.534±0.057	12.75±0.04	12.73±0.06	12.99±0.06
84	16.383±0.038	14.902±0.017	14.232±0.020	13.811±0.013	13.554±0.009	12.90±0.03	12.60±0.03	12.65±0.04
85	16.172±0.025	14.462±0.004	13.726±0.008	13.314±0.003	13.054±0.006	12.42±0.03	12.19±0.03	12.47±0.04
86	13.802±0.009	11.810±0.004	11.025±0.005	10.604±0.004	10.338±0.002	9.66±0.01	9.46±0.01	9.70±0.01
87	15.874±0.016	14.539±0.005	13.897±0.004	13.570±0.003	13.364±0.005	12.79±0.02	12.63±0.02	12.85±0.03
88	16.982±0.053	15.172±0.008	14.434±0.008	14.037±0.009	13.763±0.013	13.06±0.03	12.70±0.03	12.76±0.04
89	16.953±0.023	15.777±0.021	15.224±0.019	14.867±0.010	14.761±0.011	14.33±0.07	14.08±0.08	14.04±0.09
90	15.217±0.008	13.863±0.002	13.181±0.028	12.838±0.016	12.615±0.003	12.24±0.02	12.04±0.02	12.28±0.03
91	16.199±0.029	14.444±0.043	13.651±0.037	13.220±0.031	12.989±0.010	12.42±0.02	12.18±0.02	12.40±0.03
92	14.273±0.010	13.252±0.004	12.881±0.007	12.773±0.005	12.955±0.018	12.44±0.03	12.39±0.04	12.58±0.05
93	14.302±0.015	13.457±0.011	13.062±0.012	12.931±0.013	12.807±0.010	12.28±0.03	12.06±0.04	12.27±0.04
94	15.783±0.013	14.655±0.004	14.207±0.004	13.860±0.004	13.785±0.007	13.12±0.03	13.06±0.04	12.95±0.04
95	15.496±0.016	14.025±0.007	13.366±0.010	13.014±0.013	12.847±0.007	12.28±0.02	12.07±0.03	12.25±0.03
96	15.042±0.010	14.025±0.004	13.647±0.003	13.481±0.003	13.444±0.009	13.12±0.05	13.09±0.06	13.14±0.06
97	16.535±0.042	15.199±0.013	14.415±0.010	14.054±0.008	13.780±0.008	13.13±0.03	12.84±0.03	12.89±0.03
98	16.843±0.142	12.749±0.002	12.027±0.001	11.612±0.001	11.695±0.006	9.98±0.03	9.75±0.04	9.97±0.04
99	14.072±0.017	13.218±0.013	12.856±0.010	12.774±0.009	12.728±0.007	12.25±0.03	12.07±0.03	12.45±0.05
100	16.093±0.016	14.504±0.014	13.759±0.013	13.375±0.012	13.133±0.007	12.50±0.03	12.34±0.04	12.61±0.05
101	14.155±0.012	12.748±0.003	12.182±0.004	11.910±0.002	11.813±0.005	11.22±0.02	11.02±0.02	11.27±0.03
102	14.717±0.018	13.273±0.004	12.827±0.008	12.674±0.005	13.002±0.015	12.25±0.04	11.99±0.04	12.16±0.05
103	16.178±0.024	14.468±0.003	13.759±0.005	13.415±0.004	13.281±0.008	12.63±0.02	12.33±0.03	12.51±0.04
104	14.260±0.007	13.214±0.007	12.854±0.011	12.660±0.005	12.616±0.007	12.26±0.02	12.19±0.03	12.57±0.04
105	15.853±0.023	14.324±0.004	13.696±0.002	13.332±0.002	13.290±0.008	12.70±0.01	12.55±0.05	12.61±0.02
106	14.268±0.021	12.696±0.006	12.074±0.002	11.731±0.002	11.611±0.010	10.71±0.01	10.50±0.05	10.73±0.04
107	17.195±0.045	15.593±0.006	14.792±0.005	14.350±0.006	14.121±0.010	13.47±0.03	13.15±0.04	13.32±0.05
108	17.297±0.044	15.730±0.022	15.001±0.019	14.504±0.017	14.235±0.018	13.26±0.04	13.04±0.05	13.13±0.05
109[b]	···	···	···	···	···	12.42±0.02	12.25±0.03	12.41±0.04
110	15.722±0.212	12.935±0.024	12.178±0.151	11.957±0.028	11.875±0.035	10.76±0.01	10.60±0.02	10.77±0.02
111	15.130±0.018	13.938±0.008	13.433±0.007	13.109±0.007	13.067±0.011	12.66±0.02	12.44±0.03	12.59±0.03
112	16.505±0.031	15.325±0.027	14.811±0.025	14.552±0.028	14.330±0.030	13.45±0.03	13.16±0.04	13.27±0.04
113	14.967±0.010	13.521±0.002	12.906±0.002	12.558±0.001	12.403±0.003	11.83±0.02	11.63±0.02	11.83±0.03
114	17.163±0.031	15.556±0.005	14.795±0.005	14.387±0.005	14.108±0.008	13.58±0.03	13.24±0.04	13.38±0.04
115	18.246±0.118	17.142±0.057	16.813±0.055	16.573±0.107	16.448±0.166	15.88±0.10	15.55±0.10	15.69±0.14
116	15.241±0.032	13.354±0.013	12.647±0.009	12.283±0.008	12.181±0.012	11.56±0.03	11.31±0.03	11.54±0.05
117	17.846±0.053	16.104±0.023	15.325±0.018	14.994±0.032	14.754±0.037	14.01±0.04	13.81±0.05	13.94±0.06
118	15.491±0.012	14.069±0.002	13.470±0.002	13.140±0.002	12.955±0.005	12.40±0.03	12.16±0.03	12.29±0.05
119	17.546±0.046	16.138±0.007	15.473±0.006	15.066±0.006	14.836±0.017	14.37±0.06	14.13±0.08	14.06±0.07
120	18.268±0.196	17.157±0.159	16.730±0.168	16.421±0.192	16.195±0.176	14.48±0.07	14.26±0.11	14.17±0.07
121	18.062±0.044	16.780±0.008	16.049±0.007	15.500±0.006	15.241±0.012	14.68±0.06	14.26±0.07	14.04±0.05
122	15.653±0.015	14.088±0.005	13.229±0.003	12.796±0.003	12.472±0.004	11.84±0.02	11.57±0.02	11.71±0.03
123	14.234±0.025	13.118±0.009	12.788±0.007	12.629±0.005	12.627±0.012	12.60±0.05	12.31±0.06	12.30±0.07
124	14.943±0.015	13.096±0.023	12.382±0.005	12.026±0.008	11.837±0.005	11.17±0.02	10.95±0.03	11.11±0.03
125	14.376±0.014	13.211±0.005	12.776±0.013	12.542±0.008	12.528±0.021	11.93±0.02	11.88±0.03	12.12±0.03
126	16.158±0.079	14.436±0.018	14.116±0.013	14.021±0.016	14.589±0.060	13.93±0.08	13.88±0.10	14.16±0.17
127	14.694±0.051	12.765±0.005	12.142±0.007	11.814±0.012	11.671±0.012	11.04±0.02	10.83±0.02	11.07±0.03
128	15.174±0.007	14.219±0.004	13.638±0.004	13.467±0.005	13.279±0.007	12.79±0.03	12.63±0.04	12.70±0.04
129	14.374±0.027	12.688±0.034	12.055±0.003	11.661±0.005	11.961±0.016	10.31±0.01	10.04±0.01	10.33±0.01
130	15.150±0.013	14.135±0.005	13.785±0.007	13.609±0.006	13.571±0.020	12.95±0.04	12.88±0.04	13.12±0.07
131	13.836±0.040	12.738±0.022	12.259±0.024	12.052±0.023	11.918±0.034	10.50±0.02	10.20±0.03	10.26±0.02
132	15.717±0.015	14.200±0.010	13.431±0.010	13.043±0.011	12.743±0.008	12.21±0.03	11.91±0.03	12.01±0.04
133	20.546±0.249	19.617±0.238	18.969±0.226	18.843±0.384	18.639±0.416	16.42±0.10	16.40±0.10	16.00±0.11
134[c]	15.413±0.085	13.862±0.128	11.993±0.013	11.011±0.005	9.92±0.2	9.69±0.02	9.52±0.02	9.76±0.03
135	16.239±0.023	14.669±0.005	13.992±0.006	13.625±0.003	13.443±0.006	13.06±0.03	12.92±0.04	13.00±0.04
136	15.307±0.016	13.673±0.005	12.957±0.009	12.612±0.012	12.490±0.018	11.77±0.03	11.62±0.03	11.76±0.04
137	14.263±0.025	12.557±0.034	11.844±0.021	11.478±0.016	11.343±0.014	10.23±0.01	10.09±0.02	10.57±0.03
138	15.875±0.013	14.512±0.003	13.852±0.002	13.513±0.003	13.337±0.005	12.75±0.03	12.50±0.03	12.71±0.04
139	16.137±0.087	14.585±0.036	13.973±0.035	13.610±0.038	13.477±0.046	12.62±0.03	12.36±0.04	12.23±0.04
140	15.579±0.023	14.502±0.013	13.989±0.008	13.781±0.008	13.524±0.007	12.98±0.03	12.83±0.03	13.08±0.05
141	17.081±0.079	15.671±0.038	15.025±0.048	14.711±0.031	14.622±0.058	13.82±0.05	13.65±0.06	13.68±0.08
142	13.797±0.020	12.498±0.014	11.954±0.018	11.660±0.012	11.533±0.007	10.98±0.02	10.68±0.02	11.04±0.03
143	14.841±0.039	13.904±0.024	13.355±0.017	13.175±0.016	13.259±0.021	12.37±0.03	12.47±0.05	12.54±0.06
144	16.363±0.018	14.459±0.004	13.694±0.004	13.318±0.004	13.056±0.006	12.47±0.02	12.24±0.03	12.33±0.03
145	15.357±0.020	14.045±0.005	13.672±0.004	13.411±0.004	13.325±0.007	12.83±0.03	12.72±0.05	12.77±0.04
146	16.307±0.027	14.917±0.030	14.364±0.030	14.065±0.025	13.931±0.019	13.30±0.04	13.00±0.03	13.20±0.04
147	14.947±0.016	13.202±0.002	12.605±0.002	12.233±0.001	12.152±0.005	11.50±0.02	11.36±0.02	11.54±0.03
148	15.435±0.015	13.725±0.006	12.943±0.005	12.571±0.005	12.299±0.004	11.60±0.02	11.34±0.02	11.42±0.03

TABLE 9 — *Continued*

SFRS			SDSS				2MASS	
	u	g	r	i	z	J	H	K_s
149	14.877±0.021	14.215±0.014	13.826±0.012	13.770±0.014	13.704±0.011	13.16±0.03	13.02±0.04	13.18±0.05
150	16.285±0.026	14.603±0.020	13.937±0.016	13.609±0.013	13.518±0.007	12.87±0.03	12.63±0.03	12.84±0.04
151	15.143±0.014	13.946±0.006	13.517±0.006	13.272±0.005	13.159±0.005	12.63±0.04	12.47±0.04	12.52±0.05
152	15.145±0.005	13.533±0.002	12.920±0.002	12.607±0.002	12.385±0.002	11.95±0.01	11.78±0.01	12.00±0.02
153	16.253±0.019	14.562±0.017	13.739±0.018	13.327±0.017	13.043±0.007	12.48±0.02	12.19±0.02	12.25±0.03
154	18.249±0.078	16.607±0.042	15.866±0.050	15.436±0.046	15.137±0.065	13.74±0.04	13.36±0.04	13.41±0.05
155	15.005±0.026	13.433±0.007	12.830±0.005	12.521±0.004	12.373±0.008	11.79±0.01	11.54±0.02	11.79±0.03
156	14.368±0.006	13.026±0.002	12.364±0.002	12.069±0.002	11.896±0.003	11.46±0.02	11.29±0.02	11.51±0.03
157	16.678±0.061	14.529±0.003	13.748±0.003	13.348±0.004	13.118±0.009	12.48±0.03	12.19±0.02	12.30±0.03
158	16.476±0.159	14.794±0.039	13.793±0.074	13.295±0.023	13.116±0.048	12.10±0.02	12.00±0.04	12.14±0.04
159	16.070±0.021	14.417±0.005	13.699±0.004	13.309±0.004	13.110±0.005	12.43±0.02	12.26±0.02	12.40±0.03
160	17.176±0.035	15.274±0.015	14.400±0.012	13.979±0.012	13.690±0.009	12.92±0.03	12.73±0.04	12.78±0.04
161	14.863±0.116	13.920±0.047	13.554±0.022	13.424±0.024	13.402±0.044	16.33±0.07	15.97±0.14	16.17±0.12
162	15.143±0.025	13.960±0.008	13.484±0.007	13.274±0.004	13.157±0.009	12.54±0.02	12.37±0.03	12.58±0.04
163	15.211±0.012	13.619±0.016	12.855±0.012	12.402±0.011	12.171±0.008	11.39±0.01	11.18±0.01	11.35±0.02
164	14.938±0.072	13.212±0.009	12.603±0.076	12.255±0.010	12.341±0.056	11.54±0.01	11.23±0.01	11.43±0.02
165	16.121±0.072	14.490±0.011	13.852±0.008	13.494±0.013	13.416±0.062	12.67±0.02	12.32±0.02	12.39±0.03
166	14.314±0.009	13.103±0.002	12.685±0.003	12.523±0.012	12.646±0.025	12.46±0.01	12.34±0.02	12.60±0.03
167	18.075±0.053	16.468±0.005	15.701±0.005	15.317±0.005	15.045±0.013	14.52±0.06	14.27±0.07	14.50±0.10
168	15.423±0.027	14.121±0.054	13.509±0.036	13.207±0.031	12.970±0.013	12.41±0.02	12.12±0.02	12.27±0.03
169	16.045±0.042	14.237±0.032	13.419±0.024	12.978±0.025	12.729±0.011	12.04±0.02	11.76±0.02	11.93±0.02
170	15.434±0.014	14.246±0.002	13.739±0.003	13.500±0.002	13.341±0.006	12.91±0.03	12.82±0.04	13.03±0.05
171	14.522±0.039	12.474±0.020	11.762±0.071	11.484±0.022	11.245±0.040	10.00±0.01	9.83±0.01	10.05±0.01
172	14.507±0.036	12.764±0.015	12.068±0.013	11.655±0.012	11.459±0.012	10.32±0.02	10.14±0.03	10.40±0.03
173	16.115±0.023	14.613±0.006	13.846±0.006	13.469±0.006	13.255±0.006	12.68±0.03	12.43±0.03	12.52±0.03
174	14.753±0.039	13.479±0.015	12.824±0.006	12.677±0.008	12.994±0.056	11.91±0.04	11.11±0.04	11.24±0.09
175	15.169±0.011	14.345±0.006	13.493±0.002	13.090±0.003	12.898±0.006	11.18±0.04	10.96±0.05	11.15±0.06
176	14.110±0.008	12.441±0.002	11.738±0.003	11.343±0.001	11.147±0.003	10.79±0.01	10.61±0.01	10.83±0.02
177	17.953±0.055	16.768±0.014	16.245±0.013	15.866±0.008	15.663±0.017	15.21±0.07	14.73±0.08	14.71±0.08
178[d]	16.614±0.258	16.270±0.912	15.344±0.484	15.907±1.621	…	11.16±0.01	10.97±0.02	11.21±0.02
179	15.385±0.040	13.603±0.009	12.778±0.003	12.554±0.005	12.537±0.010	10.76±0.05	10.73±0.07	11.41±0.03
180	17.653±0.058	16.701±0.022	16.231±0.024	15.783±0.026	15.690±0.052	14.91±0.10	14.63±0.11	14.62±0.15
181	15.533±0.229	14.107±0.037	13.491±0.020	13.141±0.033	13.020±0.069	10.82±0.03	10.69±0.04	10.75±0.04
182	14.303±0.019	13.248±0.010	12.667±0.010	12.470±0.013	12.208±0.010	11.50±0.02	11.29±0.02	11.47±0.02
183	15.154±0.035	14.087±0.008	13.636±0.004	13.477±0.006	13.570±0.018	13.12±0.05	13.71±0.04	13.68±0.09
184	15.108±0.033	13.299±0.003	12.546±0.003	12.163±0.003	11.947±0.006	11.35±0.02	11.12±0.02	11.28±0.03
185	16.968±0.033	15.015±0.017	14.225±0.015	13.841±0.014	13.557±0.010	12.97±0.03	12.65±0.03	12.89±0.04
186	14.600±0.016	13.363±0.004	12.912±0.002	12.711±0.003	12.737±0.009	12.92±0.03	12.87±0.08	13.02±0.05
187	13.987±0.010	12.376±0.001	11.697±0.002	11.314±0.001	11.093±0.003	10.44±0.01	10.21±0.01	10.45±0.02
188	13.838±0.025	11.934±0.003	11.438±0.003	11.077±0.005	11.337±0.009	9.43±0.03	9.33±0.03	9.56±0.05
189	15.008±0.009	13.499±0.001	12.871±0.001	12.595±0.001	12.422±0.003	11.97±0.02	11.73±0.03	11.68±0.02
190	16.177±0.021	14.818±0.005	14.151±0.003	13.815±0.003	13.558±0.006	13.03±0.03	12.76±0.03	12.97±0.04
191	14.923±0.020	12.924±0.002	12.214±0.001	11.863±0.002	11.863±0.007	11.13±0.02	10.95±0.02	11.14±0.03
192	14.469±0.041	13.343±0.058	12.750±0.054	12.703±0.030	12.736±0.077	11.45±0.04	11.54±0.06	11.54±0.07
193	13.556±0.147	11.743±0.265	10.992±0.256	10.587±0.257	10.287±0.239	9.39±0.01	9.18±0.02	9.40±0.01
194	14.394±0.011	13.069±0.001	12.477±0.002	12.219±0.003	12.166±0.006	11.51±0.03	11.37±0.03	11.62±0.05
195[e]	10.73±0.4	10.24±0.15	9.94±0.15	10.20±0.15	10.35±0.15	11.55±0.03	11.60±0.05	11.82±0.06
196[b]	…	…	…	…	…	11.93±0.05	11.81±0.07	12.18±0.08
197	14.381±0.011	12.972±0.002	12.426±0.001	12.226±0.003	12.315±0.009	11.62±0.04	11.53±0.04	11.49±0.05
198	15.475±0.026	13.648±0.003	12.948±0.005	12.576±0.014	12.422±0.009	11.91±0.02	11.71±0.03	11.96±0.05
199	13.980±0.011	12.676±0.003	12.230±0.002	12.031±0.002	12.013±0.011	11.38±0.02	11.24±0.02	11.50±0.04
200	14.549±0.066	12.623±0.019	11.996±0.044	11.759±0.027	11.801±0.041	10.74±0.02	10.62±0.03	10.93±0.04
201	13.552±0.004	11.666±0.006	10.880±0.007	10.450±0.006	10.176±0.006	9.32±0.01	8.52±0.01	9.14±0.02
202	13.680±0.007	11.684±0.004	10.782±0.005	10.289±0.004	9.967±0.001	9.12±0.02	8.91±0.02	9.11±0.02
203	14.297±0.034	12.026±0.001	11.221±0.003	10.771±0.001	10.480±0.003	9.60±0.02	9.41±0.02	9.65±0.02
204	12.683±0.001	12.807±0.000	12.732±0.001	12.480±0.001	12.723±0.001	12.59±0.02	12.31±0.02	11.77±0.02
205	14.022±0.007	12.900±0.002	12.464±0.001	12.233±0.002	12.213±0.006	11.75±0.03	11.66±0.04	11.96±0.05
206	17.973±0.042	16.454±0.005	15.602±0.004	15.201±0.004	14.920±0.012	14.42±0.08	14.16±0.09	14.04±0.10
207	15.124±0.019	13.327±0.003	12.643±0.002	12.276±0.002	12.140±0.006	11.56±0.03	11.42±0.04	11.72±0.05
208	14.381±0.012	13.070±0.037	12.533±0.031	12.266±0.027	12.116±0.010	11.54±0.01	11.42±0.02	11.58±0.02
209	15.817±0.028	14.065±0.004	13.380±0.006	13.053±0.008	12.900±0.016	12.15±0.02	11.87±0.03	11.98±0.03
210	14.709±0.015	13.623±0.006	13.203±0.005	13.042±0.005	12.952±0.011	12.62±0.05	12.76±0.08	12.75±0.07
211	15.232±0.024	14.376±0.014	14.184±0.017	14.131±0.018	14.092±0.024	14.38±0.09	14.05±0.08	14.55±0.14
212	14.566±0.021	12.924±0.004	12.480±0.002	12.360±0.004	12.617±0.011	11.39±0.04	11.30±0.05	11.39±0.06
213	14.363±0.021	12.007±0.019	11.245±0.015	10.781±0.015	10.450±0.014	8.88±0.02	8.73±0.03	8.96±0.03
214	17.130±0.051	15.825±0.028	15.244±0.014	14.891±0.014	14.692±0.020	14.22±0.05	13.98±0.06	14.02±0.07
215	15.867±0.017	14.458±0.009	13.757±0.007	13.406±0.006	13.157±0.005	12.69±0.02	12.47±0.03	12.57±0.03
216	13.626±0.007	12.499±0.009	12.149±0.006	12.024±0.002	12.105±0.026	11.87±0.01	11.76±0.02	12.06±0.03
217	18.852±4.030	13.599±0.049	12.817±0.005	12.379±0.049	12.179±0.066	11.62±0.01	11.31±0.02	11.42±0.02
218	14.668±0.013	13.115±0.003	12.559±0.001	12.317±0.002	12.322±0.005	11.52±0.03	11.29±0.04	11.59±0.05
219	14.796±0.018	13.539±0.009	12.861±0.006	12.603±0.007	12.616±0.012	11.62±0.04	11.56±0.05	11.73±0.07
220	16.839±0.036	15.198±0.009	14.523±0.007	14.098±0.007	14.016±0.010	13.35±0.05	13.11±0.05	13.10±0.07
221	15.242±0.007	14.440±0.005	14.131±0.006	14.002±0.007	13.798±0.008	13.55±0.03	13.25±0.03	13.53±0.05
222	16.399±0.024	14.736±0.004	13.982±0.003	13.581±0.004	13.358±0.009	12.87±0.03	12.77±0.04	12.84±0.04

TABLE 9 — *Continued*

SFRS	SDSS					2MASS		
	u	g	r	i	z	J	H	K_s
223	16.006±0.025	14.319±0.028	13.587±0.030	13.197±0.027	12.952±0.017	12.25±0.02	11.98±0.03	12.15±0.03
224	13.713±0.019	12.944±0.012	12.588±0.008	12.488±0.010	12.430±0.008	12.18±0.02	12.10±0.03	12.25±0.04
225	16.068±0.025	14.488±0.015	13.754±0.014	13.352±0.012	13.128±0.006	12.57±0.03	12.29±0.03	12.48±0.04
226	17.955±0.098	16.162±0.024	15.140±0.017	14.681±0.023	14.260±0.027	13.33±0.04	12.90±0.04	12.81±0.04
227[f]	···	11.2	10.7	···	···	9.63±0.03	9.41±0.04	9.80±0.05
228	16.166±0.068	14.337±0.027	13.863±0.017	13.674±0.008	13.715±0.022	13.20±0.09	12.68±0.06	13.00±0.10
229	16.295±0.046	14.255±0.004	13.589±0.004	13.239±0.003	13.189±0.010	12.69±0.04	12.48±0.06	12.53±0.05
230	14.262±0.010	12.954±0.006	12.490±0.006	12.263±0.006	12.208±0.007	11.58±0.03	11.42±0.03	11.61±0.04
231	20.110±0.202	18.551±0.016	17.750±0.013	17.244±0.013	16.952±0.031	16.36±0.12	16.28±0.18	15.86±0.12
232	17.000±0.022	16.110±0.005	15.829±0.005	15.558±0.007	15.506±0.025	15.16±0.08	14.91±0.11	15.14±0.12
233	17.021±0.036	15.183±0.004	14.458±0.005	14.006±0.006	13.723±0.008	13.05±0.03	12.78±0.04	12.79±0.04
234	15.005±0.033	13.211±0.016	12.655±0.004	12.418±0.024	12.552±0.043	11.81±0.03	11.54±0.05	12.13±0.03
235	15.805±0.020	14.252±0.005	13.536±0.003	13.150±0.002	12.870±0.007	12.28±0.02	11.94±0.02	12.09±0.03
236	14.158±0.008	13.315±0.004	12.959±0.004	12.832±0.005	12.817±0.004	12.51±0.03	12.33±0.04	12.66±0.06
237	17.395±0.082	16.179±0.040	15.769±0.058	15.230±0.056	15.129±0.069	14.48±0.06	14.22±0.07	14.42±0.10
238	15.392±0.157	13.914±0.009	13.458±0.245	13.282±0.026	13.787±0.387	13.31±0.04	13.08±0.05	13.82±0.12
239	15.030±0.008	13.784±0.008	13.908±0.021	12.988±0.014	12.706±0.009	11.89±0.02	11.24±0.02	10.65±0.02
240	15.461±0.034	13.994±0.014	13.410±0.014	13.048±0.021	12.919±0.033	12.46±0.03	12.23±0.12	12.36±0.03
241	17.191±0.023	16.444±0.011	16.233±0.013	15.823±0.015	15.797±0.024	15.55±0.15	15.17±0.15	15.01±0.16
242[b]	···	···	···	···	···	13.34±0.05	13.52±0.09	13.61±0.11
243	15.012±0.058	13.662±0.109	12.791±0.028	12.469±0.014	12.418±0.060	11.35±0.01	11.12±0.02	11.35±0.02
244	15.791±0.016	13.903±0.008	13.089±0.008	12.688±0.008	12.430±0.007	11.72±0.02	11.45±0.02	11.67±0.03
245	16.571±0.092	14.630±0.004	13.944±0.002	13.562±0.010	13.528±0.035	12.78±0.03	12.57±0.03	12.59±0.04
246	15.720±0.026	14.136±0.006	13.440±0.011	13.123±0.006	12.884±0.005	12.38±0.03	12.14±0.03	12.27±0.04
247	15.836±0.024	14.558±0.006	13.983±0.047	13.676±0.005	13.405±0.010	13.02±0.03	12.73±0.03	12.87±0.03
248	16.891±0.039	15.191±0.014	14.480±0.011	14.100±0.012	13.856±0.016	13.38±0.04	12.99±0.04	13.30±0.05
249	14.706±0.023	13.338±0.018	12.745±0.014	12.444±0.014	12.276±0.009	11.84±0.01	11.65±0.02	11.95±0.02
250	14.492±0.027	12.627±0.012	12.010±0.003	11.633±0.003	11.407±0.022	10.62±0.01	10.38±0.02	10.60±0.02
251	18.394±0.065	16.913±0.026	16.135±0.023	15.690±0.021	15.383±0.017	14.33±0.05	14.13±0.07	14.06±0.06
252	15.710±0.013	14.055±0.002	13.397±0.002	13.059±0.002	12.860±0.004	12.43±0.02	12.17±0.02	12.43±0.03
253	17.085±0.015	16.245±0.009	15.842±0.012	15.355±0.011	15.322±0.010	14.71±0.08	14.22±0.09	13.50±0.04
254	15.820±0.031	13.947±0.003	13.299±0.003	12.938±0.004	12.805±0.008	12.35±0.03	12.00±0.03	12.15±0.04
255	15.595±0.012	14.341±0.006	13.842±0.006	13.539±0.005	13.370±0.008	12.89±0.03	12.65±0.03	12.85±0.05
256	16.334±0.022	14.785±0.010	14.032±0.006	13.638±0.009	13.371±0.006	12.77±0.04	12.47±0.04	12.55±0.05
257	16.277±0.027	14.677±0.013	14.162±0.018	13.874±0.021	13.662±0.031	12.86±0.02	12.59±0.03	12.77±0.03
258	16.049±0.020	14.521±0.007	13.748±0.007	13.327±0.007	13.111±0.005	12.42±0.03	12.14±0.03	12.25±0.04
259	15.687±0.017	13.998±0.016	13.174±0.012	12.726±0.013	12.431±0.004	11.74±0.03	11.50±0.04	11.58±0.03
260[c]	14.796±0.029	13.726±0.010	13.419±0.023	13.260±0.013	12.68±0.05	13.06±0.03	13.10±0.05	13.33±0.07
261[d]	15.111±0.202	13.368±0.007	12.958±0.025	12.631±0.038	···	11.74±0.03	11.65±0.04	11.86±0.05
262	15.673±0.038	13.621±0.004	12.987±0.003	12.691±0.003	12.660±0.008	11.96±0.03	11.74±0.03	11.89±0.04
263	19.054±0.063	18.373±0.014	17.612±0.011	17.126±0.011	17.007±0.030	16.05±0.23	15.27±0.15	13.89±0.05
264	16.464±0.020	15.364±0.005	14.866±0.003	14.494±0.004	14.339±0.010	13.88±0.04	13.76±0.06	13.71±0.06
265	13.959±0.092	12.583±0.091	12.978±0.107	12.069±0.089	12.256±0.139	11.44±0.04	11.26±0.04	11.56±0.06
266	13.465±0.009	12.436±0.002	12.125±0.002	11.983±0.004	12.167±0.016	11.11±0.03	11.00±0.05	11.35±0.06
267	16.209±0.254	15.381±0.131	15.072±0.083	14.812±0.072	14.537±0.048	14.76±0.05	14.57±0.13	14.20±0.10
268	14.830±0.013	13.668±0.003	13.229±0.003	13.006±0.003	12.971±0.008	12.36±0.03	12.30±0.04	12.48±0.04
269[d]	15.121±0.202	13.376±0.007	12.971±0.025	12.636±0.038	···	11.46±0.03	11.16±0.03	11.67±0.05
270	15.330±0.004	14.629±0.002	14.306±0.002	13.774±0.002	13.846±0.003	13.54±0.03	13.02±0.03	12.29±0.02
271	15.950±0.084	14.574±0.047	14.052±0.037	13.693±0.034	13.556±0.064	12.14±0.05	11.88±0.06	11.64±0.05
272	16.242±0.029	14.679±0.018	13.976±0.014	13.627±0.010	13.455±0.009	12.87±0.04	12.60±0.04	12.73±0.06
273	15.724±0.042	14.067±0.009	13.421±0.010	13.046±0.005	12.833±0.020	12.10±0.02	11.87±0.03	12.01±0.03
274	16.097±0.019	14.558±0.010	13.826±0.012	13.439±0.010	13.198±0.007	12.77±0.04	12.48±0.04	12.63±0.05
275	16.062±0.017	14.683±0.004	14.054±0.003	13.729±0.002	13.514±0.005	13.04±0.03	12.86±0.04	13.00±0.06
276	16.295±0.020	14.671±0.006	13.931±0.007	13.554±0.007	13.309±0.006	12.65±0.03	12.51±0.03	12.72±0.03
277	16.074±0.044	14.597±0.025	13.867±0.024	13.450±0.024	13.192±0.028	12.12±0.02	11.99±0.03	12.11±0.03
278	14.711±0.017	12.538±0.002	11.833±0.001	11.473±0.002	11.376±0.005	10.37±0.01	10.19±0.02	10.50±0.02
279	15.796±0.037	14.235±0.008	13.658±0.007	13.344±0.016	13.272±0.017	12.79±0.02	12.59±0.03	12.71±0.04
280	16.524±0.145	14.634±0.007	13.936±0.013	13.598±0.009	13.371±0.023	12.66±0.03	12.35±0.03	12.60±0.05
281	16.421±0.019	14.788±0.006	14.225±0.005	13.842±0.004	13.588±0.005	13.05±0.03	12.77±0.03	12.73±0.03
282	15.055±0.120	12.719±0.013	11.988±0.016	11.631±0.005	11.460±0.011	10.71±0.02	10.53±0.02	10.73±0.03
283	15.864±0.009	14.783±0.004	14.212±0.004	13.939±0.005	13.690±0.006	13.19±0.03	12.87±0.03	12.93±0.04
284	16.851±0.033	15.168±0.003	14.411±0.002	14.046±0.002	13.785±0.005	13.31±0.05	12.92±0.05	12.94±0.06
285	14.320±0.044	13.268±0.042	12.844±0.044	12.630±0.007	12.509±0.039	11.97±0.02	11.88±0.02	12.07±0.03
286	14.194±0.009	12.648±0.002	11.899±0.001	11.570±0.001	11.308±0.002	10.67±0.01	10.47±0.01	10.66±0.02
287	16.512±0.022	14.928±0.016	14.198±0.016	13.767±0.014	13.514±0.010	12.89±0.03	12.61±0.03	12.73±0.04
288	15.741±0.038	13.258±0.002	12.587±0.002	12.271±0.002	12.242±0.005	11.49±0.03	11.33±0.04	11.48±0.04
289	14.521±0.018	12.548±0.002	11.832±0.001	11.493±0.003	11.544±0.007	10.11±0.01	10.23±0.02	10.46±0.03
290	15.466±0.021	13.733±0.001	13.059±0.001	12.733±0.001	12.531±0.004	12.01±0.02	11.82±0.02	12.04±0.03
291	15.557±0.010	14.059±0.009	13.351±0.009	13.014±0.010	12.791±0.005	12.20±0.02	12.06±0.02	12.16±0.03
292	15.677±0.011	14.459±0.003	14.106±0.003	13.714±0.003	13.585±0.006	13.47±0.04	13.08±0.04	12.24±0.03
293	17.212±0.049	15.728±0.011	15.107±0.010	14.719±0.010	14.437±0.018	13.75±0.05	13.43±0.06	13.50±0.06
294	14.999±0.022	13.299±0.003	12.672±0.002	12.459±0.004	12.301±0.005	11.41±0.03	11.29±0.04	11.54±0.05
295	16.153±0.072	13.985±0.039	13.198±0.020	12.863±0.025	12.606±0.008	11.79±0.02	11.58±0.02	11.79±0.03
296	16.415±0.139	13.720±0.012	12.910±0.023	12.416±0.004	12.193±0.026	11.18±0.02	10.85±0.02	10.96±0.03

TABLE 9 — *Continued*

SFRS			SDSS				2MASS	
	u	g	r	i	z	J	H	K_s
297	17.570±0.062	15.960±0.016	15.151±0.014	14.700±0.014	14.410±0.010	13.84±0.04	13.62±0.05	13.67±0.06
298	14.755±0.010	13.704±0.008	13.327±0.009	13.158±0.010	13.091±0.006	12.84±0.03	12.73±0.04	13.04±0.06
299	16.764±0.051	14.907±0.038	14.142±0.030	13.735±0.025	13.517±0.023	12.81±0.03	12.54±0.03	12.83±0.05
300	14.395±0.008	13.238±0.055	12.791±0.006	12.581±0.007	12.497±0.006	11.10±0.02	10.92±0.03	11.32±0.04
301	14.137±0.009	12.820±0.002	12.266±0.006	12.034±0.002	11.989±0.005	11.24±0.03	11.09±0.03	11.30±0.04
302	17.176±0.036	15.532±0.007	14.710±0.004	14.311±0.004	14.070±0.009	13.41±0.03	12.91±0.04	13.11±0.04
303	16.752±0.037	15.001±0.003	14.287±0.003	13.920±0.003	13.717±0.009	13.29±0.03	12.99±0.03	13.20±0.05
304	15.044±0.023	13.310±0.006	12.762±0.003	12.488±0.003	12.347±0.006	11.75±0.02	11.61±0.02	11.81±0.03
305	15.337±0.013	13.767±0.017	13.107±0.013	12.743±0.014	12.489±0.004	11.93±0.02	11.64±0.02	11.77±0.02
306	15.348±0.043	14.078±0.012	13.415±0.005	13.087±0.019	12.883±0.027	12.28±0.02	12.03±0.03	12.16±0.03
307	15.408±0.032	13.728±0.052	13.049±0.068	12.649±0.035	12.395±0.013	11.86±0.02	11.62±0.03	11.75±0.03
308	15.028±0.011	13.668±0.011	13.116±0.021	12.802±0.023	12.622±0.012	12.00±0.02	11.75±0.02	11.86±0.02
309	16.234±0.091	14.387±0.030	13.711±0.025	13.322±0.022	13.203±0.021	12.42±0.02	12.19±0.02	12.29±0.02
310	16.619±0.052	14.900±0.011	13.967±0.006	13.508±0.007	13.193±0.023	12.41±0.02	12.08±0.02	12.13±0.03
311	16.931±0.020	15.327±0.002	14.579±0.002	14.181±0.002	13.884±0.005	13.42±0.03	13.08±0.04	13.14±0.04
312	14.186±0.017	12.882±0.002	12.395±0.002	12.153±0.002	12.515±0.024	11.10±0.03	10.93±0.04	11.34±0.05
313	16.001±0.017	14.489±0.004	13.762±0.003	13.359±0.003	13.077±0.005	12.51±0.03	12.27±0.03	12.43±0.03
314	14.945±0.039	13.329±0.012	12.888±0.014	12.728±0.015	13.013±0.038	11.70±0.02	11.41±0.02	11.79±0.07
315	14.177±0.005	12.902±0.002	12.339±0.002	12.045±0.001	11.916±0.002	11.39±0.02	11.22±0.02	11.43±0.02
316	15.060±0.070	13.358±0.022	12.669±0.008	12.274±0.008	12.367±0.018	11.13±0.03	10.90±0.03	11.23±0.04
317	14.215±0.010	12.793±0.002	12.191±0.002	11.880±0.001	11.701±0.004	11.21±0.02	10.99±0.02	11.19±0.03
318	15.741±0.030	14.084±0.042	13.393±0.035	13.062±0.030	12.859±0.016	12.23±0.01	12.00±0.02	12.22±0.02
319	16.909±0.029	15.502±0.006	14.969±0.008	14.611±0.008	14.436±0.010	14.01±0.05	13.70±0.06	13.73±0.07
320	16.642±0.030	14.706±0.027	14.069±0.029	13.732±0.026	13.501±0.016	11.70±0.02	11.41±0.02	11.79±0.07
321	15.254±0.013	14.029±0.005	13.524±0.004	13.244±0.003	13.086±0.005	12.56±0.02	12.41±0.04	12.53±0.03
322	14.271±0.003	13.913±0.003	13.546±0.005	13.303±0.005	13.121±0.005	12.43±0.02	12.16±0.03	12.33±0.02
323	15.392±0.020	13.615±0.003	12.963±0.001	12.619±0.002	12.655±0.006	12.11±0.03	11.94±0.03	12.13±0.05
324	14.432±0.021	13.141±0.005	12.645±0.005	12.421±0.005	12.466±0.009	11.71±0.03	11.50±0.03	11.81±0.05
325	16.010±0.016	14.340±0.004	13.630±0.004	13.269±0.004	13.037±0.004	12.53±0.03	12.22±0.03	12.35±0.04
326	16.893±0.038	15.429±0.007	14.705±0.004	14.293±0.004	14.014±0.009	13.45±0.03	13.18±0.04	13.19±0.04
327	15.061±0.012	14.695±0.017	14.562±0.019	14.687±0.023	14.576±0.027	14.47±0.06	14.42±0.08	14.64±0.12
328	15.225±0.012	14.109±0.005	13.625±0.006	13.382±0.005	13.245±0.006	12.76±0.02	12.54±0.03	12.82±0.04
329	19.105±0.108	17.684±0.025	16.726±0.014	16.256±0.015	15.885±0.021	15.04±0.10	14.37±0.09	14.25±0.07
330	16.116±0.868	14.139±0.121	13.455±0.067	13.024±0.108	12.515±0.354	11.93±0.03	11.64±0.02	11.74±0.02
331	16.757±0.120	15.037±0.149	14.196±0.103	13.734±0.085	13.440±0.023	12.50±0.03	12.12±0.03	12.08±0.03
332	15.762±0.015	14.209±0.007	13.560±0.006	13.184±0.007	13.034±0.006	12.43±0.03	12.16±0.03	12.33±0.03
333	17.396±0.046	16.660±0.100	16.004±0.101	15.564±0.103	15.293±0.117	15.04±0.08	14.03±0.01	13.99±0.01
334	14.023±0.016	12.357±0.034	11.712±0.027	11.416±0.022	11.228±0.005	10.55±0.01	10.34±0.01	10.63±0.02
335	18.124±0.083	16.686±0.026	15.990±0.029	15.589±0.033	15.354±0.030	13.63±0.05	13.56±0.06	13.73±0.06
336	15.004±0.070	12.860±0.029	12.002±0.057	11.644±0.035	11.371±0.032	10.49±0.03	10.35±0.03	10.43±0.02
337	15.693±0.035	13.389±0.002	12.668±0.004	12.247±0.002	12.130±0.004	11.34±0.02	11.20±0.02	11.35±0.03
338	16.614±0.028	15.304±0.019	14.793±0.022	14.464±0.022	14.320±0.024	13.52±0.04	13.29±0.05	13.38±0.06
339	15.669±0.022	13.801±0.003	13.089±0.002	12.682±0.002	12.467±0.005	11.90±0.03	11.66±0.03	11.69±0.04
340	14.971±0.017	14.186±0.005	13.791±0.006	13.608±0.020	13.408±0.011	13.25±0.04	13.12±0.04	13.24±0.10
341	15.338±0.021	13.615±0.004	13.001±0.003	12.647±0.002	12.531±0.006	11.89±0.02	11.70±0.02	11.86±0.03
342	16.130±0.018	14.857±0.003	14.208±0.004	13.872±0.003	13.653±0.007	13.12±0.04	12.95±0.05	13.05±0.05
343	16.115±0.051	14.199±0.004	13.289±0.002	12.831±0.002	12.540±0.008	11.90±0.02	11.66±0.02	11.79±0.03
344	14.925±0.030	13.247±0.004	12.543±0.006	12.167±0.002	11.980±0.008	11.39±0.02	11.10±0.02	11.28±0.02
345	15.435±0.015	14.263±0.022	13.912±0.014	13.714±0.012	13.658±0.008	13.08±0.04	13.15±0.06	13.14±0.06
346	14.475±0.013	13.387±0.006	13.009±0.005	12.805±0.004	12.798±0.008	12.37±0.03	12.17±0.04	12.25±0.04
347	18.439±0.109	17.023±0.062	16.538±0.119	16.089±0.108	16.018±0.182	14.74±0.07	14.49±0.10	14.22±0.07
348	15.263±0.005	14.400±0.002	14.104±0.002	13.886±0.002	13.735±0.004	13.54±0.03	13.25±0.04	13.46±0.06
349	15.929±0.012	14.386±0.007	13.631±0.007	13.259±0.007	12.984±0.006	12.22±0.03	12.13±0.03	12.54±0.05
350	15.554±0.017	14.509±0.003	13.960±0.003	13.661±0.002	13.577±0.012	13.01±0.04	12.88±0.05	12.82±0.04
351^{f}	···	14.5	13.7	···	···	12.37±0.02	12.16±0.03	12.37±0.04
352	16.968±0.025	14.977±0.003	13.990±0.002	13.490±0.002	13.150±0.004	12.77±0.03	12.55±0.03	12.79±0.04
353	14.383±0.010	13.611±0.005	13.424±0.004	13.377±0.002	13.302±0.005	13.11±0.03	13.06±0.04	13.38±0.06
354	18.942±0.107	17.274±0.009	16.445±0.007	15.912±0.008	15.655±0.030	14.96±0.09	14.36±0.07	14.48±0.09
355	15.102±0.873	13.842±0.945	13.228±0.860	13.995±1.052	11.806±0.559	13.26±0.04	13.04±0.05	13.08±0.05
356^{g}	15.0	14.3	13.9	···	···	12.83±0.05	12.68±0.06	12.70±0.07
357	16.763±0.111	15.572±0.055	15.088±0.132	14.732±0.053	14.519±0.024	14.11±0.05	14.70±0.00	13.95±0.07
358	18.800±0.118	17.284±0.035	16.480±0.030	16.033±0.039	15.635±0.034	14.86±0.07	14.59±0.08	14.66±0.09
359	15.953±0.041	14.427±0.005	13.724±0.004	13.340±0.008	13.064±0.017	12.50±0.03	12.27±0.03	12.37±0.03
360	15.508±0.035	14.115±0.010	13.465±0.010	13.128±0.019	12.918±0.005	12.35±0.02	12.14±0.02	12.31±0.03
361	16.665±0.045	14.926±0.020	14.265±0.025	13.875±0.021	13.655±0.023	13.13±0.03	13.00±0.05	12.98±0.05
362	15.972±0.068	15.090±0.045	14.626±0.027	14.478±0.026	14.477±0.036	13.86±0.07	13.84±0.11	13.65±0.10
363	15.762±0.013	14.398±0.002	13.786±0.002	13.464±0.002	13.300±0.004	12.85±0.03	12.58±0.04	12.79±0.04
364	15.399±0.038	13.409±0.016	12.631±0.027	12.208±0.012	12.139±0.017	11.50±0.02	11.22±0.02	11.44±0.02
365	17.474±0.058	15.744±0.012	14.875±0.016	14.429±0.008	14.110±0.012	13.41±0.03	13.19±0.04	13.31±0.04
366	16.263±0.049	14.935±0.009	14.494±0.006	14.249±0.015	14.410±0.072	13.54±0.04	13.31±0.06	13.45±0.06
367	17.624±0.060	16.000±0.030	15.272±0.029	14.883±0.030	14.601±0.016	14.02±0.04	13.84±0.05	13.96±0.07
368	16.678±0.028	15.129±0.003	14.363±0.002	13.947±0.002	13.665±0.009	13.13±0.03	12.83±0.03	12.94±0.04
369	17.781±0.028	16.217±0.005	15.440±0.004	14.926±0.004	14.662±0.008	14.03±0.03	13.72±0.04	13.64±0.03

TABLE 9 — *Continued*

SFRS			SDSS				2MASS	
	u	g	r	i	z	J	H	K_s

Note. — SDSS DR7 Petrosian magnitudes and 2MASS total magnitudes for the SFRS galaxies. Where the SDSS photometry is unreliable due to shredding, no values are given. Uncertainties are taken from the 2MASS extended source catalog and reflect measurement errors only. Issues pertaining to systematic errors in the 2MASS data are discussed in Sec. 4.3.2 Uncertainties are taken from the 2MASS extended source catalog and reflect measurement errors only. Issues pertaining to systematic errors in the 2MASS data are discussed in Sec. 4.3.2 All magnitudes are expressed on the AB system.

[a] SDSS u photometry was replaced by an estimate based on applying the Jester et al. (2005) filter transformations to the global $BVRI$ photometry from Hyperleda.

[b] Available SDSS $ugriz$ photometry corresponds only to a portion of this source.

[c] SDSS z photometry was replaced by an estimate based on applying the Jester et al. (2005) filter transformations to the global $BVRI$ photometry from Hyperleda.

[d] Available SDSS z photometry corresponds only to a portion of this source.

[e] SDSS $ugriz$ photometry was replaced by an estimate based on applying the Jester et al. (2005) filter transformations to the global $BVRI$ photometry from Hyperleda.

[f] SDSS gr photometry was replaced by an estimate based on applying the Jester et al. (2005) filter transformations to the global $BVRI$ photometry from Hyperleda.

[g] SDSS ugr photometry was replaced by an estimate based on applying the Jester et al. (2005) filter transformations to the global $BVRI$ photometry from Hyperleda.